

# **Human Descending Thoracic Aorta, a Mechanical Characterization**

Giulio Franchini

Department of Mechanical Engineering

McGill University

Montréal, Québec

2022-04-10

A thesis submitted to McGill University in partial fulfilment of the  
requirement of the degree of Doctor of Philosophy in Mechanical  
Engineering

© Giulio Franchini 2022



A tutte le nonne del mondo

To all grandmothers

给所有的祖母

الى جميع الجدات

## **Acknowledgements**

First of all, I thank Professor Marco Amabili for welcoming me into his laboratory and introducing me to the exciting world of vibrations.

I need to thank Dr. Giovanni Ferrari and Dr. Prabakaran Balasubramanian who have shown great skills and patience in teaching me their lab secrets, as well as technicians Mathieu Beauchesne and Lydia Dyda.

I would like to thank the financial support of the Natural Sciences and Engineering Research Council of Canada that supported this research and Transplant Québec that provided the human aortas.

## Abstract

PTFE and Dacron grafts are implanted today for repair of large human vessels like the aorta. They were originally designed more than half a century ago. While they are biocompatible, they alter the mechanics and physiology of the natural arteries. Researchers are now proposing a new generation of mechanically compatible grafts. The human aorta is a complex laminated structure with hyperelastic and viscoelastic material properties. This study aims to characterize the nonlinear static and viscoelastic properties of ex-vivo human descending thoracic aortas. The characterization is obtained on both strips subjected to static and dynamic tensile tests and on aortic segments tested in a mock circulatory loop. The loop is capable to reproduce the physiological pulsatile pressure and blood flow. Another research activity was dedicated to investigate the relationship between the vascular smooth muscle (VSM) activation and the mechanical properties of the aorta, and to develop a suitable model of the active mechanical response to help with the graft design. Since the VSM is mainly located in the tunica media, the activation strain can be attributed to this aortic layer. VSM activation is only possible for a small number of hours after the explantation from a heart-beating donor and when the tissue is kept refrigerated in organ preservation solution all the time before testing. Tests were carried out in a thermally controlled Krebs-Henseleit buffer solution, which was bubbled with oxygen. Potassium depolarization (KCl) and noradrenaline were used as vasoactive agents to induce VSM contraction. Experimental data and a suitable material model for human aortas with VSM activation are not available in the literature despite the need for the development of advanced grafts. Results show a significant effect of the pre-stretch on the dynamic stiffness ratio, while the pre-stretch has a smaller effect on the loss factor; the largest values of the dynamic stiffness ratio were obtained for the physiological conditions (about 50 kPa of engineering stress). All layers contribute in a similar way to the viscoelastic (passive) behavior. In active condition, results show that Vascular Smooth Muscles activation has a significant quasi-static stiffness increase of the descending thoracic aortic tissue in both the circumferential and longitudinal directions. Moreover, the viscoelastic effects increase in case of Vascular Smooth Muscles activation.

## Abrégé

Des greffes de PTFE et de Dacron sont implantées aujourd'hui pour la réparation de gros vaisseaux humains comme l'aorte. Ils ont été conçus à l'origine il y a plus d'un demi-siècle. Bien qu'ils soient biocompatibles, ils modifient la mécanique et la physiologie des artères naturelles. Les chercheurs proposent aujourd'hui une nouvelle génération de greffons mécaniquement compatibles. L'aorte humaine est une structure stratifiée complexe avec des propriétés matérielles hyperélastiques et viscoélastiques. Cette étude vise à caractériser les propriétés statiques et viscoélastiques non linéaires des aortes thoraciques descendantes humaines ex vivo. La caractérisation est obtenue à la fois sur des bandelettes soumises à des essais de traction statique et dynamique et sur des segments aortiques testés en boucle circulatoire fictive. La boucle est capable de reproduire la pression pulsatile physiologique et le débit sanguin. Une autre activité de recherche a été consacrée à étudier la relation entre l'activation du muscle lisse vasculaire (VSM) et les propriétés mécaniques de l'aorte, et à développer un modèle approprié de la réponse mécanique active pour aider à la conception de la greffe. Étant donné que le VSM est principalement situé dans la tunique médiane, la souche d'activation peut être attribuée à cette couche aortique. L'activation du VSM n'est possible que pendant un petit nombre d'heures après l'explantation d'un donneur au cœur battant et lorsque le tissu est conservé au réfrigérateur dans une solution de conservation d'organes tout le temps avant le test. Les tests ont été effectués dans une solution tampon de Krebs-Henseleit thermiquement contrôlée, qui a été barbotée avec de l'oxygène. La dépolarisation du potassium (KCl) et la noradrénaline ont été utilisées comme agents vasoactifs pour induire la contraction du VSM. Les données expérimentales et un modèle de matériau approprié pour les aortes humaines avec activation VSM ne sont pas disponibles dans la littérature malgré la nécessité de développer des greffes avancées. Les résultats montrent un effet significatif du pré-étirement sur le rapport de rigidité dynamique, tandis que le pré-étirement a un effet moindre sur le facteur de perte ; et les valeurs les plus élevées du rapport de rigidité dynamique ont été obtenues pour les conditions physiologiques (environ 50 kPa de contrainte technique). Mais plus important encore, toutes les couches contribuent de la même manière au comportement viscoélastique (passif). En condition active, les résultats montrent que l'activation des muscles lisses vasculaires entraîne une augmentation significative de la rigidité quasi-statique du tissu aortique thoracique descendant

dans les directions circonférentielle et longitudinale. De plus, les effets viscoélastiques augmentent en cas d'activation des muscles lisses vasculaires.

# Chapter 1

## Introduction

A major goal of researchers should be the improvement of any biomedical prosthesis to keep up the technological progress. The aim is to improve the quality of life of patients who undergoes surgery for prosthetic implantation. The technological progress cannot afford to stop in a field of application of such importance as that of biomedical prostheses for human patients. In the present thesis, we have chosen to focus on the mechanical characterization of the human thoracic descending aorta, which is the crossroads of the blood that flows into our body. The human aorta, after an initial ascending tract, deviates its direction forming an arch, which then continues in a descending direction. This can be divided in two sections: the first is the thoracic part up to the diaphragm, followed by the abdominal section. At the top of the arch, the arteries that supply the upper limbs and the brain depart.

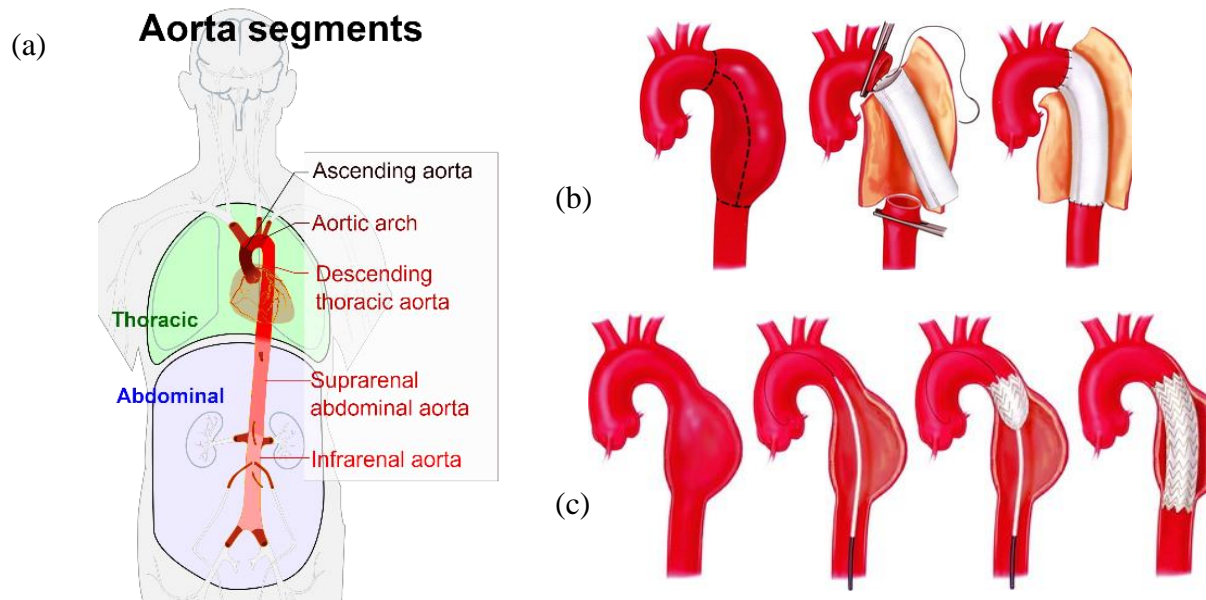


Figure 1. (a) Aortic segments. (b) Open surgery for aortic repair after aneurysm. (c) Endovascular surgery for aortic repair. [E. M. Isselbacher, Thoracic and Abdominal Aortic Aneurysms. *Circulation* 2005;111:816–828]

The thoracic descending section of the aorta can be affected by aneurysms or by acute dissections, which can require open or endovascular surgery for repair (see Fig. 1). In this thesis, we identify the parameters and mechanical properties of the aortic tissue. Undoubtedly, a purely mechanical approach is not sufficient for such complex material, considering its “living” nature with its ability to remodel. However, it becomes necessary to fully understand its active and passive mechanical behaviour in order to develop improved or revolutionary aortic grafts. This document shifts the focus on the mechanical aspects of the aortic material. The author hopes that this mechanical approach will become a fundamental guideline for future prosthetic design, enriching the already rich literature.

### The aorta: a layered structure

The human aorta is the largest artery in the human body and consists of three distinct biological layers with their own mechanical, material and biological characteristics. Each aortic layer is fibrous and can be described as an anisotropic fiber-reinforced structure (see Fig. 2).

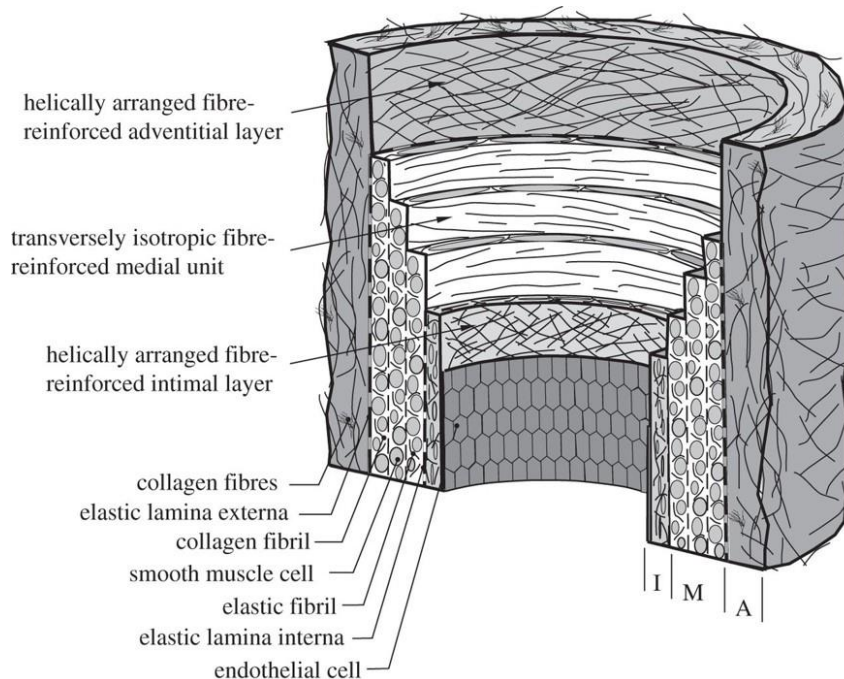


Figure 2. Example of healthy aorta with the three main layers: Intima, Media and Adventitia. [G. A. Holzapfel, T. C. Gasser & R. W. Ogden, A New Constitutive Framework for Arterial Wall Mechanics and a Comparative Study of Material Models. *Journal of elasticity and the physical science of solids*, volume 61, 1–48 (2000).]

- Tunica adventitia. It is the outermost layer with a helically arranged fiber distribution. Results in the literature describe the collagen fiber orientation as approximately at 45 degrees with respect to the longitudinal axis. Its average thickness is about 0.7 mm (as observed after mechanical layer separation).
- Tunica media. It is the intermediate layer and the main responsible of the aortic stiffness and contains vascular smooth muscle, which is the source of the active behaviour. Its average thickness is about 0.9 mm (as observed after mechanical layer separation).
- Tunica intima. It is the innermost layer, composed by endothelial cells in contact with the blood flow and elastic tissue. It has the biological function of being the interface layer with the blood. Its average thickness is about 0.2 mm.

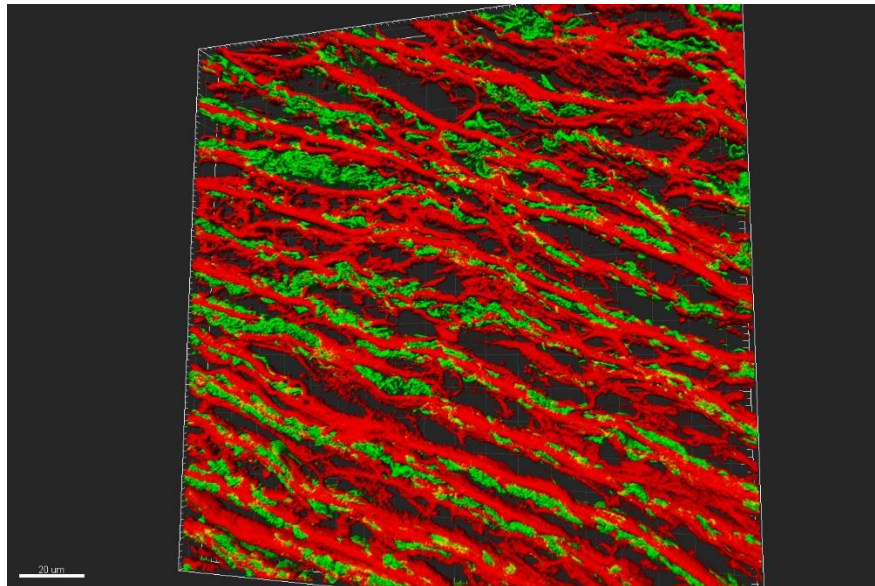


Figure 3. Elastin (red) and collagen (green) network of fibers in a sample of human aorta.

The results obtained of this thesis by papers are presented in the three following chapters, which exactly replicate the publications printed in peer-review prestigious journals. These chapters are summarized below. Chapter 2 and 3 deal with the passive mechanical identification of the layer-specific and global response of the wall. Tests are performed on aortic strips (Chapter 2) and tubular segments (Chapter 3). The active and passive mechanical responses of the full wall are measured and compared in Chapter 4, where a mechanical model of the active tissue is proposed.

**Chapter 2** - Viscoelastic characterization of human descending thoracic aortas under cyclic load. *Acta Biomaterialia*, vol. 130, pp. 291-307, (2021).

Experiments were carried out on 15 human descending thoracic aortas from heart-beating healthy donors who donated organs for transplant. The aortas were kept refrigerated in organ preservation solution and tests were completed within 48 hours from explant. Donors' age was comprised between 25 and 70 years, with an average of  $51.7 \pm 12.8$  years. Quasi-static and dynamic uniaxial tensile tests were carried out in thermally controlled physiological saline solution in order to characterize the viscoelastic behavior. Strips were tested under harmonic deformation of different frequency, between 1 and 11 Hz, at three initial pre-stretches. Cyclic deformations of two different amplitudes were used: a physiological one and a small one, the latter one for comparison purposes to understand the accuracy limits of viscoelastic models. Aortic strips in circumferential and longitudinal directions were cut from each aorta. Some strips were dissected to separate the three layers: intima, media and adventitia. They were tested individually in order to obtain layer-specific data. However, strips of the intact wall were also tested. Therefore, 8 strips per donors were tested. Viscoelastic parameters are accurately evaluated from the hysteresis loops. Results show that small-amplitude cyclic strain over-estimate the storage modulus and under-estimate the loss-factor. Therefore, cyclic deformation of physiological amplitude is necessary to obtain correct viscoelastic data of aortic tissue. The value of the applied pre-stretch is significant on the dynamic stiffness ratio (storage modulus divided by the corresponding quasi-static stiffness), while it is less significant for the loss factor. The median of the dynamic stiffness ratios, in physiological conditions, varies between 1.14 and 1.33 for the different layers and the intact wall; the corresponding median of the loss factors varies between 0.050 and 0.066. The lowest dynamic stiffness ratios and loss factors were obtained from donors of the youngest age group.

**Chapter 3** - Viscoelasticity of human descending thoracic aorta in a mock circulatory. *Journal of the Mechanical Behavior of Biomedical Materials*, vol. 130, 105205 (2022).

Healthy human descending thoracic aortas, obtained during organ donation for transplant and research, were tested in a mock circulatory loop to measure the mechanical response to physiological pulsatile pressure and flow. The viscoelastic properties of the aortic segments were investigated at three different pulse rates. The same aortic segments were also subjected to quasi-static pressure tests in order to identify the aortic dynamic stiffness ratio, which is defined as the ratio between the stiffness in case of pulsatile pressure and the stiffness measured for static pressurization, both at the same value of pressure. The loss factor was also identified. The shape of the deformed aorta under static and dynamic pressure was measured by image processing to verify the compatibility of the end supports with the natural deformation of the aorta in the human body. In addition, layer-specific experiments on 10 human descending thoracic aortas allowed to precisely identify the mass density of the aortic tissue, which is an important parameter in cardiovascular dynamic models.

**Chapter 4** - Role of smooth muscle activation in the static and dynamic mechanical characterization of Human aortas. *PNAS (Proceedings of the National Academy of Sciences of the United States of America)*, vol. 119, No. 3, e2117232119 (2022).

Experimental data and a suitable material model for human aortas with smooth muscle activation are not available in the literature despite the need for developing advanced grafts; the present study closes this gap. Mechanical characterization of human descending thoracic aortas was performed with and without vascular smooth muscle (VSM) activation. Specimens were taken from 13 heart-beating donors. The aortic segments were cooled in Belzer UW solution during transport and tested within a few hours after explantation. VSM activation was achieved through the use of potassium depolarization and noradrenaline as vasoactive agents. In addition to isometric activation experiments, the quasistatic passive and active stress–strain curves were obtained for circumferential and longitudinal strips of the aortic material. This characterization made it possible to create an original mechanical model of the active aortic material that accurately fits the experimental data. The dynamic mechanical characterization was executed using cyclic strain at

different frequencies of physiological interest. An initial pre-stretch, which corresponded to the physiological conditions, was applied before cyclic loading. Dynamic tests made it possible to identify the differences in the viscoelastic behavior of the passive and active tissue. This work illustrates the importance of VSM activation for the static and dynamic mechanical response of human aortas. Most importantly, this study provides material data and a material model for the development of a future generation of active aortic grafts that mimic the natural behavior and help regulating blood pressure.

## **Chapter 2**

# **Viscoelastic characterization of human descending thoracic aortas under cyclic load**

Giulio Franchini<sup>1</sup>, Ivan D. Breslavsky<sup>1</sup>, Gerhard A. Holzapfel<sup>2,3</sup>, Marco Amabili<sup>1,4</sup>

(1) Department of Mechanical Engineering, McGill University, Montreal, Canada

(2) Institute of Biomechanics, Graz University of Technology, Austria

(3) Department of Structural Engineering, Norwegian University of Science and Technology  
Trondheim, Norway

(4) Dipartimento di Ingegneria e Architettura, University of Parma, Parma, Italy

Keywords: Human aorta; viscoelasticity; layer-specific; experiments;

### **Abstract**

Experiments were carried out on 15 human descending thoracic aortas from heart-beating healthy donors who donated organs for transplant. The aortas were kept refrigerated in organ preservation solution and tested were completed within 48 hours from explant. Donors' age was comprised between 25 and 70 years, with an average of  $51.7 \pm 12.8$  years. Quasi-static and dynamic uniaxial tensile test were carried out in thermally controlled physiological saline solution in order to characterize the viscoelastic behavior. Strips were tested under harmonic deformation of different frequency, between 1 and 11 Hz, at three initial pre-stretches. Cyclic deformations of two different amplitudes were used: a physiological one and a small one, the latter one for comparison purposes to understand the accuracy limits of viscoelastic models. Aortic strips in circumferential and longitudinal directions were cut from each aorta. Some strips were dissected to separate the three layers: intima, media and adventitia. They were tested individually in order to obtain layer-specific data. However, strips of the intact wall were also tested. Therefore, 8 strips per donors were tested. Viscoelastic parameters are accurately evaluated from the hysteresis loops. Results show that

small-amplitude cyclic strain over-estimate the storage modulus and under-estimate the loss-factor. Therefore, cyclic deformation of physiological amplitude is necessary to obtain correct viscoelastic data of aortic tissue. The value of the applied pre-stretch is significant on the dynamic stiffness ratio (storage modulus divided by the corresponding quasi-static stiffness), while it is less significant for the loss factor. The median of the dynamic stiffness ratios, in physiological conditions, varies between 1.14 and 1.33 for the different layers and the intact wall; the corresponding median of the loss factors varies between 0.050 and 0.066. The lowest dynamic stiffness ratios and loss factors were obtained from donors of the youngest age group.

## **Statement of Significance**

There is an increasing interest in replacing traditional Dacron grafts used to repair thoracic aortas after acute dissection and aneurysm, with grafts in innovative biomaterials that mimic the mechanical properties and the dynamic behavior of the aorta. The human aorta is a complex laminated structure with hyperelastic and viscoelastic material properties and residual stresses. This study aims to characterize the nonlinear viscoelastic properties of *ex-vivo* human descending thoracic aortas by measuring hysteresis loops of physiological amplitude under harmonic strain. Results show the necessity to characterize the viscoelastic material properties of the aorta under physiological conditions, as well as the necessity to introduce improved models that take better into account the influence of the initial pre-stretch and amplitude of the cyclic load.

## **1. Introduction**

The characterization of the mechanical response of aortic tissue to dynamic loads is a paramount significance to develop a future generation of aortic grafts that can mimic the natural behavior of the aorta. This is important not to alter the Windkessel effect, which is a function of the natural aorta that allows to accumulate blood volume during the systole in the elastic vessel and to release it during diastole [1]. This has the positive effect of smoothing the pulsatile nature of the flow, which is beneficial to the perfusion. Experimental studies have shown that the cyclic expansion of the descending thoracic aorta under physiologically pulsating blood flow is 10 % of the diameter

in young individuals and can be reduced to 1 % over 70 years of age, with values progressively decreasing with age [2, 3]. The stiffness of arteries increases with age, which is a significant health issue. On the other hand, the cyclic expansion of currently used Dacron grafts is practically negligible [4-6], which completely cancels the Windkessel effect for the portion of the aorta replaced by the graft.

The human aorta is composed of three layers [7]: the intima is the inner layer, which is in contact with the blood; the media is the central layer and contains also the smooth muscle; the adventitia is the outer layer. Each one of the three layers has different mechanical properties.

While the static mechanical characterization of the aortic tissue has been studied more extensively [8-15] and sophisticated hyperelastic constitutive models have been developed [16-22], the literature reporting viscoelastic tests is still relatively scarce. However, it is recognized that the arterial dynamic stiffness is a risk factor for clinical hypertension [23] and, therefore, more experiments are needed, as well as studies linking viscoelastic mechanical properties to age. Bergel [24] used harmonic volumetric inflation of human aortic segments with liquid pushed by a syringe connected to a mechanism to characterize the dynamic behavior. He observed that the dynamic stiffness was between 1.05 and 1.1 times the static stiffness for the thoracic aorta, and the loss tangent grew with frequency, ranging from 0.079 to 0.15. Westerhof and Noordergraaf [25] critically reviewed most of the reported experimental results on arterial viscoelasticity up to their time. They also introduced a model of the systematic arterial tree for the purpose of studying the effect of the viscous properties of the wall.

The viscoelasticity of the entire aorta was examined by *in vivo* ultrasound measurement. Fifteen human abdominal aortas were characterized *in vivo* at rest condition, specifically around 72 beats per minute, by Imura et al. [26]; a similar study by Imura et al. [27] obtained data from 61 aortas. They used an ultrasonic sensor to measure the wall displacement and a catheter to obtain the intra-aortic pulsatile pressure. Results show an average loss tangent of 0.12 and a storage modulus of 604 kPa.

Mock circulatory loops were developed to characterize the viscoelastic behavior of arteries *in vitro* by recreating physiological pulsatile blood flow conditions by avoiding invasive pressure measurement. Tests on eleven Merino sheep descending thoracic aortas at 108 and 110 bpm [28, 29], seven human common carotid arteries at 70 bpm [30], and canine descending thoracic aortas subjected to vasoactive agent for smooth muscle activation [31], were reported in the literature. By

using the experimental results of previous studies, Ghigo et al. [32] described the viscoelastic behavior of the arterial wall and its influence on the pulse wave. Amabili et al. [3] used a mock circulatory loop to obtain the viscoelastic properties of eleven *ex vivo* human descending thoracic aortas of healthy donors in the full range of physiological heart rates.

Courtial et al. [33] tested samples of four healthy human abdominal aortas at low shear strain with a rotational rheometer, reporting loss tangent values from 0.04 to 0.1 and storage moduli gradually increasing with frequency.

Layer-specific viscoelastic experiments on axial and circumferential strips of 12 healthy descending thoracic aortas were performed by the research group of Amabili [13, 34]. It was found that the storage modulus increased by 1.2 to 3.5 times with respect to the static stiffness, and the loss tangent varied from 0.06 to 0.21, for small-amplitude cyclic strain. Specifically, the amplitude was 50  $\mu\text{m}$  for a strip with free length of about 25 mm, giving a cyclic engineering strain of 0.2%. Due to the small cycles, linear viscoelasticity was assumed around the pre-stretched configuration; then, the storage modulus and the loss tangent were obtained by using the amplitude and phase of the complex modulus. Layer-specific viscoelastic experiments on a chronic type A dissected human aorta were carried out by Amabili et al. [35] using the same approach.

Results in [13, 24, 25, 34] show that the mechanical behavior of each aortic layer is nonlinearly viscoelastic. The viscoelasticity is responsible for a slight delay between the blood pressure wave and the displacement of the aortic wall, which favors the accumulation of blood during the systole. In addition, the dynamic stiffness of the aortic tissue increases compared to that observed under static load, which is also an effect of viscoelasticity [13, 24, 25, 34, 35].

The complex nonlinear viscoelastic behavior of the aorta is usually modeled by using quasi-linear viscoelasticity [36, 37] or nonlinear viscoelasticity with internal variables [37, 38]. It is interesting to observe that, even if the two approaches start from different perspectives, they are based on similar hypotheses and they lead to similar results [37, 39]. It is necessary to understand if these models agree with experimental results.

In the present study, a quasi-static and dynamic mechanical characterization were carried out on 15 human descending thoracic aortas from heart-beating healthy donors who donated organs for transplant. Some strips were dissected to separate the three layers: intima, media and adventitia. They were tested individually in order to obtain layer-specific data. However, strips of the intact wall were also tested

## 2. Materials and Methods

This section describes (i) the specimen preparation, (ii) the quasi-static and dynamic uniaxial tensile tests, and (iii) the viscoelastic parameter identification. The constitutive model is given in Appendix A2.

### 2.1 Donors and preparation of strips

Transplant Québec, the organ donation coordinator in Québec, Canada, provided the 15 human descending thoracic aortas for the present study between September 2019 and October 2020. The present study was authorized by the ethical committee of McGill University. Donors' age was comprised between 25 and 70 years, with an average of 51.7 and a standard deviation of 12.8 years. Table 1 presents information on the donors' age, gender, weight, height and cause of death. All donors were screened for organ donation and were considered healthy for this purpose. The donors were maintained heart-beating after cerebral death was assessed for the purpose of organ donation for transplant. Aortas were removed at the end of the organ explant operation and were kept refrigerated at 4° C in Belzer UW organ preservation solution [40].

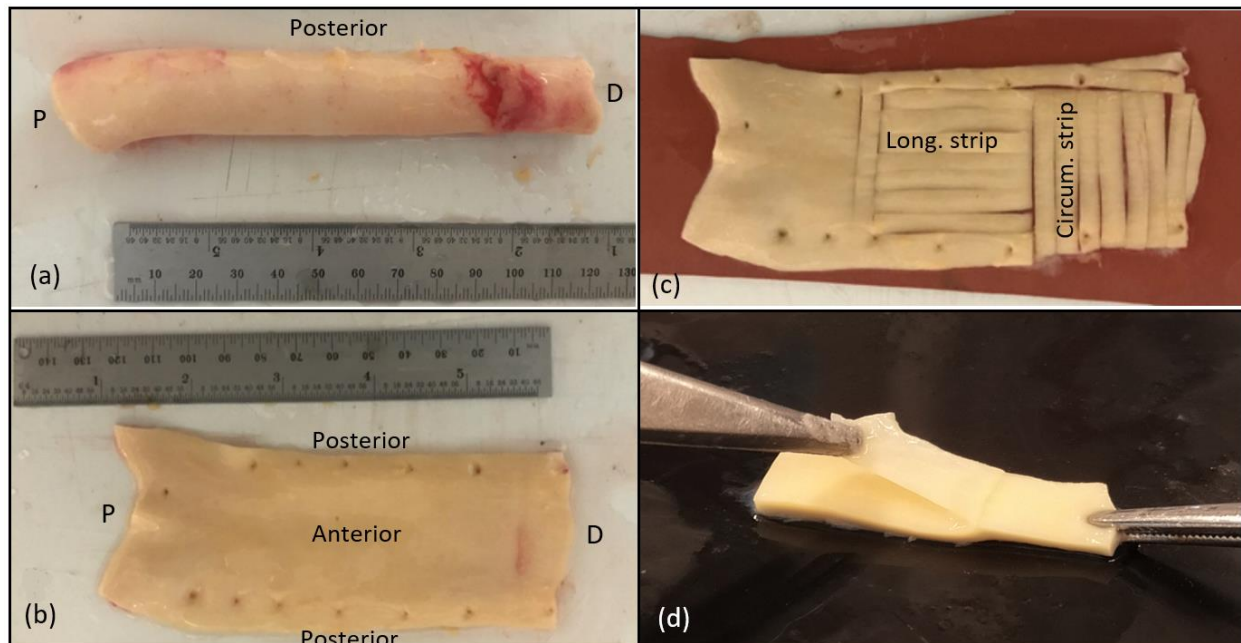


Figure 1 Preparation of the aorta from donor #9: (a) descending thoracic aorta cleaned from periaortic connective tissue and bifurcating arteries; P = proximal side; D = distal side; (b) descending thoracic aorta opened with a longitudinal cut made on the poster

Table 1. Data on 15 donors: TBI = traumatic brain injury; CVA = cerebrovascular accident; HAI = hypoxic/anoxic injury. Thickness and standard deviation (mm) of the descending thoracic aorta are also given. Ten thickness measurement were made: five on the longitudinal strip and five on the circumferential strip.

Donor #	1	2	3	4	5	6	7	8	9	10	11	12	13	14	15	
Age	66	45	47	70	54	46	65	63	50	48	25	30	47	59	60	
Gender	M	M	M	M	M	M	F	M	F	M	F	M	M	F	M	
Weight (kg)	86	74	92	91.5	80	103	50	53	110	81	75	72	115	76.4	72.6	
Height (cm)	162	172	188	183	175	178	155	172	168	175	159	158	187	165	171	
Death	TBI	CVA	CVA	CVA	CVA	HAI	CVA	CVA	CVA	CVA	TBI	HAI	HAI	CVA	CVA	
Thickness (mm)	1.75		1.77	1.52	1.67	1.62	1.45	1.98	1.71	1.68	1.81	1.57	1.61	1.63	1.67	1.57
St. dev. ( $\pm$ mm)	0.19	0.36	0.36	0.22	0.23	0.13	0.25	0.14	0.34	0.21	0.11	0.25	0.30	0.20	0.15	

They were tested immediately after arrival in the laboratory and tests were completed within 48 hours from explant. Figure 1(a) shows a descending thoracic aorta after removal of the bifurcating arteries and the periaortic connective tissue.

The aorta was then opened up with a longitudinal cut along the posterior part, in between the holes of the bifurcating intercostal arteries; in this way, the holes appear near both edges of the opened-up aorta and the anterior portion of the aortic tissue is in the central part, as shown in Fig. 1(b). Strips with width of about 5 mm and length of about 35 mm were cut in the circumferential and longitudinal directions, with the arrangement shown in Fig. 1(c). Some strips were kept with the intact wall, while other strips were dissected to separate the three layers (intima, media and adventitia), as shown in Fig. 1(d). A few strips were split, which allowed to choose the one with the best layer separation. Histology and microscopy imaging were used to verify the quality of the layer separation. Fig. 2 shows one example of a Masson trichrome staining of the cross-section of the three separated layers and the intact wall of donor #4. In fact, the smooth muscle appears in red color with trichrome staining and allows to assess the quality of the layer separation since the smooth muscle is confined to the media.

Transition zones were observed in-between the layers, around the membrana elastica interna and the externa one, as previously described in [12]. During the layer separation, the transition layer around the membrana elastica externa tended to stick to the adventitia. Each strip thickness was measured by using a Micro-Epsilon triangulation laser sensor (model optoNCDT1402) at five different locations. The thickness and standard deviation of the descending thoracic aortas from different donors is given in Table 1, obtained from 10 measurements (5 from the circumferential strip and 5 from the longitudinal strip). The width of each strip was also measured at five locations to calculate the cross-section area.

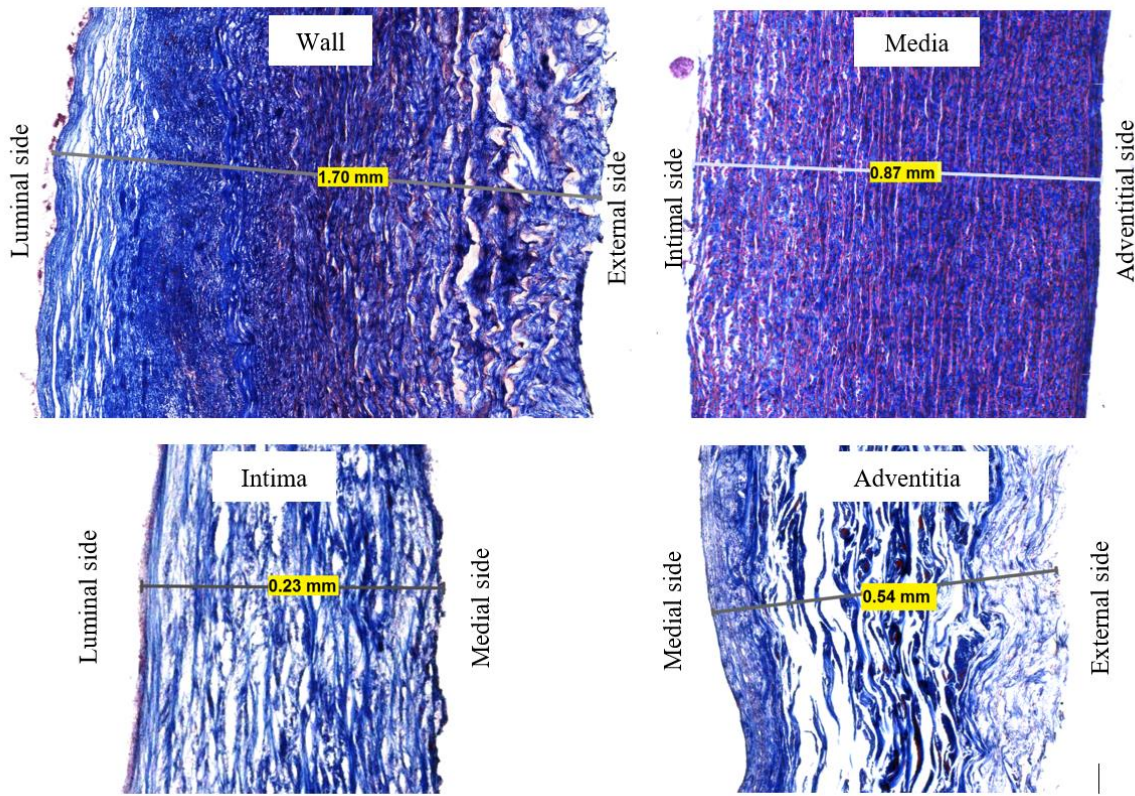


Figure 2 . Cross-sections of the wall and of the three separated layers of a descending thoracic aorta (donor #4) in order to verify the quality of the layer separation. Masson trichrome stain, thickness 10  $\mu\text{m}$ . Leica Aperio digital slide scanner.

## 2.2 Quasi-static and dynamic uniaxial tensile tests

Quasi-static and dynamic uniaxial tensile tests were carried out on a specifically developed system consisting of: (i) a Brüel & Kjær electrodynamic exciter model 4824 combined with a power amplifier B&K Type 2732 to impose quasi-static and dynamic displacements to the mobile

strip holder; (ii) a self-developed Simulink code within a dSPACE hardware to control the electrodynamic exciter; (iii) a LMS SCADAS data acquisition system with the Siemens LMS TestLab software to record displacement, force and strain during the test; (iv) a Polytec laser Doppler vibrometer OFV 5000 with displacement decoder to measure the displacement of the mobile strip holder; (v) an Interface WMCFP-1000g load cell connected to the fixed strip holder to measure the force; (vi) an Epsilon ONE-52PT video extensometer (equipped with telecentric lens to minimize potential inaccuracies caused by out-of-plane motions; distance of about 5 mm between markers on tested specimens; absolute error not exceeding  $\pm 5 \mu\text{m}$ ); (vii) a plexiglass case containing a temperature controlled thermal bath that contained the handles and the aortic strips. The system presents a fixed grip connected to the force sensors and a moving grip connected to the electrodynamic exciter. The distance between the grips and the tensile forces had accuracy reading of  $\pm 1 \mu\text{m}$  and  $\pm 0.01 \text{ N}$ , respectively. Aluminum grips were used together with cyanoacrylate glue to avoid any slippage. The thermal bath of physiological saline solution (0.9 % NaCl in volume) was kept at  $37^\circ\text{C}$ . A photo of the experimental setup is given in Fig. A1 in the Appendix A1.

Quasi-static tensile tests were carried out after eight pre-conditioning cycles at a displacement rate of 0.05 mm/s. This rate was considered sufficiently slow to minimize viscoelastic effects, as verified by the negligible hysteresis between loading and unloading after preconditioning. Displacement control was implemented, with displacement inversion at the desired stress level (0.1 MPa in most experiments) being given as engineering stress. The distance between the grips was initially adjusted in order to find the load-free configuration of the strip. This configuration was adjusted (if necessary) at the end of the pre-conditioning cycles, without stopping the test, and the corresponding strain was zeroed.

Dynamic tests were designed to identify the viscoelastic parameters of the aortic tissue in conditions close to the physiological ones. Each aortic strip was tested under harmonic cyclic strain at frequency varying from 1 to 11 Hz, with a two Hz step increment; 30 dynamic cycles were recorded at each frequency and the last one was presented. The amplitude of each cycle, defined as the difference between maximum and minimum strain, was about 0.07 engineering strain (i.e. 7%), with the only exception of donor #4, the oldest donor of age 70 years, for which the cycle amplitudes were reduced to 0.03 engineering strain (3%). Amabili et al. [3] have shown that the amplitude of the cyclic strain of aortas under physiological pulsatile flow and pressure varies

between 9% (for age around 20 years) and 2% (for age around 70 years). Therefore, the imposed cyclic strain amplitude falls in the physiological values. In physiological conditions, the aorta is always pressurized (between 80 and 120 mmHg for a healthy individual at rest conditions). Therefore, the dynamic load is superimposed to a static load that is generating a pre-stretch in physiological conditions. For this reason, the present study investigates the effect of dynamic loading on a pre-loaded (pre-stretched) strip. The pre-load level is attributed to the central point of the cyclic loop. Harmonic strain cycles started from a central point at a given initial pre-stretch. Three pre-stretch levels, giving about 12.5, 50, 100 kPa of engineering stress, were selected. Among these three levels, 50 kPa is a reference stress level to represent a physiological condition. In fact, the approximate formula for a thin pressurized cylinder  $S = pR/h$ , for mean blood pressure  $p = 93.3$  mmHg (obtained in case of pulsatile pressure between 80 and 12 mmHg as  $80+40/3$  mmHg), mean aortic radius  $R = 10$  mm and wall thickness  $h = 2$  mm, gives 62 kPa, which is close enough to the 50 kPa level. This is a rough calculation; for an accurate calculation considering residual stresses see, e.g., Breslavsky and Amabili [41]. The 100 kPa level was added to investigate the effect of higher pressures (e.g., hypertension), while the 12.5 level was chosen to study the viscoelastic response of tissue when the involvement of collagen fibers in the aortic tissue response is modest.

In addition to this physiological viscoelastic characterization, small dynamic cycles of amplitude 0.005 engineering strain (0.5%) were also imposed in order to verify the effect of the reduced amplitude on the viscoelastic properties of the aortic tissue. Three pre-stretch levels were considered and the frequency range was comprised between 1 and 11 Hz.

The measurement process for each strip consisted of: (i) pre-conditioning and quasi-static uniaxial tensile tests at displacement rate of 0.05 mm/s for a total of 10 loading and unloading cycles; (ii) application of the first pre-stretch level, followed by 30 cycles of amplitude 0.5% at each frequency from 1 to 11 Hz with a 2 Hz increment; (iii) 30 cycles of amplitude 7% at each frequency from 1 to 11 Hz with a 2 Hz increment; (iv) repetition of steps (ii) and (iii) for the second and then the third pre-stretch level. The number of measured points per cycle was 790 at 1 Hz and decreased proportionally with increasing frequency. The time sequence of the quasi-static and dynamic tests on one strip is given in Fig. A2 in the Appendix.

### 2.3 Identification of the nonlinear viscoelastic parameters and viscoelastic model

One schematic hysteresis loop of the harmonic cyclic strain is shown in Fig. 3 together with the quasi-static stress-strain curve. The middle curve of the loop is obtained as an average of the top and bottom curves of the loop. On this middle curve lies the loop center. The corresponding point to the loop center on the quasi-static stress-strain curve is indicated in Fig. 3 as the intersection between this curve and the minimal distance line. Ideally, the center of the loop should be located on the quasi-static curve, but due to minimal relaxation, creep and inelasticity occurring between the quasi-static test and the dynamic test, small differences can arise. The slope of the tangent to the middle line of the loop at the loop center is indicated as  $\alpha_L$ , hence  $\tan(\alpha_L)$  gives the storage modulus. The slope of the tangent to the quasi-static curve at the point corresponding to the loop center is denoted by  $\alpha_S$ , hence  $\tan(\alpha_S)$  gives the corresponding static modulus. The dynamic stiffness ratio  $\delta$  is introduced as the ratio between the storage modulus and the corresponding static modulus. This parameter indicates the increase of stiffness of the aortic tissue of the strip when loaded dynamically with respect to a quasi-static load. It depends on the pre-stretch level, on the amplitude of the harmonic cyclic strain and on the frequency of the dynamic load.

The hysteresis loop in Fig. 3 is also used to calculate the loss factor  $\eta$ . For a complete vibration cycle, the energy dissipated per unit volume, say  $\Delta W_d$ , by the aortic strip subjected to harmonic strain is [37]

$$\Delta W_d = \int_{cycle} \sigma d\varepsilon, \quad (1)$$

where  $\sigma$  is the dynamic stress and  $\varepsilon$  is the dynamic strain. Equation (1) gives the area contained within the hysteresis loop.

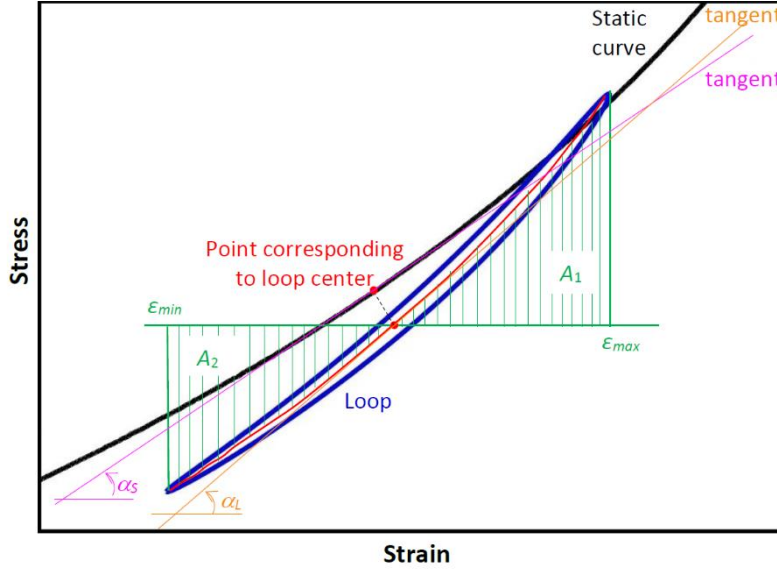


Figure 3 Hysteresis loop (—) and static curve (—) of an aortic strip under harmonic load in the stress-strain plane. The area inside the loop is proportional to the energy loss. The average of the areas  $A_1$  and  $A_2$ , found using the middle curve of the loop (—) and the horizontal line passing through the center of the loop, is proportional to the storage energy. The slope of the tangent to the middle line of the loop (—) at the loop center is  $\alpha_L$ , and  $\tan(\alpha_L)$  gives the storage modulus; the slope of the tangent to the static curve (—), at the point corresponding to the loop center, is  $\alpha_S$  and  $\tan(\alpha_S)$  gives the corresponding static modulus.

The hysteresis loop (Fig. 3) can be divided into two curves: the top half refers to loading and the lower half to unloading. They join at the two extrema of the strain values taken by the loop,  $\varepsilon_{min}$  and  $\varepsilon_{max}$ . The dynamic elastic relationship describing the stress-strain curve of the viscoelastic aorta, under harmonic strain, is assumed to be the average of the upper half and the lower half of the loop; it is the backbone curve of the loop drawn in red in Fig. 3. The storage energy per unit volume, say  $W_S$ , for one quarter of the cycle [37], is given by

$$W_S = \frac{A_1 + A_2}{2}, \quad (2)$$

where  $A_1$  and  $A_2$  are the areas of the two curvilinear triangles shown in Fig. 3. Due to the nonlinearity of the dynamic elastic relationship, the areas  $A_1$  and  $A_2$  are different and an average of the two is introduced in equation (2). Then, the loss factor  $\eta$  is obtained as [3, 37]

$$\eta = \frac{\Delta W_d}{2\pi W_S} = \frac{\Delta W_d}{\pi(A_1 + A_2)}. \quad (3)$$

Since equation (3) is a ratio of the two areas, it does not carry measurement units.

It is convenient to introduce a simple model to describe the viscoelastic behavior of the material versus frequency: the generalized Maxwell viscoelastic material model with  $N_s$  springs, developed in the framework of the nonlinear viscoelasticity with internal variables [37, 38]. The dynamic stiffness ratio  $\delta$  is given by

$$\delta(\omega) = \frac{E'(\omega)}{E_\infty} = \left[ 1 + \sum_{m=1}^{N_s} \beta_m^\infty \frac{(\omega \tau_m)^2}{1 + (\omega \tau_m)^2} \right], \quad (4)$$

where  $E'$  is the storage modulus,  $E_\infty$  is the static modulus (Pa),  $\omega$  (rad/s) is the harmonic oscillation frequency,  $\beta_m^\infty > 0$ ,  $m = 1, \dots, N_s$ , are non-dimensional stiffness coefficients and  $\tau_m$ ,  $m = 1, \dots, N_s$ , are time constants (s). The loss tangent  $\eta$  is represented by

$$\eta(\omega) = \frac{\sum_{m=1}^{N_s} \beta_m^\infty \frac{\omega \tau_m}{1 + (\omega \tau_m)^2}}{1 + \sum_{m=1}^{N_s} \beta_m^\infty \frac{(\omega \tau_m)^2}{1 + (\omega \tau_m)^2}}. \quad (5)$$

The dynamic stiffness ratio and the loss factor are also functions of the initial pre-stretch and the amplitude of the cyclic strain  $\varepsilon_{\max} - \varepsilon_{\min}$ . Therefore, different sets of model parameters must be obtained for any initial pre-stretch level, as well as for different amplitudes of the cyclic strain. In addition, different sets of parameters are necessary for each strip of aortic tissue. The static modulus  $E_\infty$  is a function of the initial pre-stretch  $\lambda$  of the strip and it can be obtained from the hyperelastic constitutive model introduced in equation (A1) in the Appendix. The integer  $N_s$  in equations (4) and (5) must be large enough to approximate with good accuracy the experimental data, while the viscoelastic parameters  $2N_s$  must be identified for each strip at a given pre-stretch. The problem of minimization of an objective function is solved with a genetic algorithm [34].

### 3. Results and Discussion

The results of the quasi-static uniaxial tensile tests and the loops obtained applying a harmonic cyclic strain of amplitude 0.07 engineering strain at frequency 1 Hz at three different pre-stretch

levels, corresponding to about 12.5, 50, 100 (kPa, engineering stress), are presented in Fig. 4 for the descending thoracic aorta from donor #12 (age 30 years); results for the eight strips from the same donor are presented. Except for a very few cases (e.g., for the longitudinal intact wall), the center of the loop is at a small distance from the quasi-static curve. Even if the loops have all the same amplitude in strain, the ones at the largest pre-stretch (100 kPa) have a larger overall size. As discussed in Section 2.2, the second pre-stretch level (50 kPa) is the closest to the physiological conditions. Even if the middle curve of the loop is not drawn in Fig. 4, it exists between the top and the bottom of each loop, which is slender. Then, results display a clear increase of the storage modulus with respect to the corresponding static modulus.

The hysteresis loops, now with zeroed strain corresponding to the loop center, are presented for the frequencies 1, 3 and 5 Hz in Fig. 5. Results for the eight strips from donor #12 are presented. Differences in the shape and size of the loops obtained at different frequencies are minor and barely visible. Some visual differences are observed for the largest pre-stretch level. Overall, a modest influence of the frequency is observed in the dynamic response of the aortic strips, which confirm results known from the literature [13, 36]. In Fig. 5 it can also be observed that the shape and the stress values of the loops are relatively similar (in both directions) for the intact wall and the media, which is the thickest layer.

The dynamic stiffness ratios and the loss factors for the eight strips from donor #12 were identified for the three different pre-stretch levels. Results are presented in Figs. 6 and 7 versus the frequency (in Hz) of the imposed cyclic strain. As previously discussed, the effect of frequency is not very relevant in the studied range of 1 to 11 Hz. On the other side, it is very important to observe the significantly different curves obtained for the dynamic stiffness ratio for the three different pre-stretch levels, see Fig. 6. This indicates a complex nonlinear viscoelastic behavior of the aortic tissues that cannot be accurately modeled by using quasi-linear viscoelasticity [36, 37] or the nonlinear viscoelasticity with internal variables [37, 38] since both theories, in the present formulation, assume that the dynamic stiffness ratio and the loss factor are independent of the initial pre-stretch. In addition, while for the strip of the intact wall and for the media, both taken in the circumferential direction, the dynamic stiffness ratio increases with the pre-stretch, the opposite is observed for the strip of the adventitia taken in the same direction. A mixed behavior is observed for the intima in both directions. The effect of the pre-stretch in Fig. 6 is significant, but it is also different for each strip. It is suggested that this effect is related to the different

arrangements of the collagen and elastin fibers in the three layers, which also behave highly anisotropic, giving rise to different viscoelastic behavior of the circumferential and the longitudinal strips of the same layer. For the loss factor, in Fig. 7 it is observed that the effect of the initial pre-stretch is minor, somehow of the same order of magnitude of the influence of frequency.

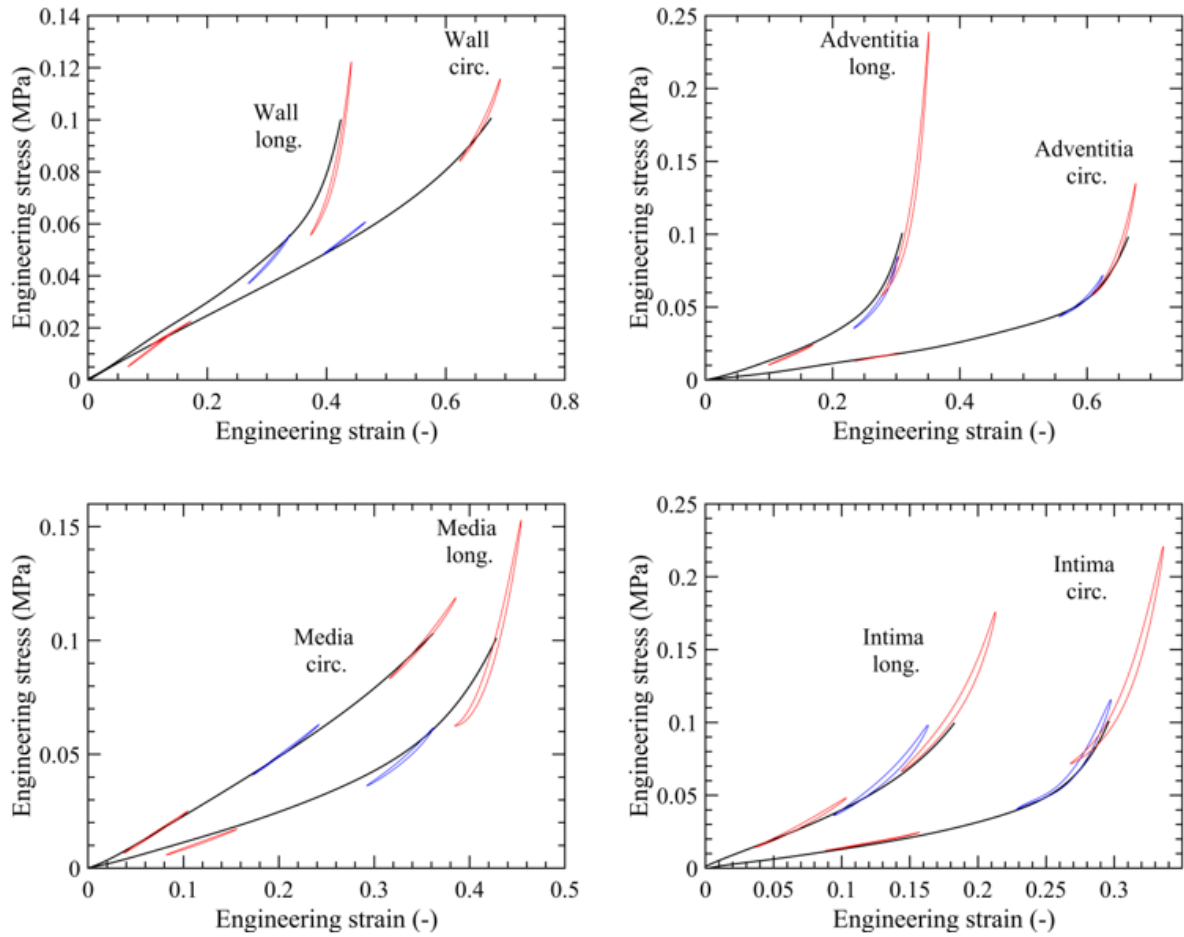
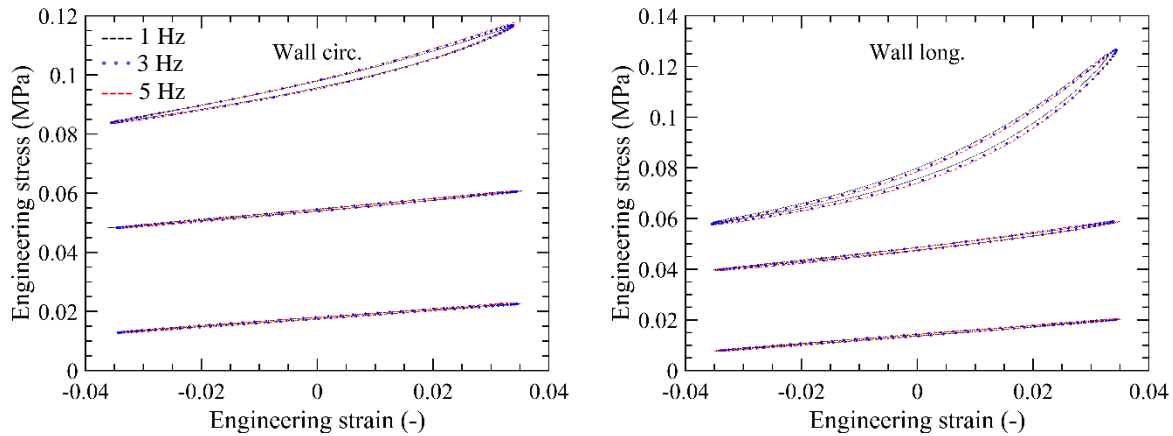


Figure 4 Hysteresis loops at 1 Hz (red or blue curves; blue for the closest to the physiological conditions) superimposed on the uniaxial tensile tests (black curves) of the circumferential and longitudinal strips from the intact wall, adventitia, media and intima from donor #12. Engineering stress (first Piola-Kirchhoff stress) versus engineering strain is given. Three cycles at different initial pre-stretch corresponding to about 12.5, 50, 100 kPa for the central point of the strain of each strip were measured. The amplitude of each cycle was about 0.07. The pre-stretch giving an engineering stress of about 50 kPa is a good reproduction of the physiological one (blue cycle).

### 3.1 Effect of the hysteresis loop amplitude

The effect of the amplitude of the hysteresis loops at 1 Hz, obtained for the circumferential strip from the intact wall and the longitudinal strip from the adventitia, both from donor #12, is shown in Fig. 8. Large loops have an amplitude of 0.07 engineering strain (7%, same as in Figs. 4-7); small loops have an amplitude of 0.005, i.e. 14 times smaller. The small loops in Fig. 8, where just two strips are shown for brevity, have a larger slope than the large loops. This is confirmed by the values of the dynamic stiffness ratio for all the strips from donor #12 reported in Table 2. For all 24 cases, the dynamic stiffness ratio is larger when small loops are considered instead of large (physiological) loops. The increase is comprised between 4 and 105% for this aorta. Table 3 presents the loss factors, which are all smaller for small cycles than for the corresponding large loops. The decrease of the loss factor for the small cycles with respect to the large (physiological) loops is comprised between 1 and 32%, showing a smaller influence of the cyclic strain amplitude on the loss factor with respect to what is observed for the dynamic stiffness ratio.



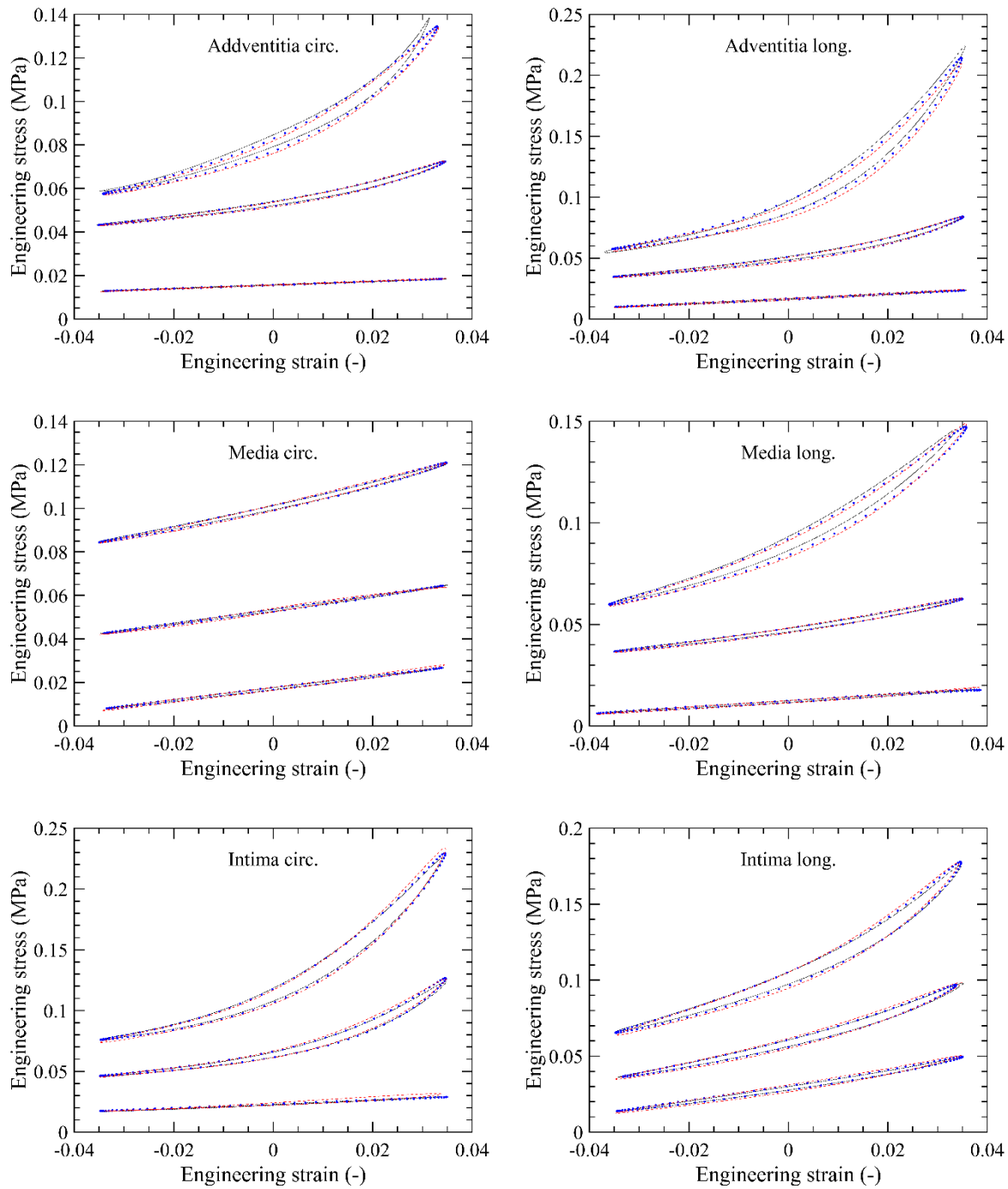
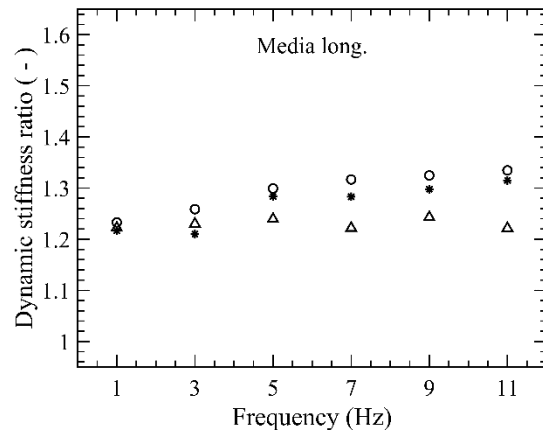
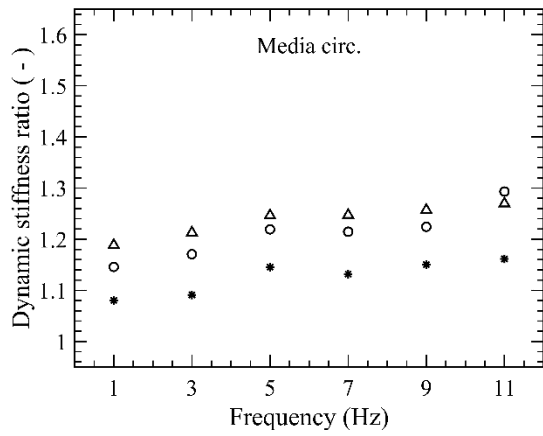
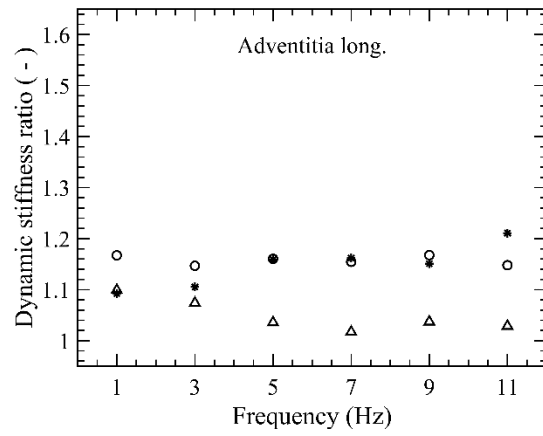
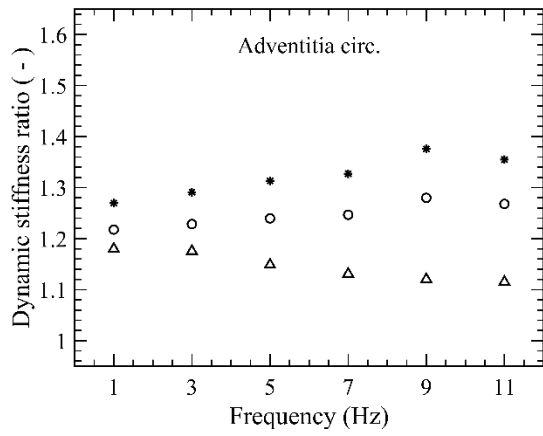
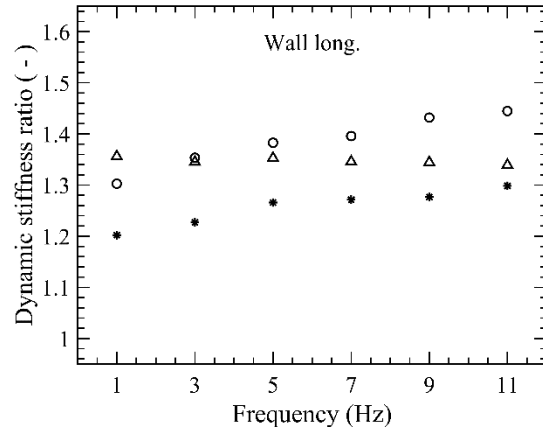
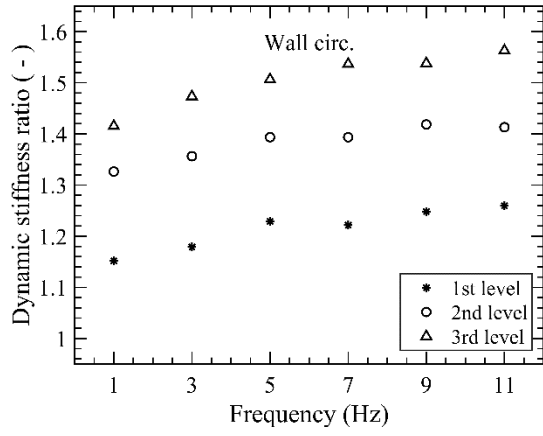


Figure 5 . Hysteresis loops at different frequency (black curve = 1 Hz, blue dots = 3 Hz, red dashes = 5 Hz) on the circumferential and longitudinal strips from the intact wall, adventitia, media and intima from donor #12. Engineering stress (first Piola-Kirchhoff stress) versus engineering strain (measured from the reference point of the loop) are given. The strain corresponding to the loop center was zeroed. Three cycles at different initial pre-stretch corresponding to about 12.5, 50, 100 kPa for the central point of the strain of each strip were measured. The amplitude of each cycle was about 0.07.



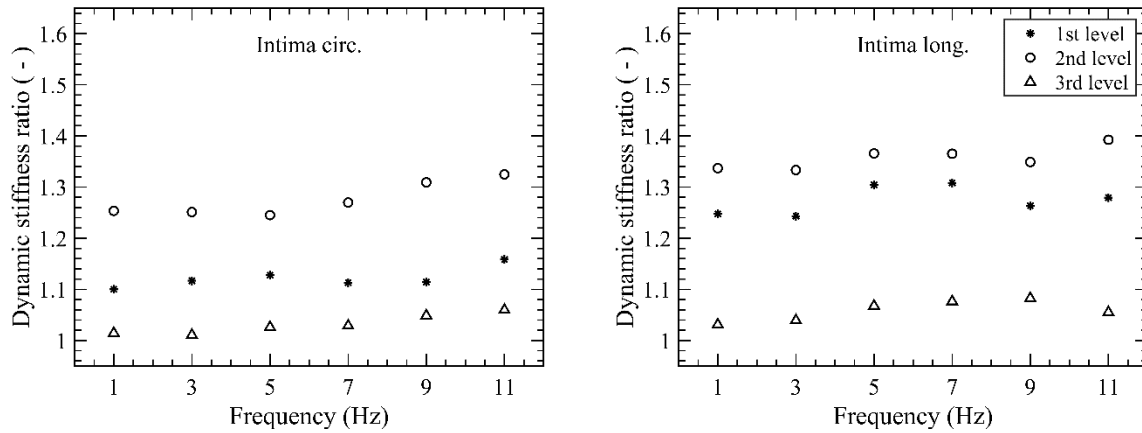
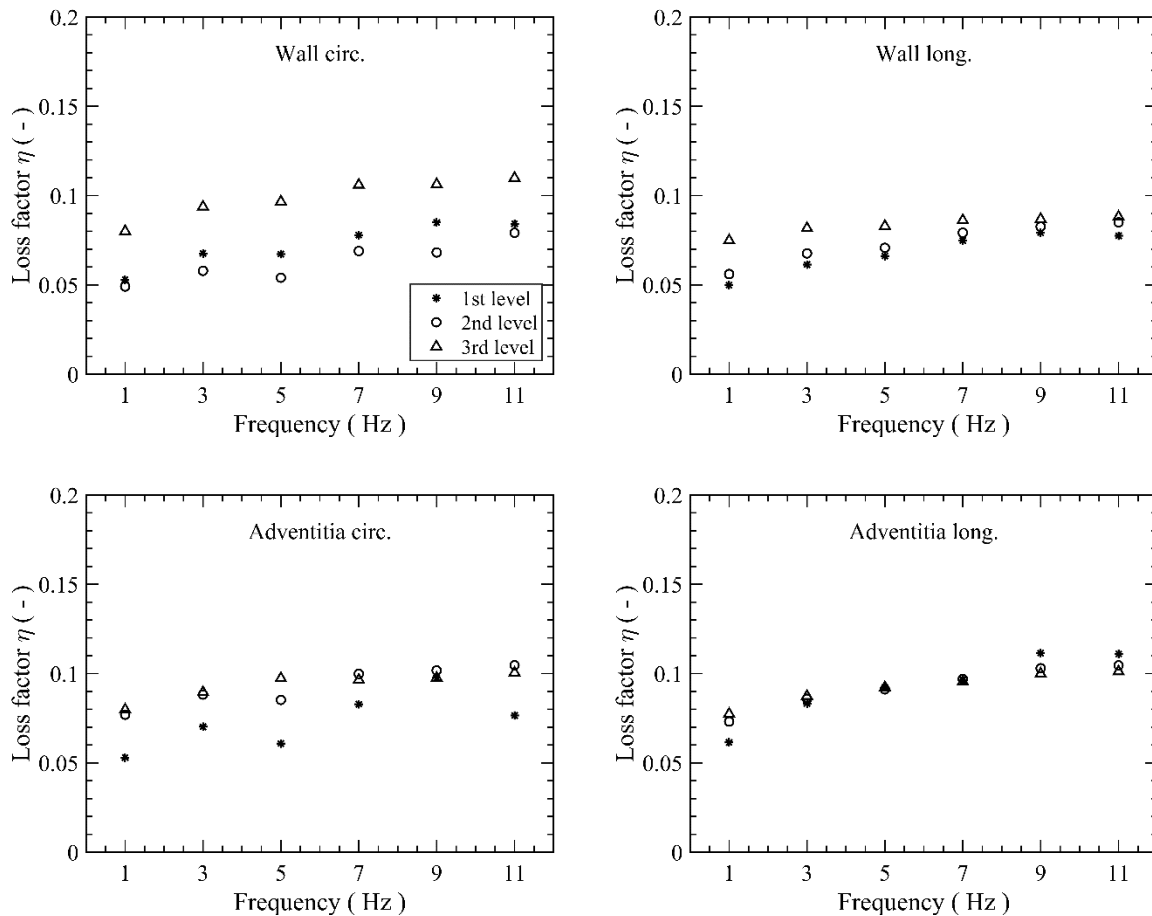


Figure 6. Dynamic stiffness ratio at three different initial stretches *versus* loading frequency (Hz) for the circumferential and longitudinal strips from the intact wall, adventitia, media and intima from donor #12. \* = first level, about 12.5 kPa (engineering stress); o = second level, about 50 kPa; Δ = third level, about 100 kPa.



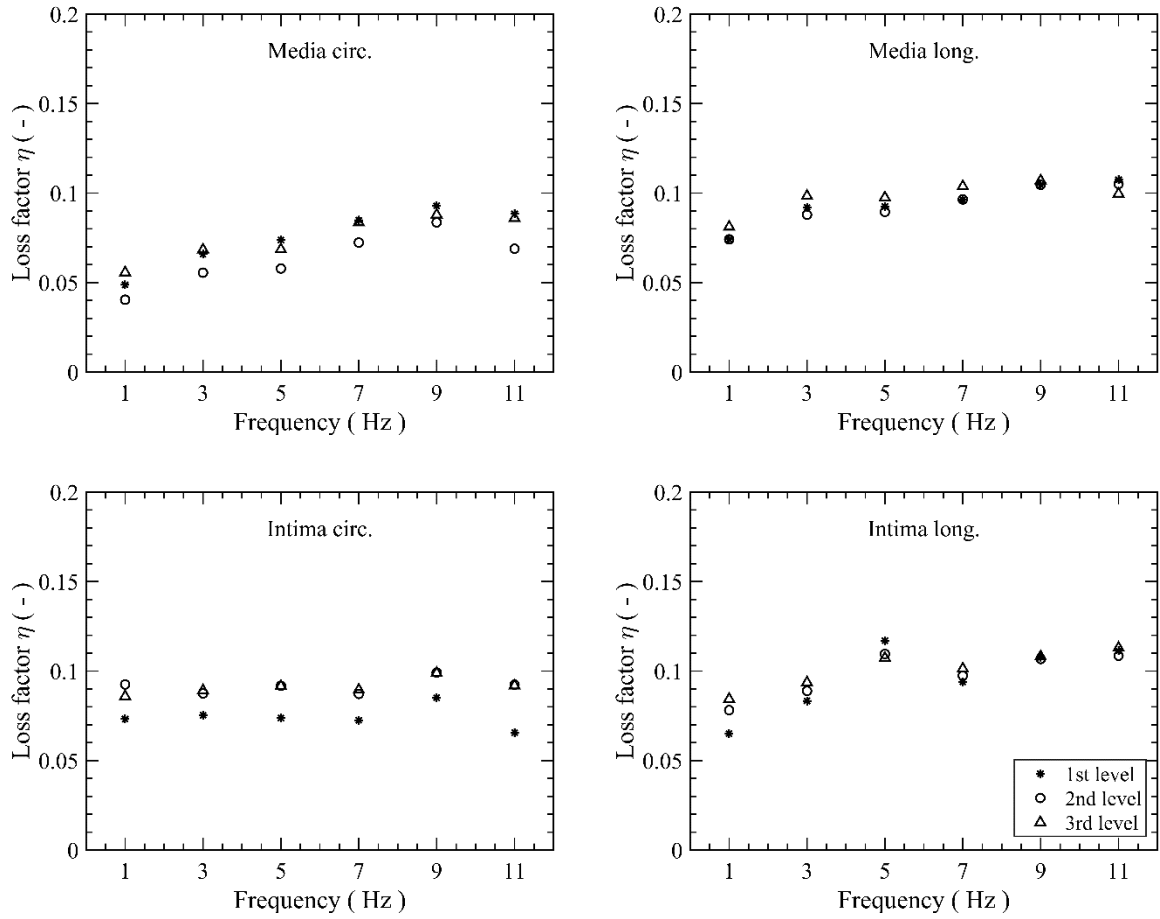


Figure 7. Loss factor  $\eta$  at three different initial stretches *versus* loading frequency (Hz) for the circumferential and longitudinal strips from the intact wall, adventitia, media and intima from donor #12. \* = first level, about 12.5 kPa (engineering stress); o = second level, about 50 kPa;  $\Delta$  = third level, about 100 kPa.

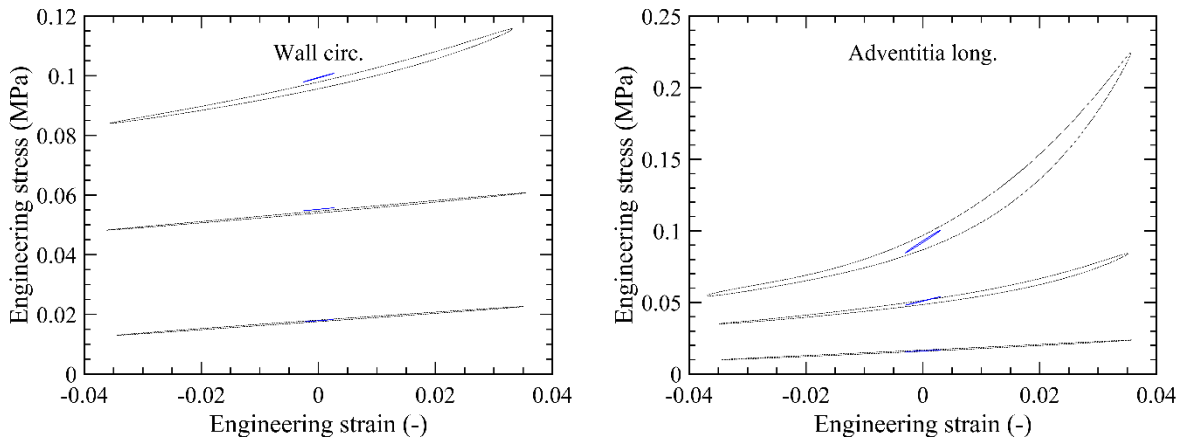


Figure 8. Hysteresis loops of two different amplitudes (large loops in black; small loops in blue) at 1 Hz on the circumferential strip from the intact wall and the longitudinal strip from adventitia, from donor #12; large loops, amplitude 0.07 engineering strain; small loops, amplitude 0.005. Engineering stress (first Piola-Kirchhoff stress) versus engineering strain (measured from the reference point of the loop) are given. Three cycles at different initial pre-stretch corresponding to about 12.5, 50, 100 kPa for the central point in strain of each strip were measured.

Table 2. Dynamic stiffness ratio at 1 Hz evaluated from the small loops and the physiological loops from the intact wall, adventitia, media and intima strips from donor #12. Three levels of pre-stretch were used: first (1<sup>st</sup>) level, about 12.5 kPa (engineering stress); second (2<sup>nd</sup>) level, about 50 kPa; third (3<sup>rd</sup>) level, about 100 kPa. The difference between each small loop and the corresponding physiological loop is computed with respect to the physiological loop.

Strip	Pre-stretch level	Small loop	Physiological loop	Difference (%)
Wall circ.	1 <sup>st</sup>	1.23	1.15	7
	2 <sup>nd</sup>	1.47	1.33	10
	3 <sup>rd</sup>	1.90	1.42	34
Wall long.	1 <sup>st</sup>	1.25	1.20	4
	2 <sup>nd</sup>	1.48	1.30	14
	3 <sup>rd</sup>	2.79	1.36	105
Adventitia circ.	1 <sup>st</sup>	1.35	1.27	6
	2 <sup>nd</sup>	1.60	1.21	32
	3 <sup>rd</sup>	1.63	1.18	38
Adventitia long.	1 <sup>st</sup>	1.27	1.09	16
	2 <sup>nd</sup>	2.08	1.17	78
	3 <sup>rd</sup>	1.80	1.18	53
Media circ.	1 <sup>st</sup>	1.13	1.08	5
	2 <sup>nd</sup>	1.28	1.15	11
	3 <sup>rd</sup>	1.40	1.19	18
Media long.	1 <sup>st</sup>	1.34	1.22	10
	2 <sup>nd</sup>	1.47	1.23	20
	3 <sup>rd</sup>	1.64	1.22	34
Intima circ.	1 <sup>st</sup>	1.58	1.10	44
	2 <sup>nd</sup>	1.63	1.25	30
	3 <sup>rd</sup>	1.44	1.01	43
Intima long.	1 <sup>st</sup>	1.39	1.25	11
	2 <sup>nd</sup>	1.75	1.34	31
	3 <sup>rd</sup>	1.89	1.03	83

### 3.2 Model fitting of experimental data

The hyperelastic model was used to fit the quasi-static uniaxial tensile tests on the strips from the three layers of the aorta from donor #12. The fitted material model of the adventitial layer versus the experimental data is shown in Fig. 9; the coefficient of determination  $R^2$  is 0.991 in this case, indicating that the model is capable to accurately fit the experimental data. The fitted parameters of the material model for the three layers are summarized in Table 4, together with the determination parameter  $R^2$ .

The fitted generalized Maxwell model with  $N_s = 3$  is presented in Fig. 10 together with the experimental data of the intact wall from donor #12. Dynamic stiffness ratio and loss factor for both strips in the circumferential and longitudinal direction are provided. The model fits better the experimental data for the circumferential strip than the axial strip, in this case. The largest pre-stretch turns out to be problematic to fit with high accuracy. The model parameters are summarized in Table 5 for the intact wall and the three layers from donor #12 in both directions.

### 3.3 Statistical analysis

Since it is impossible, for sake of brevity, to present data for all 15 aortas that were tested with the same depth of those shown for donor #12, statistical analyses of the most significant viscoelastic parameters that were identified from all the aortas, i.e. the dynamic stiffness ratio and the loss factor, are subsequently presented. The statistical methods are presented in Appendix A.4.

Table 3. Loss factor at 1 Hz evaluated from the small loops and the physiological loops from the intact wall, adventitia, media and intima strips from donor #12. Three levels of pre-stretch were used: first (1<sup>st</sup>) level, about 12.5 kPa (engineering stress); second (2<sup>nd</sup>) level, about 50 kPa; third (3<sup>rd</sup>) level, about 100 kPa. The difference between each small loop and the corresponding physiological loop is computed with respect to the physiological loop.

Strip	Pre-stretch level	Small loop	Physiological loop	Difference (%)
Wall circ.	1 <sup>st</sup>	0.0449	0.0529	-15
	2 <sup>nd</sup>	0.0399	0.0491	-19
	3 <sup>rd</sup>	0.0595	0.0800	-26
Wall long.	1 <sup>st</sup>	0.0416	0.0499	-17
	2 <sup>nd</sup>	0.0550	0.0561	-2
	3 <sup>rd</sup>	0.0538	0.0749	-28
Adventitia circ.	1 <sup>st</sup>	0.0410	0.0530	-23
	2 <sup>nd</sup>	0.0646	0.0770	-16
	3 <sup>rd</sup>	0.0571	0.0798	-28
Adventitia long.	1 <sup>st</sup>	0.0543	0.0615	-12
	2 <sup>nd</sup>	0.0675	0.0732	-8
	3 <sup>rd</sup>	0.0718	0.0775	-7
Media circ.	1 <sup>st</sup>	0.0402	0.0487	-17
	2 <sup>nd</sup>	0.0374	0.0404	-7
	3 <sup>rd</sup>	0.0380	0.0556	-32
Media long.	1 <sup>st</sup>	0.0718	0.0742	-3
	2 <sup>nd</sup>	0.0628	0.0741	-15
	3 <sup>rd</sup>	0.0653	0.0811	-19
Intima circ.	1 <sup>st</sup>	0.0535	0.0732	-27
	2 <sup>nd</sup>	0.0652	0.0925	-30
	3 <sup>rd</sup>	0.0683	0.0859	-20
Intima long.	1 <sup>st</sup>	0.0582	0.0650	-11
	2 <sup>nd</sup>	0.0695	0.0782	-11
	3 <sup>rd</sup>	0.0838	0.0844	-1

Table 4. Parameters of the hyperelastic model obtained by fitting the quasi-static uniaxial tensile tests of the three aortic layers and the intact wall from donor #12. The coefficient of determination  $R^2$  is also provided.

Layer	$\mu$ (kPa)	$\mu_1$ (kPa)	$\mu_2$	$\alpha$ (rad)	$K_{OP}$ (-)	$k_{IP}$ (-)	$R^2$ (-)
Intima	19.29	1708.00	2.05	1.063	0.370	0.340	0.968
Media	40.42	309.03	1.91	0.696	0.386	0.251	0.971
Adventitia	21.63	67.26	19.25	1.069	0.406	0.276	0.991
Wall	41.03	36.63	3.27	0.983	0.452	0.310	0.995

Table 5. Parameters of the generalized Maxwell model obtained by fitting the viscoelastic tests of the aortic strips from donor #12.

Strip	Pre-stretch level	$\beta_1^\infty$ (-)	$\beta_2^\infty$ (-)	$\beta_3^\infty$ (-)	$\tau_1$ (s)	$\tau_2$ (s)	$\tau_3$ (s)
Wall circ.	1 <sup>st</sup>	3.64	0.122	0.115	0.001	0.074	1916.0
	2 <sup>nd</sup>	0.27	0.124	0.269	0.005	0.078	926.0
	3 <sup>rd</sup>	0.35	0.229	0.336	0.006	0.072	509.0
Wall long.	1 <sup>st</sup>	1.65	0.129	0.161	0.001	0.064	66.7
	2 <sup>nd</sup>	0.94	0.155	0.267	0.001	0.070	685.3
	3 <sup>rd</sup>	0.78	0.141	0.242	0.002	0.114	1125.0
Adventitia circ.	1 <sup>st</sup>	2.22	0.136	0.217	0.001	0.069	1261.0
	2 <sup>nd</sup>	1.07	0.142	0.143	0.002	0.102	613.5
	3 <sup>rd</sup>	0.92	0.110	0.039	0.002	0.153	339.4
Adventitia long.	1 <sup>st</sup>	1.51	0.106	0.055	0.001	0.074	764.8
	2 <sup>nd</sup>	5.43	0.101	0.082	0.001	0.133	671.9
	3 <sup>rd</sup>	4.50	0.127	0.003	0.001	0.239	415.5
Media circ.	1 <sup>st</sup>	6.69	0.124	0.055	0.001	0.047	3422.0
	2 <sup>nd</sup>	0.18	0.068	0.131	0.011	0.088	286.1
	3 <sup>rd</sup>	0.37	0.124	0.146	0.004	0.078	865.3
Media long.	1 <sup>st</sup>	0.22	0.216	0.151	0.049	0.004	3692.0
	2 <sup>nd</sup>	0.23	0.142	0.164	0.010	0.095	901.1
	3 <sup>rd</sup>	2.61	0.142	0.126	0.001	0.108	1056.0
Intima circ.	1 <sup>st</sup>	0.79	0.106	0.036	0.002	0.118	1168.0
	2 <sup>nd</sup>	2.01	0.160	0.144	0.001	0.119	345.5
	3 <sup>rd</sup>	1.05	0.136	0.001	0.003	0.056	1660.0
Intima long.	1 <sup>st</sup>	2.18	0.141	0.177	0.001	0.066	2116.0
	2 <sup>nd</sup>	0.41	0.129	0.226	0.007	0.121	2095.0
	3 <sup>rd</sup>	0.55	0.064	0.011	0.003	0.070	749.9

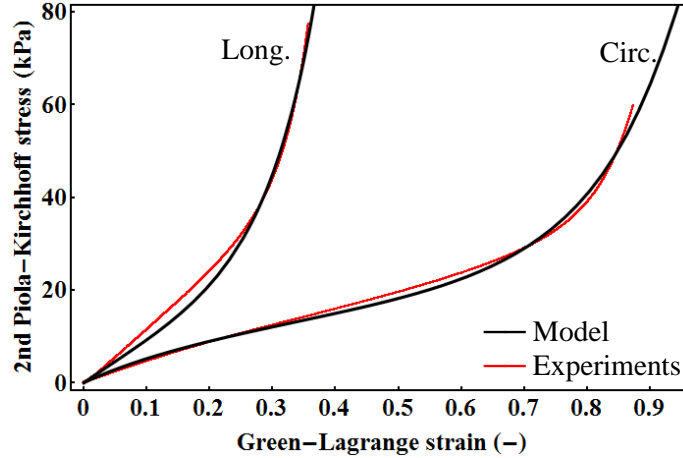


Figure 9. Fitted material model (black curve) of the adventitial layer versus experimental data (red curve) of uniaxial tensile tests on circumferential and longitudinal strips from donor #12. Second Piola-Kirchhoff stress versus Green-Lagrange strain is given. The experiments have an engineering stress of up to 100 kPa, which gives different values when converted into the second Piola-Kirchhoff stress.

Only large (physiological) loops are considered. The samples from donor #4, which were tested for age-related reasons with reduced cyclic strain (3 %), are also included in the statistical analyses. Figure 11 shows the statistical analysis of the dynamic stiffness ratio and loss factor for the circumferential and longitudinal strips from the intact wall, adventitia, media and intima from all 15 donors at 1 Hz and at a pre-stretch corresponding to 50 kPa (engineering stress), which is the closest to the physiological condition. In both directions the intact wall presents the largest values of the dynamic stiffness ratio. Figure 11(a) shows that the dynamic stiffness ratio of the entire wall cannot be obtained as the weighted average of the responses of the constitutive layers because it is the largest value than any other layer even if differences are not large. This can be justified by the fact that the entire wall has interfaces between layers of significantly different stiffness, which can create a localized viscoelastic effect, and also has residual stresses released when the layers are separated. Therefore, a viscoelastic model of the entire wall should take into account the hyperelastic and viscoelastic characteristics of each layer, which are provided in the present study, as well as the layer-specific residual stresses. The median of the dynamic stiffness ratios varies between 1.14 and 1.33 for the different layers and the intact wall. All values from different strips are comprised between 1 and 2, largely reducing the data dispersion observed in Amabili et al. [13,

34] where cycles of small amplitude were used. This shows that the use of large cycles of the physiological amplitude is the preferred method to identify the viscoelastic properties of the aortic tissue. The median of the loss factors varies between 0.050 and 0.066 for the different layers and the intact wall. Therefore, values are quite close to each other. The smaller medians are observed for the media in both directions. The one-way ANOVA test ran on the four groups of loss factor values (three layers and intact wall) indicates that there is statistical difference between the groups (the p-value associated to no difference is  $5.7 \times 10^{-7}$ ). The post-hoc Dunnett test performed taking the group of loss factors of the media as control indicates that the media loss factors sample is different from all the other three groups. All values from the different strips are comprised between 0.03 and 0.09.

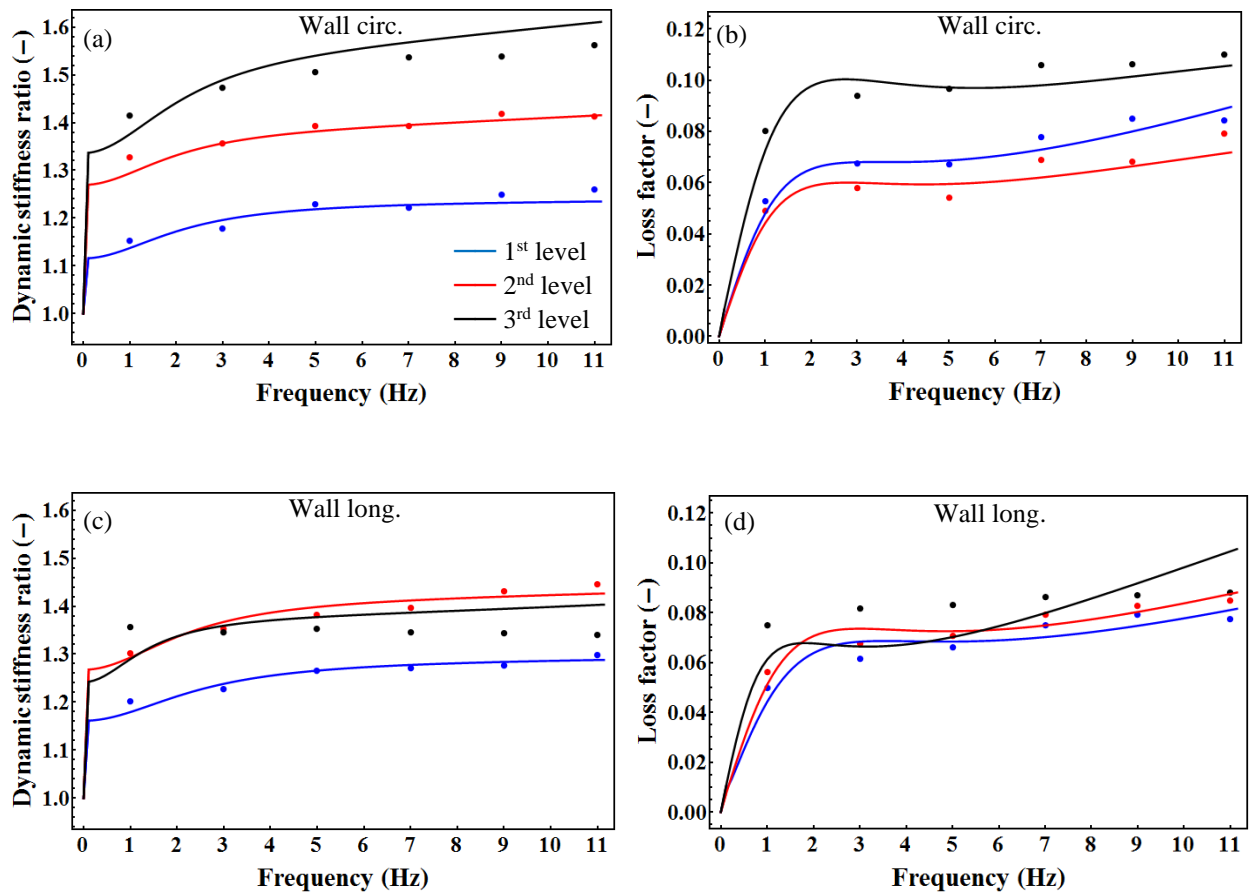


Figure 10. Results of the fitting using the generalized Maxwell model ( $N_s = 3$ ) for the dynamic stiffness ratio and the loss factor at three different initial pre-stretches for the wall from donor #12 *versus* the loading frequency (Hz). Experimental data: ● = first level, about 12.5 kPa (engineering

stress); ● = second level, about 50 kPa; ● = third level, about 100 kPa. Material model: — = first level, about 12.5 kPa; — = second level, about 50 kPa; — = third level, about 100 kPa: (a) dynamic stiffness ratio for the circumferential wall; (b) loss factor for the circumferential wall; (c) dynamic stiffness ratio for the longitudinal wall; (d) loss factor for the longitudinal wall.

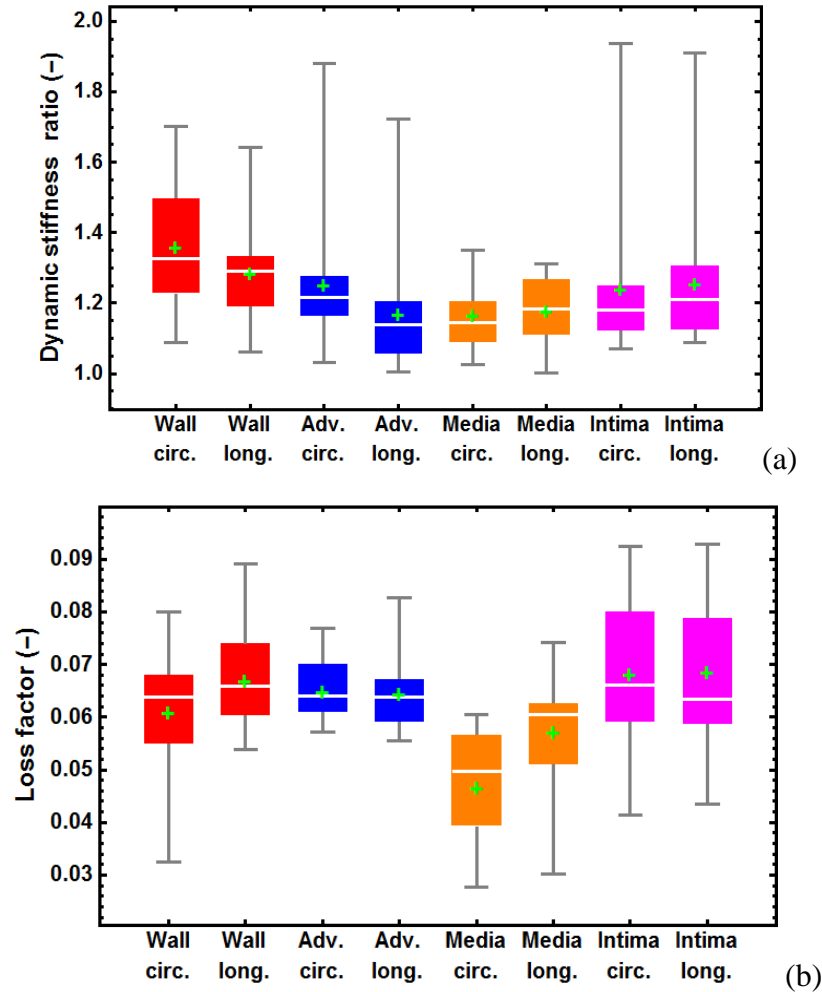


Figure 11. Statistical analysis of the dynamic stiffness ratio and the loss factor for the circumferential and longitudinal strips from the intact wall, adventitia, media and intima from all 15 donors at a pre-stretch corresponding to 50 kPa (engineering stress); maximum, minimum, first quartile, third quartile, median (white horizontal line in the box) and average (+) are reported: (a) dynamic stiffness ratio at 1 Hz loading frequency; (b) loss factor at 1 Hz loading frequency.

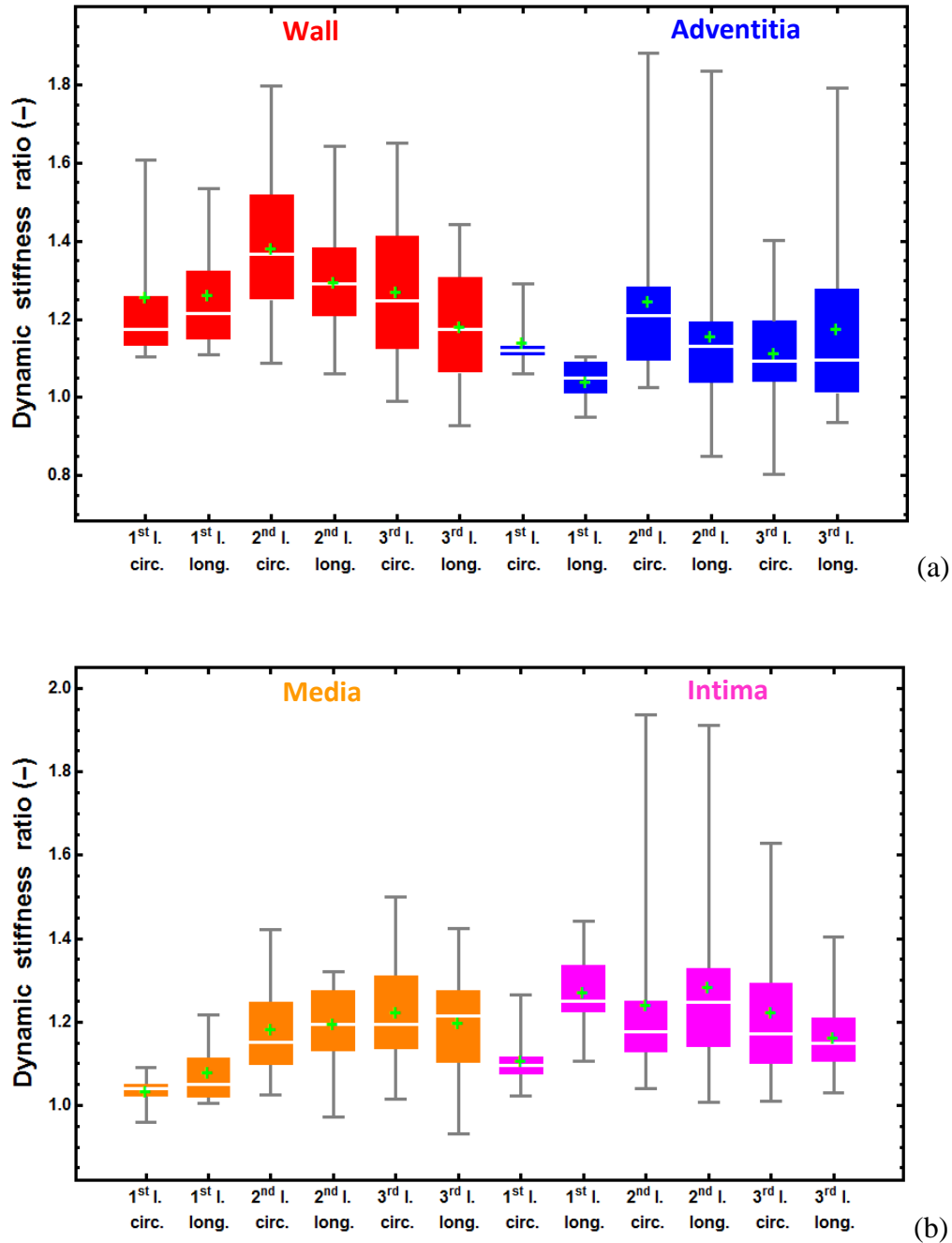


Figure 12. Statistical analysis of the dynamic stiffness ratio at 1 and 3 Hz (combined) for the circumferential and longitudinal strips from the intact wall, adventitia, media and intima from all 15 donors at three pre-stretch levels (1<sup>st</sup> level, about 12.5 kPa; 2<sup>nd</sup> level, about 50 kPa; 3<sup>rd</sup> level, about 100 kPa – engineering stress); maximum, minimum, 1<sup>st</sup> quartile, 3<sup>rd</sup> quartile, median (white horizontal line in the box) and average (+) are reported: (a) intact wall and adventitia; (b) media and intima.

The statistical analysis of the dynamic stiffness ratio at 1 and 3 Hz (combined together, since those are the physiological frequencies corresponding to 60 to 180 heart beats per minute) for the circumferential and longitudinal strips from the intact wall, adventitia, media and intima from all 15 donors at the three pre-stretch levels is shown in Fig. 12. A significant increase of the dynamic stiffness ratio can be observed between the median values obtained at the first pre-stretch level and those identified at the second level for all strips, except for the circumferential intima, which is almost unchanged. The first pre-stretch level is modest and barely involve collagen fibers, which are initially crimped. On the other hand, the second pre-stretch level is associated with a significant contribution of collagen fibers. This seems to be the reason for a significant increase of the dynamic stiffening of the tissue, and it could be attributed to an intrinsic difference in viscoelasticity of the elastin and collagen fibers. However, recent studies are starting to highlight the possible mechanism of kinematic contribution to viscoelasticity of interwind networks of elastin and collagen fibers [42]. Differences between the second and the third pre-stretch level are smaller, except for the intact wall, and often show a decrease of the values. The reduction of the dynamic stiffness ratio observed for the third pre-stretch level is possibly associated to the large increase in the size of the hysteresis loop due to the large slope of the stress-strain curve around 100 kPa. The intact wall, in both directions, presents the largest values of the dynamic stiffness ratio than any of the three individual layers. In particular, the median of the intact wall in the circumferential direction varies from 1.17 for the first pre-stretch level to 1.37 for the second level; the median of the longitudinal direction changes from 1.21 at the first level to 1.29 at the second level.

Figure 13 is analogous to Fig. 12 but presents the loss factors instead of the dynamic stiffness ratios. Except for a single case (intima in the circumferential direction for the first pre-stretch level), the results indicate an increase of the loss factor with pre-stretch within the same layer in both directions. The intact wall and the three layers have also similar values for the same pre-stretch.

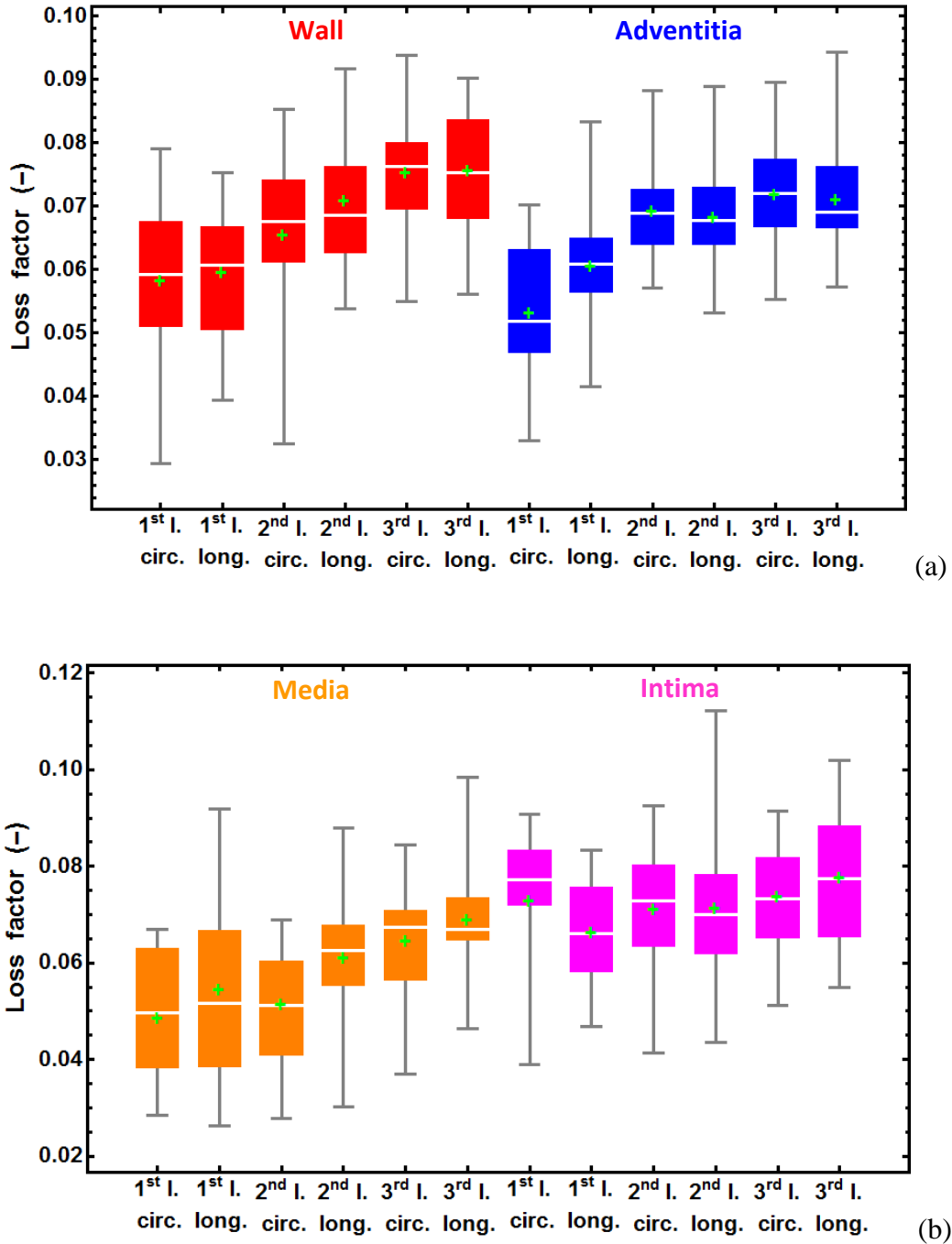


Figure 13. Statistical analysis of the loss factor at 1 and 3 Hz (combined) for the circumferential and longitudinal strips from the intact wall, adventitia, media and intima from all 15 donors at three pre-stretch levels (1<sup>st</sup> level, about 12.5 kPa; 2<sup>nd</sup> level, about 50 kPa; 3<sup>rd</sup> level, about 100 kPa – engineering stress); maximum, minimum, 1<sup>st</sup> quartile, 3<sup>rd</sup> quartile, median (white horizontal line in the box) and average (+) are reported: (a) intact wall and adventitia; (b) media and intima.

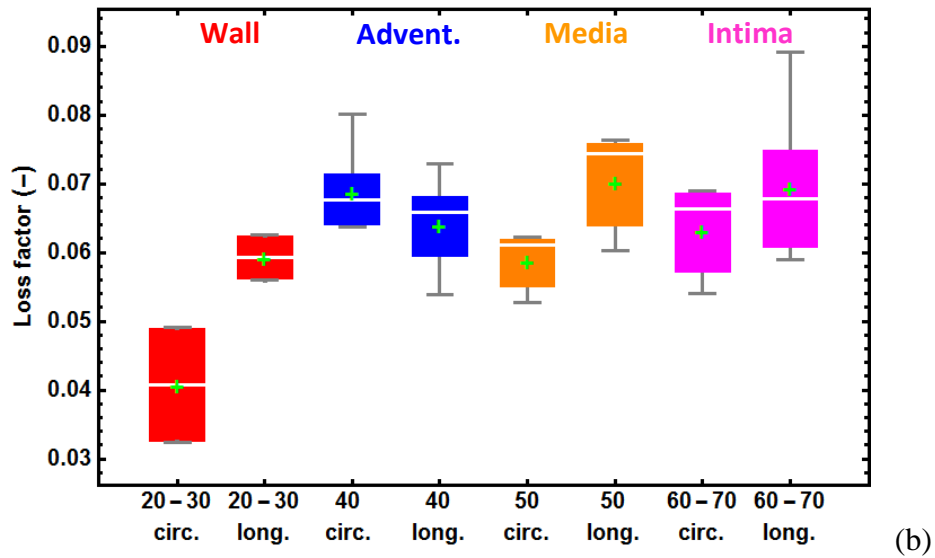
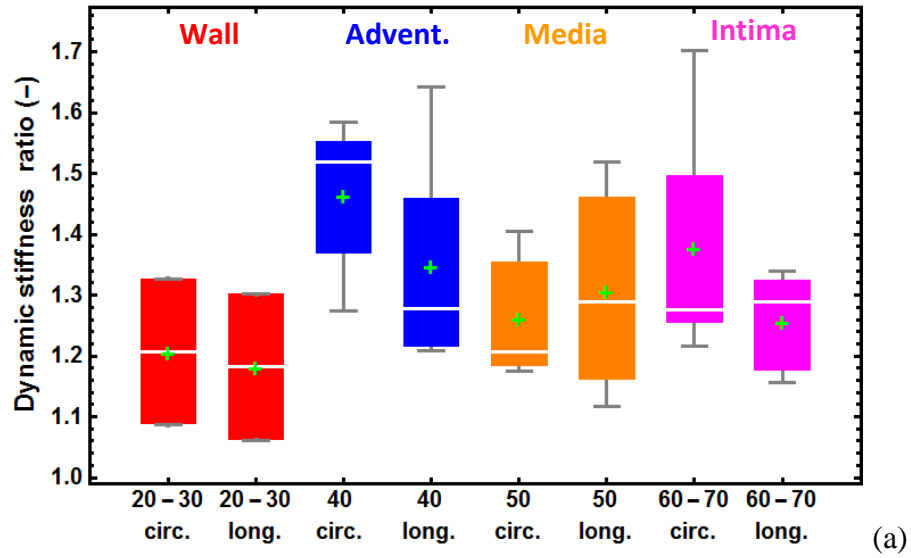


Figure 14. Statistical analysis of the dynamic stiffness ratio and the loss factor for the circumferential and longitudinal strips from the intact wall from all 15 donors divided in four age groups at a pre-stretch corresponding to 50 kPa (engineering stress); maximum, minimum, 1<sup>st</sup> quartile, 3<sup>rd</sup> quartile, median (white horizontal line in the box) and average (+) are reported. Age groups: 20-30 years, 2 donors; 40 years, 5 donors; 50 years, 3 donors; 60-70 years, 5 donors: (a) dynamic stiffness ratio at 1 Hz loading frequency; (b) loss factor at 1 Hz loading frequency.

The effect of age on the dynamic stiffness ratio and the loss factor is summarized in Fig. 14. Data are presented for the circumferential and longitudinal strips from the intact wall from all 15 donors, divided in 4 age groups at pre-stretch corresponding to 50 kPa (engineering stress), and 1 Hz. The age groups are: 20-30 years, 2 donors; 40 years, 5 donors; 50 years, 3 donors; 60-70 years, 5 donors. Both the dynamic stiffness ratio and the loss factor are smaller for the youngest age group (20-30 years), while no significant difference is observed among the other age groups. In particular, a statistical comparison of the 20-30 year group for both strips and all the other groups together was carried out by a Kruskal-Wallis test due to the very different size of the two groups (4 strips versus 26); p-values of 0.1643 (dynamic stiffness ratio) and 0.014 (loss factor) were calculated, confirming that these two groups of data, at least for the loss factor, are likely to be statistically different.

#### **4. Conclusions**

The identification of the viscoelastic properties of the intact aortic wall and the individual layers of 15 human descending thoracic aortas was carried out by using harmonic cyclic loads of physiological amplitudes. The dynamic stiffness ratio and the loss factors were obtained from the hysteresis loops. Tensile tests were uniaxial which is a limitation but, being simple, allows precise control of the parameters in dynamic tests. The most significant results of the experimental study show: (i) a significant effect of the pre-stretch on the dynamic stiffness ratio, while the pre-stretch has a smaller effect on the loss factor; (ii) the largest values of the dynamic stiffness ratio were obtained for the second pre-stretch level, which is the closest one to the physiological conditions (about 50 kPa of engineering stress); (iii) a large effect of the amplitude of the cyclic load on the viscoelastic parameters; (vi) a small effect of the loading frequency on the viscoelasticity within the range of 1 and 11 Hz; (v) the age group of 20 to 30 years presents the smallest values of the dynamic stiffness ratio and loss factor than any other age group. This study shows limits of the present viscoelastic models of soft biological tissues and paves the way to future refined nonlinear modeling by providing data that were never obtained before.

## Appendix

### A.1 Experimental setup

Figure A1 shows the experimental setup used in the experiments. The time sequence of the quasi-static and dynamic tests on one adventitial strip from donor #11 is shown in Fig. A2.

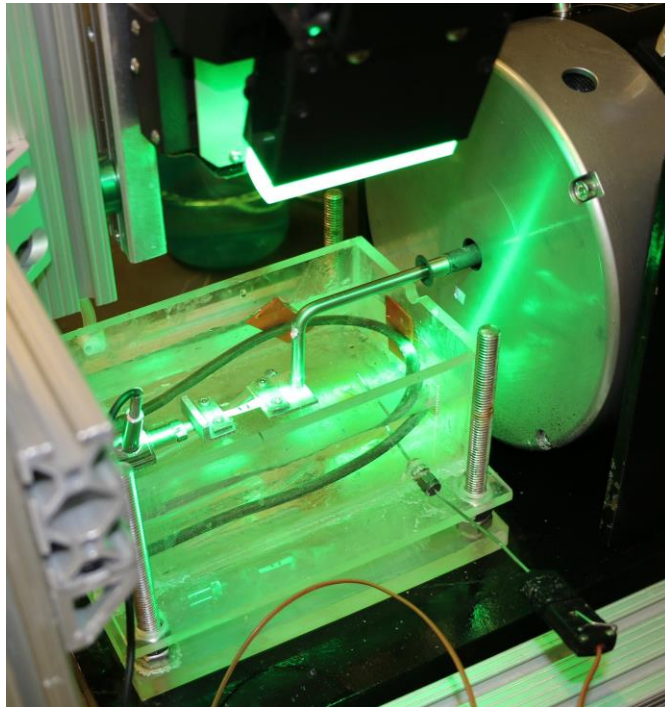


Figure A1. Experimental setup with the thermally controlled bath, the video extensometer that generates the green light for the alignment, the electrodynamic actuator from Bruel&Kjaer, the load cell and the handles that hold the aortic tissue.

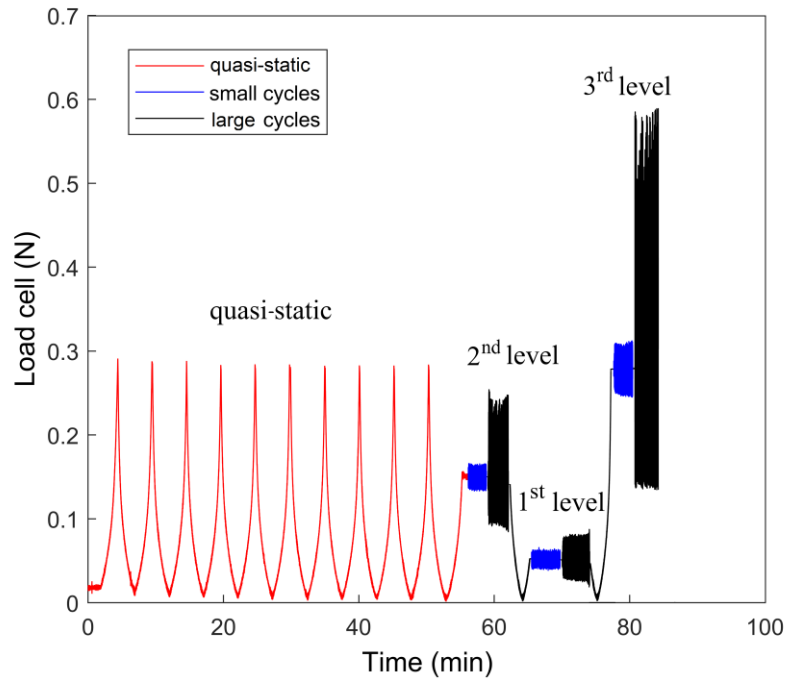


Figure A2. Scheme representing the time sequence of the quasi-static and dynamic tests on each strip.

## A.2 Hyperelastic constitutive model

Each aortic layer is assumed to be composed by an isotropic ground substance and two families of collagen fibers which are aligned symmetrically with respect to the circumferential direction of the aorta. The hyperelastic constitutive model considered in the present study was introduced by Holzapfel et al. [21] and is described by the following strain-energy function

$$W = \frac{\mu}{2}(I_1 - 3) + \frac{\mu_1}{2\mu_2} \left\{ \exp[\mu_2 E_4^2] + \exp[\mu_2 E_6^2] - 2 \right\}, \quad (\text{A1})$$

where the first term describes the response of the non-collagenous ground substance, which is modeled as a neo-Hookean material, and the second term accounts for the response of the collagen fibers. In equation (A1),  $I_1$  is the first invariant of the right Cauchy-Green tensor  $\mathbf{C}$ ,  $\mu$  is a dimensional material parameter (analogous to the shear modulus for a linearly elastic material),  $\mu_1$  is a second dimensional material parameter, while the parameter  $\mu_2$  is non-dimensional. In addition,

$$E_4 = 2\kappa_{OP}\kappa_{IP}I_1 + 2\kappa_{OP}(1 - 2\kappa_{IP})I_4 + (1 - 2\kappa_{OP}(\kappa_{IP} + 1))I_n - 1, \quad (\text{A2a})$$

$$E_6 = 2\kappa_{OP}\kappa_{IP}I_1 + 2\kappa_{OP}(1 - 2\kappa_{IP})I_6 + (1 - 2\kappa_{OP}(\kappa_{IP} + 1))I_n - 1, \quad (\text{A2b})$$

where  $I_4$  and  $I_6$  are pseudo-invariants, as characterized below, and  $I_n$  is a pseudo-invariant equal to the square of the stretch in the direction normal to the middle surface of the aorta. The out-of-plane dispersion parameter  $\kappa_{OP}$  varies from 0 (all fibers are orthogonal to the middle surface of the aorta) to 0.5 (all fibers are parallel to the middle surface), with  $\kappa_{OP} = 1/3$  corresponding to the isotropic out-of-plane fiber distribution; for human aortas  $0.33 < \kappa_{OP} < 0.5$ . The in-plane dispersion parameter  $\kappa_{IP}$  has a value  $\kappa_{IP} = 0$  for perfectly aligned fibers and  $\kappa_{IP} = 0.5$  in the case of in-plane isotropy; in general,  $0 \leq \kappa_{IP} \leq 0.5$ . The cylindrical coordinates  $x, \theta, z$  are considered for the aorta, being the longitudinal, circumferential and radial coordinate, respectively. Two relevant invariants of the right Cauchy-Green deformation tensor are [37]:

$$I_1 = 2(\varepsilon_{xx} + \varepsilon_{\theta\theta} + \varepsilon_{zz}) + 3, \quad (\text{A3a})$$

$$I_3 = (2\varepsilon_{xx} + 1)(2\varepsilon_{\theta\theta} + 1)(2\varepsilon_{zz} + 1) - (2\varepsilon_{xx} + 1)\gamma_{\theta z}^2 - (2\varepsilon_{\theta\theta} + 1)\gamma_{xz}^2 - (2\varepsilon_{zz} + 1)\gamma_{x\theta}^2 + 2\gamma_{x\theta}\gamma_{xz}\gamma_{\theta z}, \quad (\text{A3b})$$

where  $\varepsilon$  and  $\gamma$  are the normal and shear Green-Lagrange strains;  $I_3$  indicates the volume change during the deformation. Since soft biological tissues can be considered as incompressible,  $I_3 = 1$ .

By using equation (A3b), the incompressibility condition  $I_3 = 1$  yields [37]

$$\varepsilon_{zz} = \frac{\gamma_{x\theta}^2 + \gamma_{xz}^2 + \gamma_{\theta z}^2 - 2(\varepsilon_{xx} + \varepsilon_{\theta\theta}) - 4\varepsilon_{xx}\varepsilon_{\theta\theta} + 2\varepsilon_{xx}\gamma_{\theta z}^2 + 2\varepsilon_{\theta\theta}\gamma_{xz}^2 - 2\gamma_{xz}\gamma_{xz}\gamma_{\theta z}}{2((2\varepsilon_{xx} + 1)(2\varepsilon_{\theta\theta} + 1) - \gamma_{x\theta}^2)}. \quad (\text{A4})$$

The mean directions of the two families of fibers form the angles  $\alpha_1$  and  $\alpha_2$  with the circumferential direction measured on a plane tangent to the middle surface of the aortic layer. For the assumed symmetry of the fiber families,  $\alpha_2 = -\alpha_1$ . The pseudo-invariants  $I_4, I_6, I_n$  of the right Cauchy-Green deformation tensor take on the following expressions [37]:

$$I_4 = 1 + 2(\varepsilon_{xx} \sin^2 \alpha_1 + \varepsilon_{\theta\theta} \cos^2 \alpha_1 + \gamma_{x\theta} \sin \alpha_1 \cos \alpha_1), \quad (\text{A5a})$$

$$I_6 = 1 + 2(\varepsilon_{xx} \sin^2 \alpha_2 + \varepsilon_{\theta\theta} \cos^2 \alpha_2 + \gamma_{x\theta} \sin \alpha_2 \cos \alpha_2), \quad (\text{A5b})$$

$$I_n = 2\varepsilon_{zz} + 1. \quad (\text{A5c})$$

The pseudo-invariants in equations (A5a)-(A5c) give the squares of the stretches in the three directions: two directions laying on the middle surface and forming the angles  $\alpha_1$  and  $\alpha_2$  with the circumferential direction, and in the direction normal to the middle surface. The effect of the exclusion of the compressed fibers in the identification of material parameters from uniaxial tensile tests on two orthogonal strips is introduced as in [22]. The six unknown parameters  $\mu, \mu_1, \mu_2, \kappa_{IP}, \kappa_{OP}$  and  $\alpha_1$  are identified from the data obtained from quasi-static uniaxial tensile tests by using a custom-built optimization code based on a genetic algorithm [13, 22]. The first three parameters ( $\mu, \mu_1, \mu_2$ ) are mechanical, obtained from mechanical tests, and the last three parameters ( $\kappa_{IP}, \kappa_{OP}, \alpha_1$ ) are micro-structural and can be obtained by analyzing images from microscopy. In the present study, all six parameters are used as phenomenological fitting parameters. Details on the fitting procedure and algorithms are given in [13, 22].

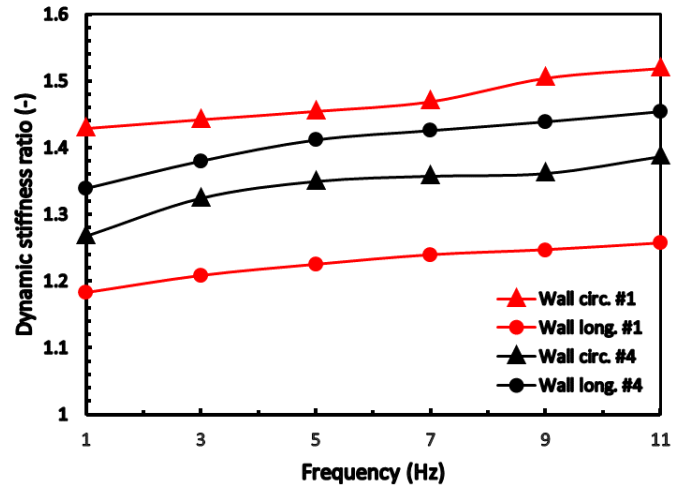


Figure A3. Dynamic stiffness ratio versus frequency for the intact wall of the two oldest donors (#1 and #4) at a pre-stretch corresponding to 50 kPa (engineering stress).

### **A.3 Additional results**

The dynamic stiffness ratio versus frequency for the intact wall of the two oldest donors (#1 and #4) is shown in Fig. A3. It confirms that the influence of frequency on dynamic stiffness is moderate even in the oldest samples.

### **A.4 Statistical methods**

The 0.05 level of significance was selected in the statistical analysis. Because of the large difference in the size of samples representing age groups, to test if the properties of aortas from young and old donors are statistically different, the Kruskal-Wallis test was applied. The ANOVA F-test was performed to check if the medians of loss-factor distributions of different layers and the intact wall were statistically different. As a post-hoc test for ANOVA, the Dunnett test was chosen since it does not require the homogeneity of variances.

### **Acknowledgments**

The authors acknowledge the financial support of the NSERC Discovery Grant and NSERC RTI grant (PI Amabili). Prabakaran Balasubramanian, Giovanni Ferrari and Francesco Giovanniello assisted with experimentation. Ali Kassab prepared the aorta samples that were provided by Transplant Québec.

### **Credit Author Statement**

**G. Franchini:** Visualization, Data curation, Investigation, Software, Formal analysis, Writing - Review & Editing. **I. Breslavsky:** Visualization, Data curation, Software, Formal analysis, Writing - Review & Editing. **G.A. Holzapfel:** Methodology, Writing - Review & Editing. **M. Amabili:** Conceptualization, Methodology, Data curation, Writing - Original Draft, Writing - Review & Editing, Project administration, Supervision.

### **References**

1. Y.C. Fung, *Biomechanics: Circulation*, second ed., Springer, New York, 1997.
2. T.M. Morrison, G. Choi, C.K. Zarins, C.A. Taylor, Circumferential and longitudinal cyclic strain of the human thoracic aorta: age-related changes, *J. Vasc. Surg.* 49 (2009) 1029-1036, doi:10.1016/j.jvs.2008.11.056.

3. M. Amabili, P. Balasubramanian, I. Bozzo, I.D. Breslavsky, G. Ferrari, G. Franchini, F. Giovanniello, C. Pogue, Nonlinear dynamics of human aortas for material characterization, *Phys. Rev. X*, 10 (2020) 011015, doi: 10.1103/PhysRevX.10.011015.
4. M. Amabili, P. Balasubramanian, I.D. Breslavsky, G. Ferrari, E. Tubaldi, Viscoelastic characterization of woven Dacron for aortic grafts by using direction-dependent quasi-linear viscoelasticity, *J. Mech. Behav. Biomed. Mater.* 82 (2018) 282-290, doi:10.1016/j.jmbbm.2018.03.038.
5. G. Ferrari, P. Balasubramanian, E. Tubaldi, F. Giovanniello, M. Amabili, Experiments on dynamic behaviour of a Dacron aortic graft in a mock circulatory loop, *J. Biomech.* 86 (2019) 132-140, doi:10.1016/j.jbiomech.2019.01.053.
6. M. Amabili, P. Balasubramanian, G. Ferrari, G. Franchini, F. Giovanniello, E. Tubaldi, Identification of viscoelastic properties of Dacron aortic grafts subjected to physiological pulsatile flow, *J. Mech. Behav. Biomed. Mater.* 110 (2020) 103804, doi: 10.1016/j.jmbbm.2020.103804.
7. J.D. Humphrey, *Cardiovascular Solid Mechanics. Cells, Tissues, and Organs*, Springer-Verlag, New York, 2002.
8. H. Weisbecker, D.M. Pierce, P. Regitnig, G.A. Holzapfel, Layer-specific damage experiments and modeling of human thoracic and abdominal aortas with non-atherosclerotic intimal thickening, *J. Mech. Behav. Biomed. Mater.* 12 (2012) 93-106, doi:10.1016/j.jmbbm.2012.03.012.
9. M.R. Labrosse, E.R. Gerson, J.P. Veinot, C.J. Beller, Mechanical characterization of human aortas from pressurization testing and a paradigm shift for circumferential residual stress, *J. Mech. Behav. Biomed. Mater.* 17 (2013) 44-55, doi:10.1016/j.jmbbm.2012.08.004.
10. S.G. Sassani, J. Kakisis, S. Tsangaris, D.P. Sokolis, Layer-dependent wall properties of abdominal aortic aneurysms: Experimental study and material characterization. *J. Mech. Behav. Biomed. Mater.* 49 (2015) 141-161, doi:10.1016/j.jmbbm.2015.04.027.
11. S.G. Sassani, S. Tsangaris, D.P. Sokolis, Layer- and region-specific material characterization of ascending thoracic aortic aneurysms by microstructure-based models, *J. Biomech.* 48 (2015) 3757-3765, doi: 10.1016/j.jbiomech.2015.08.028.
12. J.A. Niestrawska, C. Viertler, P. Regitnig, T.U. Cohnert, G. Sommer, G.A. Holzapfel, Microstructure and mechanics of healthy and aneurysmatic abdominal aortas: experimental analysis and modelling, *J. R. Soc. Interface*, 13 (2016) 20160620, doi: 10.1098/rsif.2016.0620.
13. M. Amabili, P. Balasubramanian, I. Bozzo, I.D. Breslavsky, G. Ferrari, Layer-specific hyperelastic and viscoelastic characterization of human descending thoracic aortas, *J. Mech. Behav. Biomed. Mater.* 99 (2019) 27-46, doi: 10.1016/j.jmbbm.2019.07.008.
14. M. Di Giuseppe, G. Alotta, V. Agnese, D. Bellavia, G.M. Raffa, V. Vetri, M. Zingales, S. Pasta, M. Pilato, Identification of circumferential regional heterogeneity of ascending thoracic aneurysmal aorta by biaxial mechanical testing, *J. Mol. Cell. Cardiol.* 130 (2019) 205-215, doi: 10.1016/j.yjmcc.2019.04.010.
15. M. Jadidi, M. Habibnezhad, E. Anttila, K. Maleckis, A. Desyatova, J. MacTaggart, A. Kamenskiy, Mechanical and structural changes in human thoracic aortas with age, *Acta Biomater.* 103 (2020) 172-188, doi: 10.1016/j.actbio.2019.12.024.
16. G.A. Holzapfel, T.C. Gasser, R.W. Ogden, A new constitutive framework for arterial wall mechanics and a comparative study of material models, *J. Elasticity* 61 (2000) 1-48, doi:10.1023/A:1010835316564.

17. G.A. Holzapfel, Determination of material models for arterial walls from uniaxial extension tests and histological structure, *J. Theor. Biol.* 238 (2006) 290-302, doi:10.1016/j.jtbi.2005.05.006.
18. T.C. Gasser, R.W. Ogden, G.A. Holzapfel, Hyperelastic modelling of arterial layers with distributed collagen fibre orientations, *J. R. Soc. Interface*, 3 (2006) 15-35, doi:10.1098/rsif.2005.0073.
19. R.W. Ogden, G. Saccomandi, Introducing mesoscopic information into constitutive equations for arterial walls, *Biomech. Model. Mechanobiol*, 6 (2007) 333-344, doi:10.1007/s10237-006-0064-8.
20. S. Federico, T.C. Gasser, Nonlinear elasticity of biological tissues with statistical fibre orientation, *J. R. Soc. Interface*, 7 (2010) 955-966, doi: 10.1098/rsif.2009.0502.
21. G.A. Holzapfel, J.A. Niestrawska, R.W. Ogden, A.J. Reinisch, A.J. Schriefl, Modelling non-symmetric collagen fibre dispersion in arterial walls, *J. R. Soc. Interface* 12 (2015) 20150188, doi:10.1098/rsif.2015.0188.
22. I.D. Breslavsky, G. Franchini, M. Amabili, Effect of fiber exclusion in uniaxial tensile tests of soft biological tissues, *J. Mech. Behav. Biomed. Mater.* 112 (2020) 104079, doi: 10.1016/j.jmbbm.2020.104079.
23. M.E. Safar, Arterial stiffness as a risk factor for clinical hypertension, *Nat. Rev. Cardiol.* 15 (2018) 97-105, doi: 10.1038/nrcardio.2017.155.
24. D.H. Bergel, The dynamic elastic properties of the arterial wall, *J. Physiology*, 156 (1961) 458-469, doi: 10.1113/jphysiol.1961.sp006686.
25. N. Westerhof, A. Noordergraaf, Arterial viscoelasticity: A generalized model, *J. Biomech.* 3 (1970) 357-379, doi: 10.1016/0021-9290(70)90036-9.
26. T. Imura, K. Yamamoto, K. Kanamori, T. Mikami, H. Yasuda, In vivo viscoelastic behavior in the human aorta, *Circ. Res.* 66 (1990) 1413-1419, doi: 10.1161/01.RES.66.5.1413.
27. T. Imura, K. Yamamoto, T. Satoh, K. Kanamori, T. Mikami, H. Yasuda, Non-invasive ultrasonic measurement of the elastic properties of the human abdominal aorta, *Cardiovasc. Res.* 20 (1986) 208-214, doi: 10.1093/cvr/20.3.208.
28. D. Valdez-Jasso, D. Bia, Y. Zocalo, R.L. Armentano, M.A. Haider, M.S. Olufsen, Linear and nonlinear viscoelastic modeling of aorta and carotid pressure–area dynamics under in vivo and ex vivo conditions, *Ann. Biomed. Eng.* 39 (2011) 1438-1456, doi:10.1007/s10439-010-0236-7.
29. D. Valdez-Jasso, M.A. Haider, H.T. Banks, S.D. Bia, G.Y. Zocalo, R.L. Armentano, M.S. Olufsen, Analysis of viscoelastic wall properties in ovine arteries. *IEEE Trans. Biomed. Eng.* 56 (2009) 210-219, doi:10.1109/TBME.2008.2003093.
30. R.L. Armentano, J. Gabriel Barra, F. Martin Pessana, D.O. Craiem, S. Graf, D. Bia Santana, R.A. Sanchez, Smart smooth muscle spring-dampers, *IEEE Eng. Med. Biol. Mag.* 26 (2007) 62-70, doi: 10.1109/MEMB.2007.289123.
31. R.L. Armentano, J.G. Barra, J. Levenson, A. Simon, R.H. Pichel, Arterial wall mechanics in conscious dogs. Assessment of viscous, inertial, and elastic moduli to characterize aortic wall behavior, *Circ. Res.* 76 (1995) 468-478, doi: 10.1161/01.RES.76.3.468.
32. A.R. Ghigo, X.-F. Wang, R. Armentano, J.M. Fullana, P.-Y. Legrée, Linear and nonlinear viscoelastic arterial wall models: applications on animals, *J. Biomech. Eng.* 139 (2017) 011003, doi: 10.1115/1.4034832.

33. E.-J. Courtial, L. Fanton, M. Orkisz, P.C. Douek, L. Huet, R. Fulchiron, Hyper-viscoelastic behavior of healthy abdominal aorta, *IRBM* 37 (2016) 158-164, doi:10.1016/j.irbm.2016.03.007.
34. M. Amabili, P. Balasubramanian, I. Breslavsky, Anisotropic fractional viscoelastic constitutive models for human descending thoracic aortas, *J. Mech. Behav. Biomed. Mater.* 99 (2019) 186-197, doi: 10.1016/j.jmbbm.2019.07.010.
35. M. Amabili, G.O. Arena, P. Balasubramanian, I.D. Breslavsky, R. Cartier, G. Ferrari, G.A. Holzapfel, A. Kassab, R. Mongrain, Biomechanical characterization of a chronic Type A dissected aorta, *J. Biomech.* 110 (2020) 109978, doi: 10.1016/j.jbiomech.2020.109978.
36. Y.C. Fung, *Biomechanics: Mechanical Properties of Living Tissues*, second ed, Springer, New York, 1993.
37. M. Amabili, *Nonlinear Mechanics of Shells and Plates in Composite, Soft and Biological Materials*, Cambridge University Press, New York, 2018.
38. G.A. Holzapfel, T.C. Gasser, M. Stadler, A structural model for the viscoelastic behavior of arterial walls: continuum formulation and finite element analysis, *European J. Mech. A/Solids* 21 (2002) 441-463, doi:10.1016/S0997-7538(01)01206-2.
39. H. Berjamine, M. Destrade, W.J. Parnell, On the thermodynamic consistency of quasi-linear viscoelastic models for soft solids, *Mech. Res. Commun.* 111 (2021) 103648, doi: 10.1016/j.mechrescom.2020.103648.
40. J.H. Southard, F.O. Belzer, The University of Wisconsin organ preservation solution: components, comparisons, and modifications, *Transplant. Rev.* 7 (1993) 176-190, doi: 10.1016/S0955-470X(05)80025-4.
41. I.D. Breslavsky, M. Amabili, Nonlinear model of human descending thoracic aortic segments with residual stresses, *Biomech. Model. Mechanobiol.* 17 (2018) 1839-1855, doi:10.1007/s10237-018-1060-5.
42. R.H. Dhume, V.H. Barocas, Emergent structure-dependent relaxation spectra in viscoelastic fiber networks in extension, *Acta Biomater.* 87 (2019) 245-255, doi: 10.1016/j.actbio.2019.01.027.

# **Chapter3**

## **Viscoelasticity of human descending thoracic aorta in a mock circulatory**

Giulio Franchini (1), Francesco Giovanniello (1), Marco Amabili (1,2)

(1) Department of Mechanical Engineering, McGill University, Montreal, Canada H3A 0C3

(2) Dipartimento di Ingegneria ed Architettura, University of Parma, Parma, Italy.

Keywords: human aorta; mock circulatory loop; hysteresis loop; viscoelasticity; mass density.

### **Abstract**

Healthy human descending thoracic aortas, obtained during organ donation for transplant and research, were tested in a mock circulatory loop to measure the mechanical response to physiological pulsatile pressure and flow. The viscoelastic properties of the aortic segments were investigated at three different pulse rates. The same aortic segments were also subjected to quasi-static pressure tests in order to identify the aortic dynamic stiffness ratio, which is defined as the ratio between the stiffness in case of pulsatile pressure and the stiffness measured for static pressurization, both at the same value of pressure. The loss factor was also identified. The shape of the deformed aorta under static and dynamic pressure was measured by image processing to verify the compatibility of the end supports with the natural deformation of the aorta in the human body. In addition, layer-specific experiments on 10 human descending thoracic aortas allowed to precisely identify the mass density of the aortic tissue, which is an important parameter in cardiovascular dynamic models.

### **1. Introduction**

The study of the mechanical behaviour of the human aorta received a lot of attention in the literature due to the great relevance in the hypertension (Safar, 2018) and in the development of mechanically compatible grafts for aortic repair after diseases as the acute dissection and large aortic aneurysms. Quasi-static layer-specific mechanical tests on aortic strips were conducted to characterize the hyperelastic properties of the aortic tissue (Weisbacker et al., 2012; Sassani et al., 2015; Amabili et al., 2019a; Holzapfel et al., 2019); bi-axial quasi-static tests were also performed (Di Giuseppe et al., 2019). Advanced material models were developed based on experimental results (Holzapfel et al., 2019; Breslavsky et al., 2020), as well as mechanical models of the aorta including residual stresses (Breslavsky et al., 2018) and fluid-structure interaction (Bazilevs et al., 2008; Chandra et al., 2013). Dynamic tests designed to characterize the viscoelastic material properties of the aortic tissue are much less diffused (Amabili et al., 2019a; Amabili et al. 2019b; Franchini et al., 2021). These mechanical tests were performed without vascular smooth muscle activation. Franchini et al. (2022) performed a quasi-static and dynamic characterization of human descending thoracic aortas with and without smooth muscle activation, which was achieved by KCl and noradrenaline as vasoactive agents. Another significant aspect is the axial pre-stretch of the natural aorta in the human body; this was experimentally investigated by Horný et al. (2014). *In-vivo* experiments were conducted by Imura et al. (1990) to determine the viscoelastic properties of human aortas. A chronic Type A dissected aorta was mechanically tested by Amabili et al. (2020c). Arterial stiffness can be obtained *in vivo* by measuring the travel time of the pulse wave through the aorta or by elastography, which uses externally induced shear waves (Damughatla et al., 2015). Ultrasound time-harmonic elastography was used by Schaafs et al. (2019) for quantifying aortic stiffness *in vivo* by measuring the shear-wave speed in the context of aging and arterial hypertension.

Mock circulatory loops are very useful to test *ex vivo* arteries by mimicking physiological pulsatile blood pressure and flow. With respect to *in-vivo* experiments, which are invasive, they offer the advantage of the simultaneous, accurate and direct measurement of (i) the flow parameters – flowrate, inlet and outlet pressures – and (ii) displacement and deformation of the arterial wall. Armentano et al. (1995) studied the response of canine descending thoracic aortas with vascular smooth muscle activation making use of a mock circulatory loop. Armentano et al. (2007) reported experiments on a mock circulatory loop of seven human common carotid arteries at 70 bpm. Valdez-Jasso et al. (2009; 2011) used a mock circulatory loop to performed experiments

on eleven Merino sheep descending thoracic aortas at 108 and 110 bpm. Amabili et al. (2020a) developed a mock circulatory loop to study 11 human descending thoracic aortas in order to obtain the viscoelastic properties. Ferrari et al. (2019) and Amabili et al. (2020b) applied the previously developed loop to study the response of an aortic Dacron graft to physiological pulsatile flow and pressure. Pejic et al. (2021) characterized the viscoelastic properties of a short segment of *ex vivo* porcine ascending aorta under pulsatile flow. Agrafiotis et al. (2021) developed a specific device to accurately reproduce pressure waveform to test arteries.

Numerical simulations of the dynamics of the human aorta and its interaction with the blood flow require the knowledge of the mass density of the aortic wall to be inserted in fluid-structure interaction models (Jayendiran et al., 2018). However, this information is scarcely available in the literature. According to (ICRP, 2009), the density of the wall of blood vessels is  $1.060 \text{ g/cm}^3$ , while it seems that no specific information is available in the literature on specific aortic layers. The density of an abdominal aortic aneurism is taken in (Chandra et al., 2013) as  $1.2 \text{ g/cm}^3$  for numerical simulations, without reporting a valid source for the assumption. The value of  $1.0 \text{ g/cm}^3$  was used in (Bazilevs et al., 2008) for numerical simulation of the wall of an abdominal aortic aneurysm. Due to the significant difference between the data reported in the literature and the availability of human tissue of descending thoracic aortas, it was decided to measure the mass density of the intact aortic wall and of the three layers – intima, media and adventitia – that were separated for another study (Amabili et al., 2019a; Amabili et al., 2021).

In the present study, healthy human descending thoracic aortas, obtained during organ donation for transplant and research, were tested in a mock circulatory loop to measure the mechanical response to physiological pulsatile pressure. The same aortic segments were also subjected to quasi-static pressure tests in order to identify the aortic dynamic stiffness ratio. This parameter is defined as the ratio between the stiffness in case of pulsatile pressure and the stiffness measured for static pressurization, both at the same value of pressure. The shape of the deformed aorta under static and dynamic pressure was also measured by image processing to verify the compatibility of the end supports with the natural deformation of the aorta in the human body. These two investigations were not reported in (Amabili et al., 2020a). In addition, layer-specific experiments on 10 human descending thoracic aortas allowed to precisely identify the mass density of the aortic tissue, which is an important parameter in cardiovascular dynamic models.

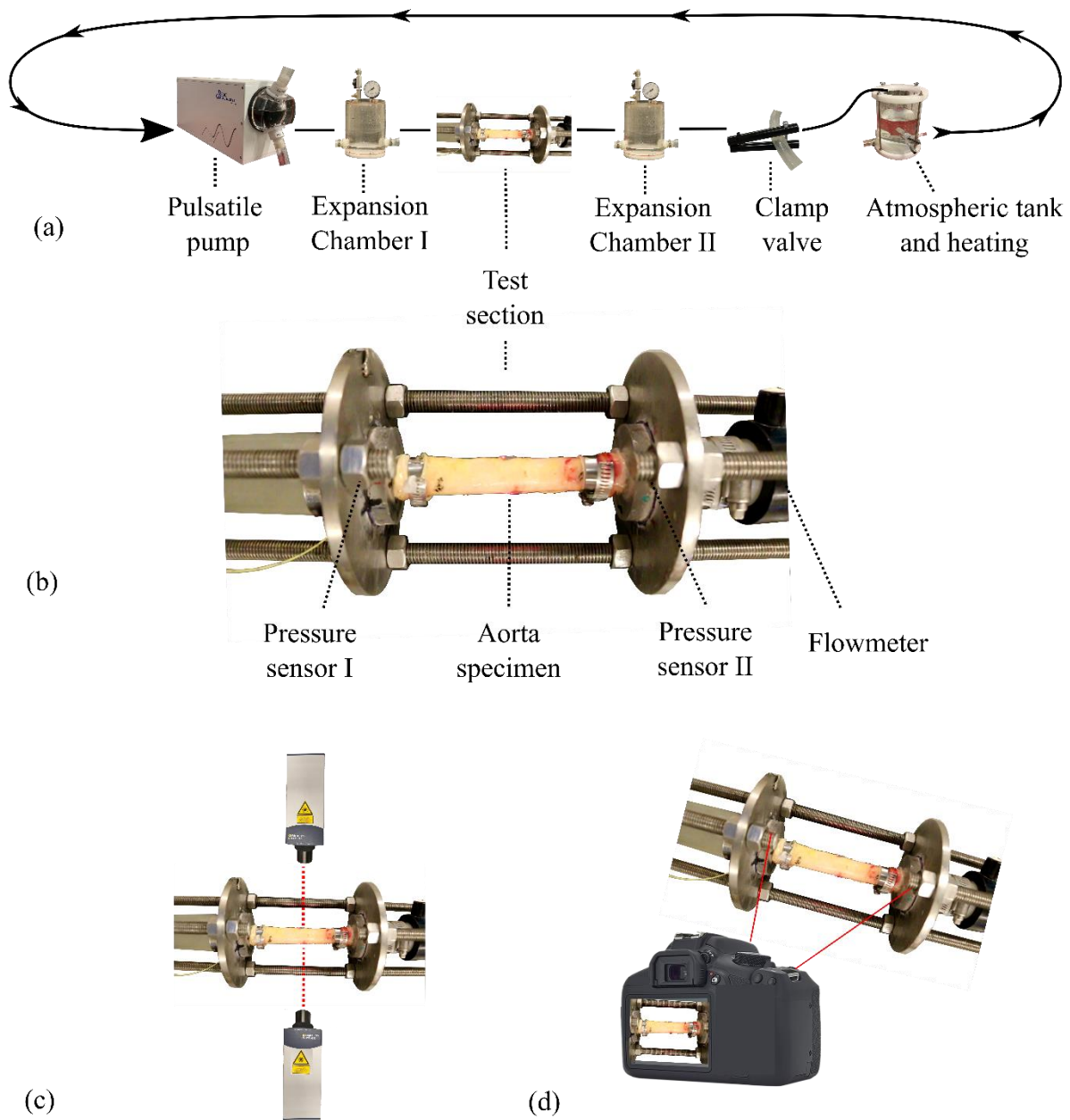


Figure 1. Illustration of the mock circulatory loop. (a) Schematic of the loop and its components. (b) Test section with the aortic segment, the two pressure sensors and the flowmeter. (c) Laser Doppler measurement of the dynamics of the aorta. (d) Digital camera used to visualize the deformation of the aorta during tests.

## 2. Materials and methods

Two different experimental activities were carried on human descending thoracic aortas, which were obtained through *Transplant Québec*, the transplant coordinator of the Province of Québec, from healthy donors of organs for transplant. The study was authorized by the ethics committee of McGill University.

Table 1. Information on donors for the tests in the mock circulatory loop. The following abbreviations are used: F = female; CVA = cerebrovascular accident.

Donor	A	B
Age (years)	61	43
Gender	F	F
Weight (kg)	68	94
Height (cm)	144	162
Cause of death	CVA	CVA
Central diameter (mm)	18.7	17.4
Wall thickness (mm)	1.73±0.16	1.59±0.14
Pre-stretch	1.04	1.05
Length between supports (mm)	68.1	80.4

### 2.1. Mock circulatory loop experiments

Two human descending thoracic aortas were tested in the mock circulatory loop shown in Fig. 1(a-d). The aortas segments were stored in saline solution at 4° C before testing within 48 hours from the removal from the body of heart-beating donors with cerebral death. The screening for transplant guaranteed that no known diseases or conditions that compromised the aorta were observed. The aortas were cleaned, removing the bifurcating branches and the periaortic connective tissue; the holes in correspondence of the bifurcations were closed with hydrogel adhesive (Yang et al., 2021). The mid-length external diameter was measured, as well as the thickness of the aortic wall. The information on the donors is given in Table 1. Cylindrical supports of appropriate diameter were used to install the aortic segment in the test section. A layer of Dacron

was placed around each extremity of the aortic segment to avoid damage during fixation with hose clamps to the supports. The proximal end of the aorta was attached to the flow inlet coming from the volumetric pump and the distal end to the flow outlet going to the atmospheric heated tank. The distance between the two supports (free length) was measured with a caliper and is reported in Table 1. An axial pre-stretch of 1.04 (4 %) and 1.05 (5 %) was imposed to the two aortas, respectively, by adjusting the distance between the two supports. The fixed axial displacements at the ends well reproduce the natural behavior of the aortic segment in the body, which is not elongating during the blood pressure pulsation. The condition of fixed radial expansion at the ends is instead not physiological. One of the scopes of the present study is to investigate the behaviour of the aortic segment in radial direction to show that the deformation during pressurization is practically constant in all the aortic segment, excluding a narrow length close to the clamps. This indicates that the fixed radial displacement at the ends does not affect the measurement in the central area of the aortic segment. When the aortic segment is in the human body, the presence of surrounding organs and bifurcating branches increases the global dissipation.

The aorta was kept moisturized during tests by wrapping it with a tissue soaked in physiological saline solution. The wet tissue was removed only during the short time of the measurement recording.

The mock circulatory loop is shown in Fig. 1(a-d) and it was designed to reproduce the pulsatile flow pumped by the heart, the peripheral resistance of the portion of the arterial tree and the Windkessel effect. The loop was built by using 3/4" ID Tygon tubing from the pump to the atmospheric tank; a larger Tygon tube was used from the tank to return to the pump. The compliance of the arterial tree upstream and downstream with respect the aorta was simulated by two expansion chambers by BDC Laboratories positioned before and after the aortic segment. Each chamber had a volume of 2.25 liters. The loop was filled with a mixture (in volume) of 55 % saline solution and 45 % glycerin, with a dynamic viscosity 3.5 mPa s at 37° C, which is the same of blood in large arteries (Fung, 1997). The mass density of the mixture was 1119 kg/m<sup>3</sup>, close to 1050 kg/m<sup>3</sup> which is the density of blood. A heated tank by BDC Laboratories, with temperature control set at 37° C and open to the atmospheric pressure, was installed to replicate the separation of the arterial tree from the venous system, which avoided suction of the pump in the aortic segment.

Air pockets of proper size were trapped at the top of each of the expansion chambers above the liquid mixture. This air volume acted as a pneumatic spring with stiffness inversely proportional to the air volume, that was regulated with pneumatic valves connected to compressed air line. A pressure gauge was installed at the top of each expansion chamber. An adjustable pinch valve was installed on the tube downstream of the aorta in order to obtain the desired resistance to the flow, which is given by the arterial tree in the body. The adjustment of the air volume contained in the expansion chambers and the right amount of squeezing introduced on the tube by the pinch valve were necessary to obtain the desired 100 mm Hg mean pressure during the pulsation, the diastolic pressure around 80 mm Hg and systolic pressure of about 120 mm Hg, which are physiological pressures at rest. The difference of systolic and diastolic pressures is referred to as the pulse pressure and was around 40 mm Hg during tests. The adjustment of the air volume and the tube squeezing was necessary at every change of the pulse rate.

The pulsatile flow was generated by a PD-1100 piston pump from BDC Laboratories. The PD-1100 pulsatile pump and accompanying software provide a particularly effective flow control for laboratory applications with physiological pulsatile flows. The pump has stroke range 0 to 290 cm<sup>3</sup>, a pulse rate 0 to 240 bpm, a flow rate 0 to 10 l/min; the software allows for waveform control. About the same mean systolic and diastolic pressures were kept at different pulse rates (60, 80 and 100 bpm) during tests to ensure that similar pressure loads were applied to the aortic segment. A FM501 Carolina Medical Electronics magnetic flowmeter with EP690 flow probe was placed at the outlet of the aorta and two SPR-524 (size 3.5 F) Millar catheter pressure sensors with PCU-2000 pressure signal conditioners were placed at the inlet and outlet of the aortic segment. The maximum error was 1.5 mm Hg for the Millar catheter pressure sensor and 0.3 l/min for the Carolina Medical magnetic flowmeter.

An illustration of the mock circulatory loop assembled for this study is given in Fig. 1(a), indicating the BDC Laboratories pump, the two expansion chambers, the test section, the squeezing clamp valve and the BDC Laboratories water tank with temperature control. An image showing the test section is presented in Fig. 1(b) where the aortic segment connected to the supports, the flowmeter and pressure transducers are visible.

Two OFV 505 Polytec laser Doppler vibrometers, with velocity and displacement decoders, were installed to measure the dynamic change of diameter of the aortic segment. They were pointing at the center of the segment along the same direction, as shown in Fig. 1(c). Tiny coupons

of thin reflective tape were placed on the aorta at the two laser target locations. Each vibrometer measured the dynamic displacement in the direction of the laser beam and the diameter change was obtained as the sum of the two laser signals. The experiments on the mock circulatory loop allow to obtain the hysteresis loops in the pressure-diameter change plane at different pulse rates.

The aortic segment installed on the loop was also subjected to a quasi-static pressurization test. This was carried out slowly increasing, and then decreasing, the air pressure in an expansion chamber once the Tygon tube was completely squeezed with two pick valves, one upstream and one downstream the aorta, to isolate it from the pump and the atmospheric tank. A digital camera was used to record the shape of the aortic segment under pulsatile flow tests and quasi-static pressurization tests, as shown in Fig. 1(d).

## 2.2. Dynamic stiffness ratio

The measurements of both the hysteresis loop and the pressurization curve allow to introduce the concept of the dynamic stiffness ratio, which was studied in (Franchini et al., 2021) for aortic strips to quantify the increase of dynamic stiffness during dynamic deformations with respect to static deformations. The dynamic stiffness ratio is obtained – see Fig. 2 – as the ratio between the dynamic stiffness, proportional to the slope of the middle line of the hysteresis loop (red line in Fig. 2), and the static stiffness, proportional to the slope of the static pressurization curve at the center of the loop (green line in Fig. 2). The ratio of the two slopes in the pressure-diameter change diagram gives the dynamic stiffness ratio. This is an important viscoelastic parameter which indicates the stiffness increase (results show that it is larger than one) in case of dynamic (pulsatile) pressure loading. The other significant viscoelastic parameter is the loss factor  $\eta$ , which is obtained from the energy loss in a cycle  $\Delta W_d$ , which is proportional to the area contained inside the hysteresis loop, and the storage energy  $W_s$ , which is obtained as the average of  $A_1$  and  $A_2$ , as shown in Fig. 3 (Amabili et al., 2020a; Franchini et al., 2021)

$$\eta = \frac{\Delta W_d}{2\pi W_s} = \frac{\Delta W_d}{\pi (A_1 + A_2)}. \quad (1)$$

An error below 10 % can be expected in the loss factor measurement.

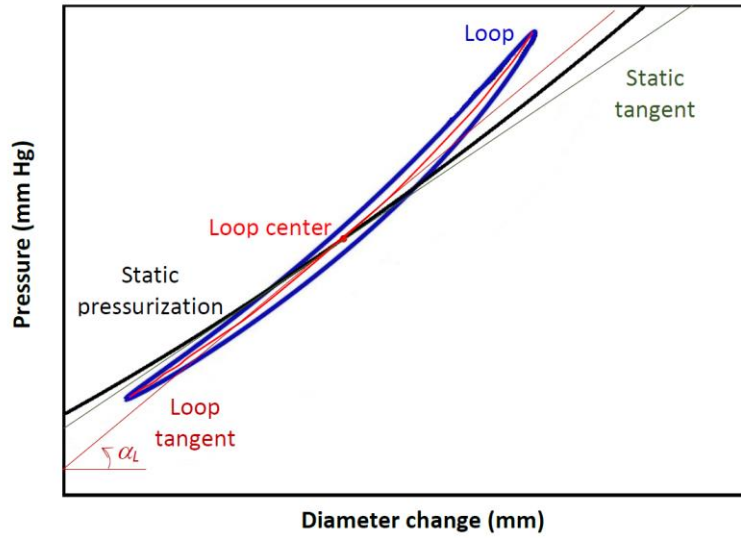


Figure 2. The dynamic stiffness ratio is obtained as the ratio between the dynamic stiffness, proportional to the slope of the middle line of the hysteresis loop (red line), and the static stiffness, proportional to the slope of the static pressurization curve (represented as average between loading and unloading) at the center of the loop (green line). The ratio of the two slopes in the pressure-diameter change diagram gives the dynamic stiffness ratio.

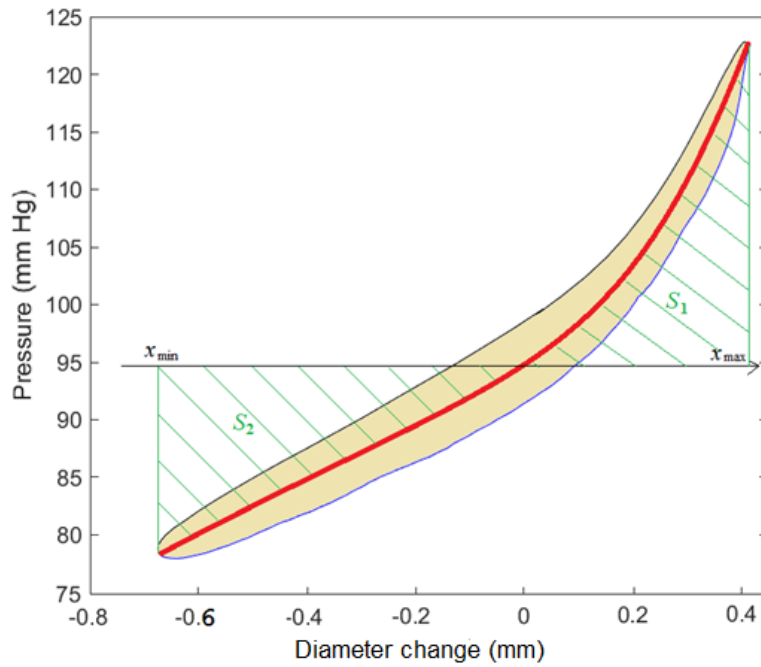


Figure 3. Hysteresis loop shown in the pressure-diameter change diagram. The area inside the loop, colored in yellow, is proportional to the energy loss in a cycle  $W$ . The average of the two areas  $S_1$  and  $S_2$  (indicated by inclined green lines), obtained by using the middle line of the loop shown in red and the horizontal line passing through it at  $x = 0$ , is proportional to the storage energy.

Table 2. Information on donors for the mass density measurements. The following abbreviations are used: M = male; F = female; CVA = cerebrovascular accident; AO = anoxia; TBI = traumatic brain injury.

Donor	1	2	3	4	5	6	7	8	9	10
Age (years)	70	54	46	65	34	63	50	32	48	55
Gender	M	M	M	F	M	M	F	F	M	F
Weight (kg)	91.5	80	103	50	83.8	53	110	105	81	59
Height (cm)	183	175	178	155	185	172	168	175	175	175
Cause of death	CVA	CVA	AO	CVA	AO	CVA	CVA	AO	CVA	TBI

### 2.3. Aortic mass density measurement

Ten human aortas were used in the present study with average age of 51.7 years; 6 males and 4 females. They were stored in saline solution at 4° C before testing within 72 hours from the removal from the body of heart-beating donors with cerebral death. The main information on the donors is given in Table 2. The aortas were cleaned, removing the periaortic connective tissue. Strips were cut, as shown in Fig. 4. Some of the strips were tested directly, while others were separated into the three layers – intima, media and adventitia – by using the procedure described in (Amabili et al., 2019a; Amabili et al., 2021).

The measurement of the mass density was achieved by weighing the single layers and the intact aortic wall in air and in water (aortic tissue is denser than water and does not float in the liquid) at room temperature. A digital scale with a resolution of 1/100 grams was employed. The weight in air was measured simply weighing the strips, while the weight in water was measured hanging the strip with a very thin wire in a known volume of water and measuring the weight variation. A photo taken during an experiment is shown in Fig. 5, where a significant quantity of aortic tissue (some strips are grouped together) is immersed in order to reduce errors. The apparent weight of the volume of water is increased by the buoyancy force  $F_b$  acting on the suspended aortic material; this force is equal to

$$F_b = \rho_w g V_f, \quad (2)$$

where  $\rho_w$  is the mass density of water,  $g$  is the gravitational constant and  $V_f$  the volume of water displaced by the immersed object (equal in the present case to the volume of the completely immersed material). In order to calculate the specific gravity  $SG$  with respect to water of the aortic tissue of mass density  $\rho_a$ , it is useful to substitute to  $\rho_w$  the ratio  $\frac{F_b}{gV_f}$ , obtained from Eq. (2):

$$SG = \frac{\rho_a}{\rho_w} = \frac{\rho_a}{\frac{F_b}{gV_f}} = \frac{\rho_a g V_f}{F_b} = \frac{W_a}{F_b}, \quad (3)$$

which shows that the specific gravity is the ratio between the weight of the aortic material in air,  $W_a$ , and the buoyancy force in water,  $F_b$ . Assuming 1.000 g/cm<sup>3</sup> the mass density of the water at 20° C, then mass density of the aortic tissue is obtained.



(a)



(b)

Figure 4. Experimental setup. (a) Aorta from donor 10; (b) preparation of strips from the aorta from donor 10 after a longitudinal cut in the posterior part.

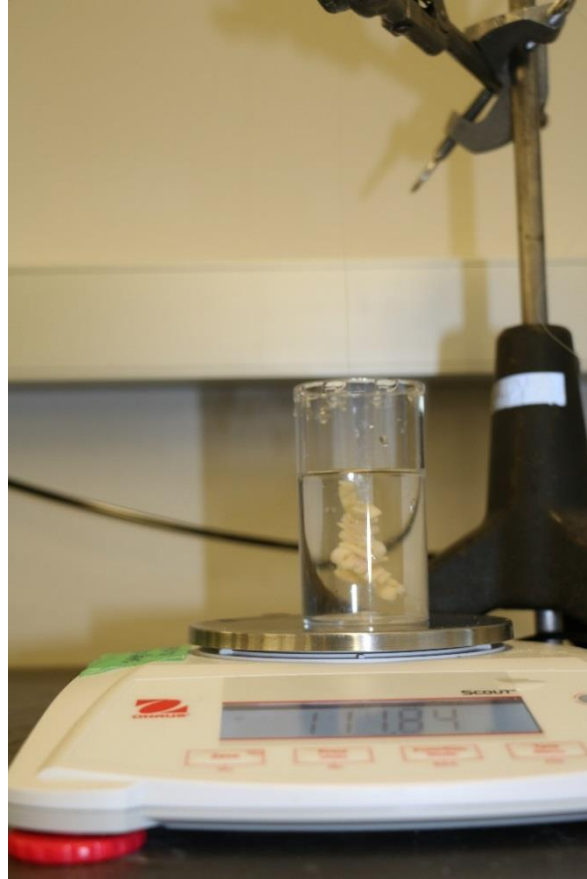


Figure 5. Measurement of the buoyancy force acting on the suspended aortic tissue.

### 3. Results of experiments on the mock circulatory loop

The results of the quasi-static pressurization of the aortic segment from donor B are shown in Fig. 6. The diameter change - pressure curve is initially almost linear; then, the aortic segment increases its stiffness and a significantly larger pressure increase is necessary to see the same diameter change. Five points are highlighted along the curve and the corresponding images of the aortic segment are presented. They show that the diameter change of the pressurized aortic segment is practically uniform along the length, except near the clamped edges. The extracted external profiles of the segment by using image processing are also shown in Fig. 6. This result clarifies that the radial boundary condition does not alter the aortic radial deformation (diameter change) of the segment, except for a small length very close to each edge. The quasi-static diameter change-pressure curve presented in Fig. 6 is the average of the two curves obtained increasing and decreasing the pressure after five cycles of preconditioning. In fact, a small hysteresis is observed during the tests. This curve is used as a reference to compare to the results of dynamic tests.

The dynamic tests were performed with pulsatile flow and pressure at different pulse rates between 60 and 100 bpm. These rates were chosen in the present study since the effect of the fluid-structure interaction on the viscoelastic behaviour of the aortic segment is significantly smaller than for larger pulse rates, as shown in (Amabili et al., 2020a). The pressure, flow and diameter change versus time for the aortic segment from donor A at pulse rates 60, 80 and 100 bpm are given in Fig. 7. Both inlet and outlet pressures are presented. Results show that the tests reproduce the physiological pressure and flow pulsation, with pressure oscillating between about 80 and 120 mm Hg with accurate waveform and presence of the dicrotic notch. The deformation of the aortic wall (diameter change) follows the average between the inlet and outlet pressures during the phase of diameter increase, while it is delayed with respect to the pressure during the phase of diameter decrease. This confirms the results presented in (Amabili et al., 2020a). This delay is the source of the viscoelastic behaviour of the aortic wall and is observed at the three different pulse rates. The maximum diameter change in a cycle is also given in Fig. 7; the measured value at 60 bpm is 0.45 mm for donor A, corresponding to a diameter change of 2.6 %.

The hysteresis loops for both the tested aortic segments are displayed in Fig. 8(a,b) for the 60, 80 and 100 bpm pulse rates. The loops at these three different pulse rates are similar and have similar area, confirming the statement that between 60 and 100 bpm the contribution of the fluid-

structure interaction to the viscoelastic behaviour of the aorta is similar for the three cases and it is smaller compared to the one obtained for larger pulse rates. In fact, a significant increase of the area inside the loop, which is associated to the loss energy per cycle, is observed at larger pulse rates (Amabili et al., 2020a). The maximum diameter change is 0.76 mm for donor B, corresponding to 4.8 %.

Fig. 9 is original for tests in mock circulatory loops. In fact, it presents the hysteresis loops from both donors at the three pulse rates (60, 80 and 100 bpm) plotted over the quasi-static pressurization curves. All the hysteresis loops present a larger slope than the quasi-static curve.

The dynamic stiffness ratios and the loss factors obtained from the experiments on the mock circulatory loop are presented in Fig. 10. An average value around 1.3 is obtained for the dynamic stiffness ratio, which is in very good agreement with the result  $1.37 \pm 0.17$  obtained in (Franchini et al., 2021) for circumferential aortic strips at 60 bpm. This shows a small effect of the fluid-structure interaction on the dynamic stiffness ratio of the aortic segment in the mock circulatory loop between 60 and 100 bpm. On the other hand, the average loss factor at 60 bpm is 0.22, which is much larger than the loss factor for circumferential aortic strips in (Franchini et al., 2021), which was found to be around  $0.061 \pm 0.01$  at 60 bpm. The observed loss factor value is instead much closer to what measured in experiments on a mock circulatory loop in (Amabili et al., 2020a), where the loss factor values varied between 0.05 and 0.21 at 60 bpm. Therefore, the fluid-structure interaction has a significant effect on the loss factor even between 60 and 100 bpm. Fig. 10 shows that the loss factor is slightly increasing with the pulse rate, while this is not observed for the dynamic stiffness ratio.

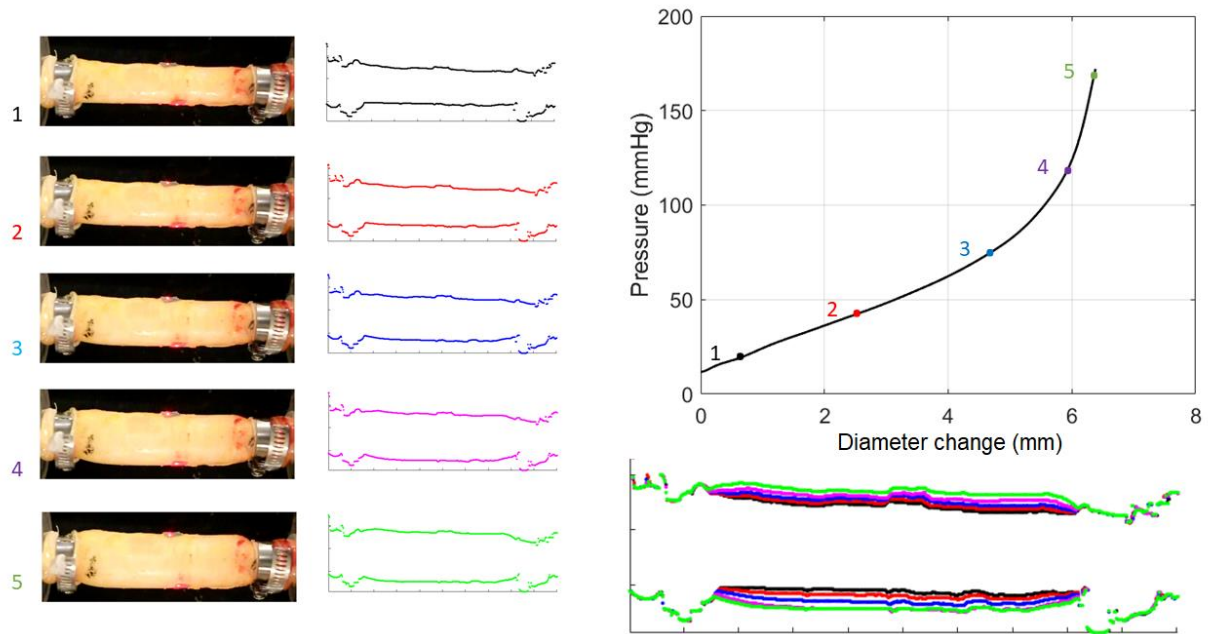


Figure 6. Quasi-static pressurization of the aortic segment from donor B. Five points are marked on the pressure-diameter expansion curve and the corresponding images of the aorta and profile extraction are shown. The arrow indicates the blood flow direction. The proximal end of the aortic segment is on the right and the distal end is on the left in the photos and the profile reconstruction.

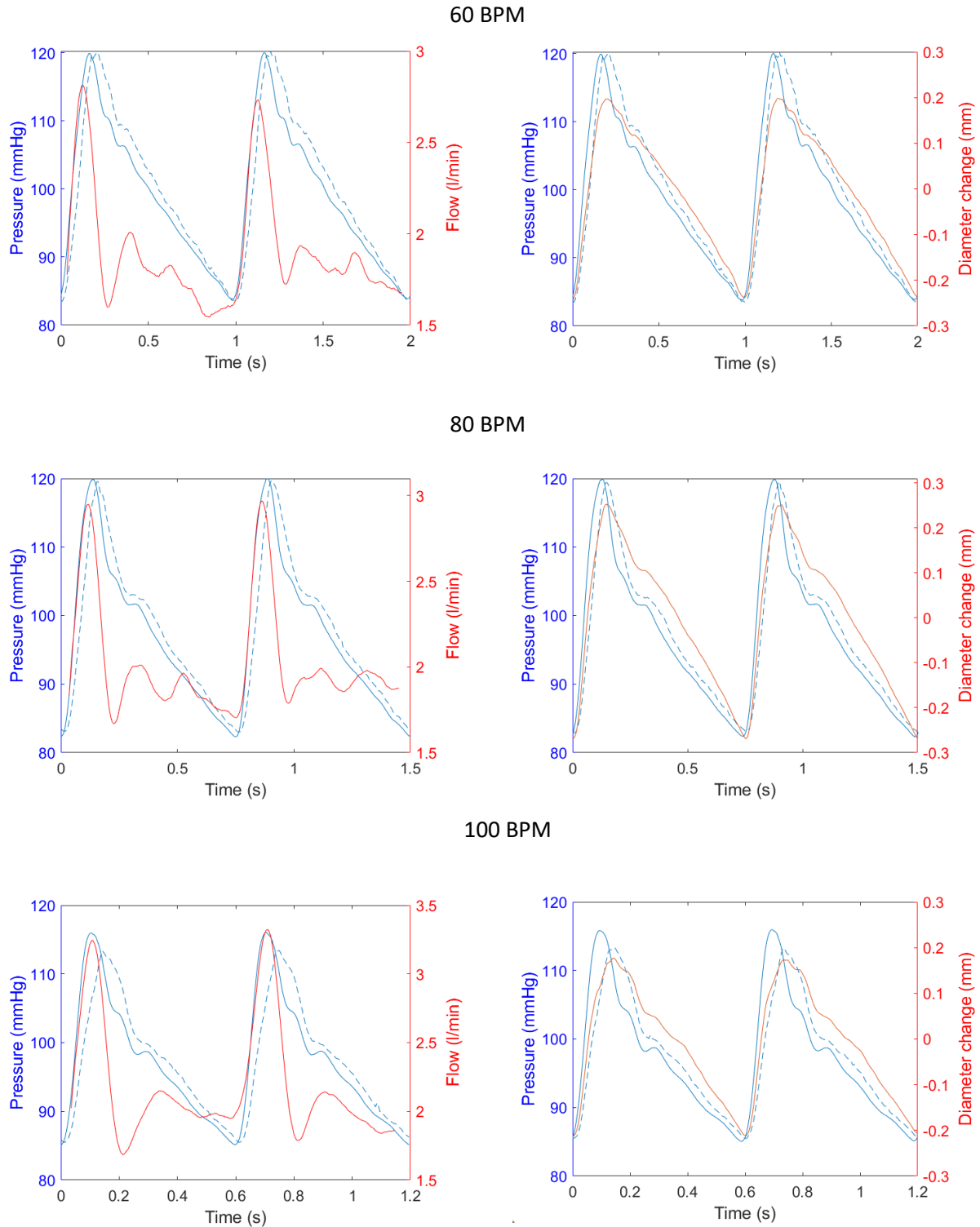


Figure 7. Pressure, flow and diameter change versus time for the aortic segment from donor A at three pulse rates: 60, 80 and 100 bpm. Left column: fluid variables; right column: cyclic change of the aortic diameter and pressures; —, inlet pressure; - - -, outlet pressure; —, outlet flowrate; —, change of the aortic diameter.

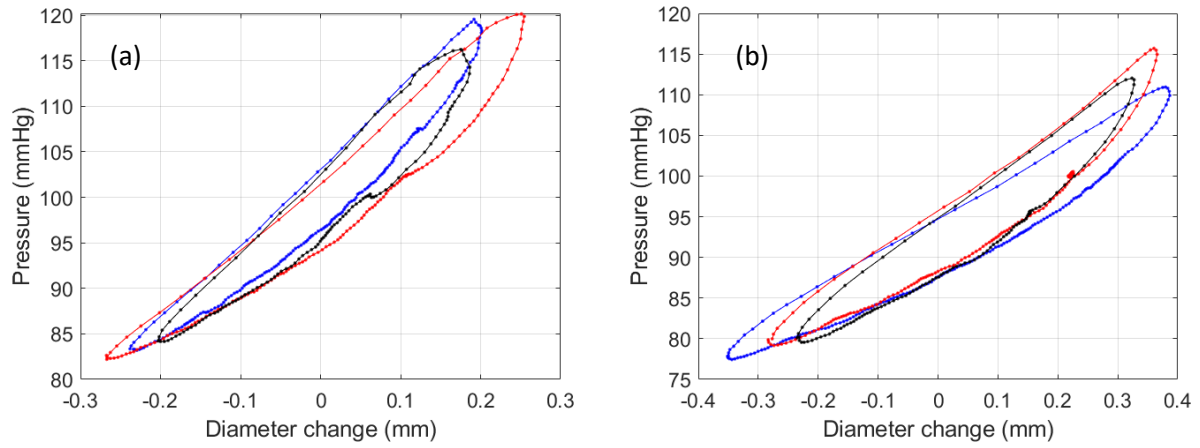


Figure 8. Hysteresis loops shown in the diameter change– pressure plane for three different pulse rates. (a) Donor A. (b) Donor B. —, 60 bpm. —, 80 bpm. —, 100 bpm.

#### **4. Results for the aortic mass density**

The results of the mass density measurement are summarized in Table 3. The average values of the mass density range between  $1.10\pm 0.04$  (media) and  $1.14\pm 0.06$  g/cm<sup>3</sup> (intima). The average values for the adventitia ( $1.11\pm 0.03$  g/cm<sup>3</sup>) and the full wall ( $1.11\pm 0.05$  g/cm<sup>3</sup>) are very close to the one of the media. The statistical analysis of the four different types of samples (i.e. the three aortic layers plus the intact wall) is carried out in Fig. 11, where the median, 1<sup>st</sup> and 3<sup>rd</sup> quartile are presented in addition to the extreme values and the average. There is no statistical difference among the four groups ( $p = 0.26$  from ANOVA test), even if a slightly larger mean value of the mass density of the intima is observed. This is not in contrast with the fact that the full wall has density very close to the media and adventitia, since the intima is thin, and its volume is a small fraction of the full wall volume.

It is interesting to observe that the present measurements give average values about 5 % larger than the one given in (ICRP, 2009) for blood vessels. Therefore, the present study is significant, because it gives a more accurate mass density data to use in numerical models of the human aorta.

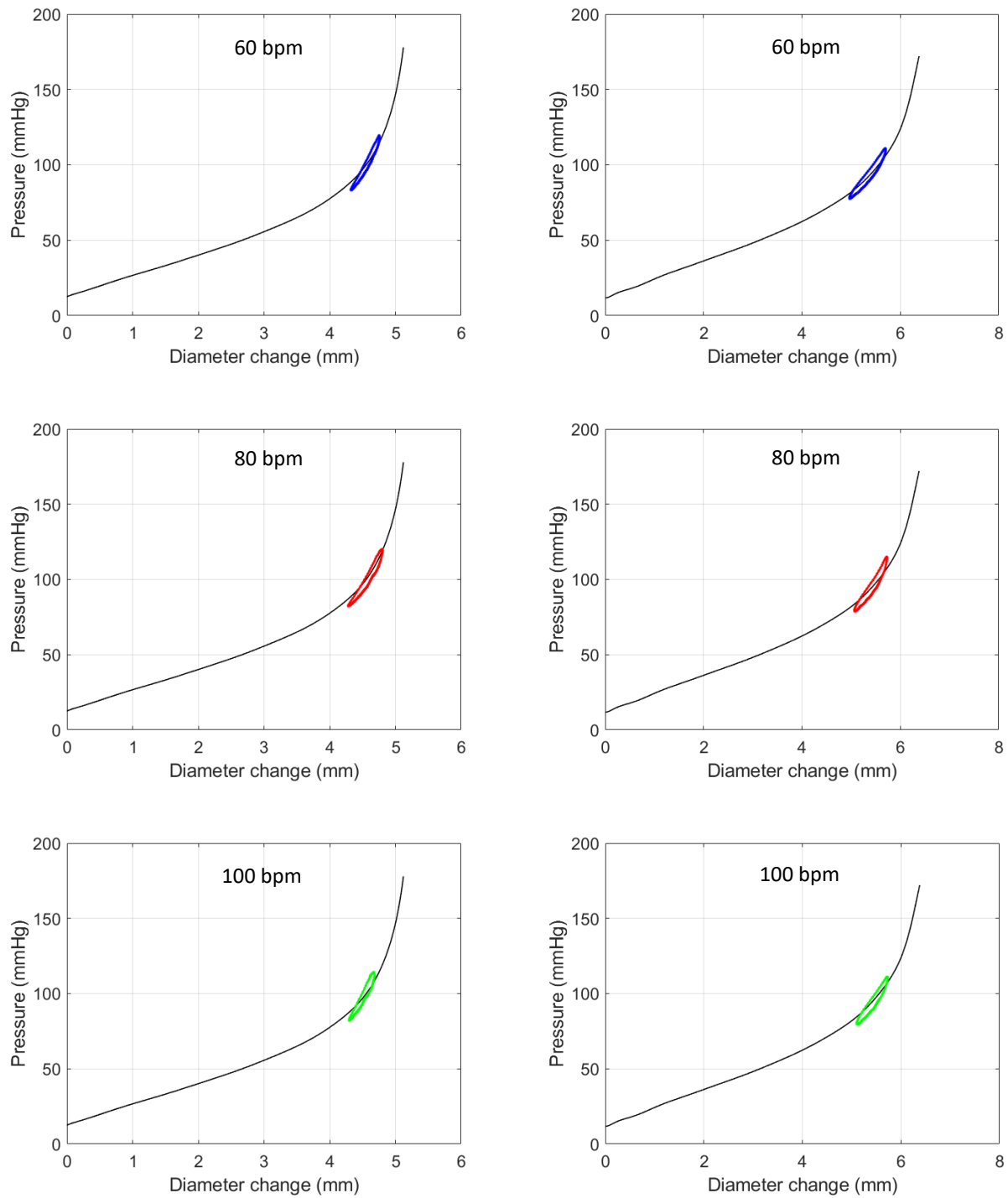


Figure 9. Hysteresis loops (colors) in the diameter change – pressure plane shown together with the quasi-static pressurization curve (black) for three different pulse rates. Left column: donor A. Right column: donor B.

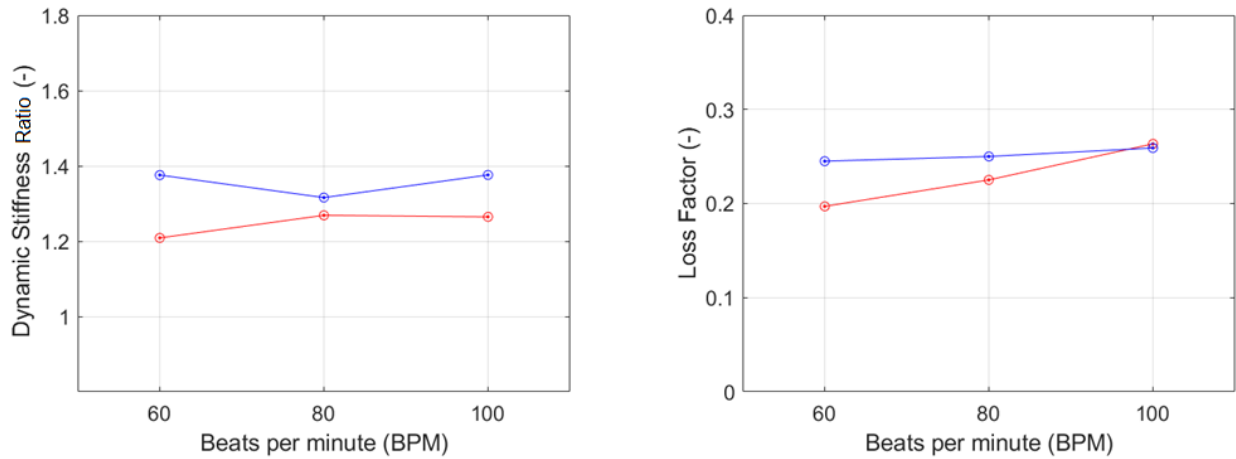


Figure 10. Dynamic stiffness ratio and loss factor versus the pulse rate. —, donor A. —, donor B.

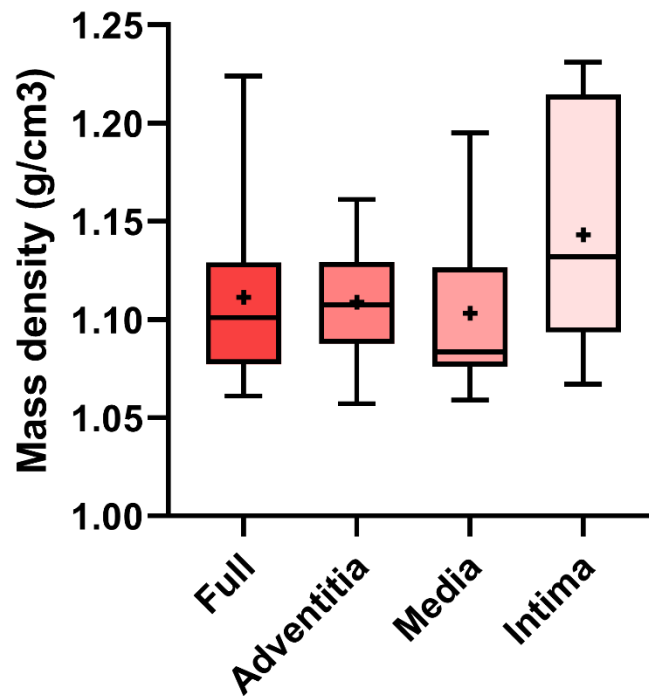


Figure 11. Statistical analysis of the mass density for the full aortic wall, adventitia, media and intima; maximum, minimum, 1<sup>st</sup> quartile, 3<sup>rd</sup> quartile, median (black horizontal line inside the box) and average (cross inside the box) are reported.

Table 3. Mass density ( $\text{g/cm}^3$ ) for each layer and for the full wall of human descending thoracic aortas; SD = standard deviation. Ten different samples were measured.

Layer	Average $\pm$ SD	Donor									
		1	2	3	4	5	6	7	8	9	10
Full	1.11 $\pm$ 0.05	1.10	1.12	1.08	1.08	1.22	1.06	1.11	1.10	1.07	1.17
Adventitia	1.11 $\pm$ 0.03	1.16	1.09	1.09	1.11	1.12	1.06	1.15	1.12	1.08	1.10
Media	1.10 $\pm$ 0.04	1.12	1.08	1.12	1.06	1.08	1.08	1.08	1.20	1.07	1.15
Intima	1.14 $\pm$ 0.06	1.11	1.23	1.07	1.15	1.10	1.11	1.16	1.07	1.21	1.22

## 5. Conclusions

Experimental results show that clamping the aortic segment to the supports in the mock circulatory loop does not alter the static and dynamic diameter expansion under static and pulsatile pressure and flow, except for a very short length close to each support. Since the aorta in the human body does not elongate during the heart beating and presents an axial pre-stretch, the clamping does not alter also the axial deformation. The study shows that it is very useful to carry on both quasi-static and dynamic tests on the aortic segment installed in the mock circulatory loop since it allows to obtain the dynamic stiffness ratio. This is an important viscoelastic parameter which indicates the stiffness increase of the aortic wall subjected to a physiological dynamic pressure load with respect to a static pressure load. The tests on the mock circulatory loop were limited to two donors since the main goal was to introduce a method to identify the dynamic stiffness ratio. Future studies could provide additional data that can be used for a statistical analysis and to study the effect of age.

Finally, this study also provides precise layer-specific measurement of the mass density of the intact human aortic wall and its three layers. Similar experimental data is not available in the literature and is necessary in numerical models. Results show average values of the mass density very similar for the full wall, media and adventitia (about 1.11 g/cm<sup>3</sup>), while the intima has slightly larger average value (1.14 g/cm<sup>3</sup>), but no statistical difference from the other layers was observed.

### Acknowledgements

The authors acknowledge the financial support of the NSERC Discovery Grant and the NSERC RTI grant. *Transplant Québec* provided the aortas used in the experiments. Ali Kassab helped with the sample preparation.

### CRedit authorship contribution statement

Giulio Franchini: Writing – original draft, Writing – review & editing, Visualization, Investigation, Data curation. Francesco Giovanniello: Writing – review & editing, Investigation. Marco Amabili: Writing – review & editing, Writing – original draft, Supervision, Methodology, Funding acquisition, Formal analysis, Data curation, Conceptualization.

### References

Agrafiotis, E., Geith, M.A., Golkani, M.A., Hergesell, V., Sommer, G., Spiliopoulos, S., Holzapfel, G.A., 2021. An active approach of pressure waveform matching for stress-based testing of arteries. *Artificial Organs* 45(12), 1562-1575.

- Amabili, M., Arena, G.O., Balasubramanian, P., Breslavsky, I.D., Cartier, R., Ferrari, G., Holzapfel, G.A., Kassab, A., Mongrain, R., 2020c. Biomechanical characterization of a chronic Type A dissected aorta. *J. Biomechanics* 110, 109978.
- Amabili, M., Asgari, M., Breslavsky, I.D., Franchini, G., Giovanniello, F., Holzapfel, G.A., 2021. Microstructural and mechanical characterization of the layers of human descending thoracic aortas. *Acta Biomaterialia* 134, 401-421.
- Amabili, M., Balasubramanian, P., Bozzo, I., Breslavsky, I., Ferrari, G., 2019a. Layer specific hyperelastic and viscoelastic characterization of human descending thoracic aortas. *J. Mech. Behavior Biomed. Mater.* 99, 27–46.
- Amabili, M., Balasubramanian, P., Bozzo, I., Breslavsky, I., Ferrari, G., Franchini, G., Giovanniello, F., Pogue, C., 2020a. Nonlinear dynamics of human aortas for material characterization. *Phys. Rev. X* 10, 011015.
- Amabili, M., Balasubramanian, P., Breslavsky, I., 2019b. Anisotropic fractional viscoelastic constitutive models for human descending thoracic aortas. *J. Mech. Behavior Biomed. Mater.* 99, 186–197.
- Amabili, M., Balasubramanian, P., Ferrari, G., Franchini, G., Giovanniello, F., Tubaldi, E., 2020b. Identification of viscoelastic properties of Dacron aortic grafts subjected to physiological pulsatile flow. *J. Mech. Behavior Biomed. Mater.* 110, 103804.
- Armentano, R.L., Barra, J.G., Levenson, J., Simon, A., Pichel, R.H., 1995. Arterial wall mechanics in conscious dogs. Assessment of viscous, inertial, and elastic moduli to characterize aortic wall behavior. *Circ. Res.* 76, 468–478.
- Armentano, R.L., Barra, J.G., Pessana, F.M., Craiem, D.O., Graf, S., Santana, D.B., Sanchez R.A., 2007. Smart smooth muscle spring-dampers. Smooth muscle smart filtering helps to more efficiently protect the arterial wall. *IEEE Eng. Med. Biol. Mag.* 26, 62–70.
- Bazilevs, Y., Calo, V.M., Hughes, T.J.R., Zhang, Y., 2008. Isogeometric fluid-structure interaction: theory, algorithms, and computations. *Computational Mechanics* 43, 3–37.
- Breslavsky, I.D., Amabili, M., 2018. Nonlinear model of human descending thoracic aortic segments with residual stresses. *Biomechanics and Modeling in Mechanobiology* 17, 1839-1855.
- Breslavsky, I.D., Franchini, G., Amabili, M., 2020. Effect of fiber exclusion in uniaxial tensile tests of soft biological tissues. *J. Mech. Behavior Biomed. Mater.* 112, 104079.
- Chandra, S., Raut, S. S., Jana, A., Biederman, R. W., Doyle, M., Muluk, S. C., Finol, E. A., 2013. Fluid-structure interaction modeling of abdominal aortic aneurysms: the impact of patient-specific inflow conditions and fluid/solid coupling. *J. Biomechanical Engineering* 135, 81001.
- Damughatla, A.R., Raterman, B., Sharkey-Toppen, T., Jin, N., Simonetti, O.P., White, R.D., Kolipaka, A., 2015. Quantification of aortic stiffness using MR Elastography and its comparison to MRI-based pulse wave velocity. *J. Magn. Reson. Imaging* 41, 44–51.
- Di Giuseppe, M., Alotta, G., Agnese, V., Bellavia, D., Raffa, G.M., Vetri, V., Zingales, M., Pasta, S., Pilato, M., 2019. Identification of circumferential regional heterogeneity of ascending thoracic aneurysmal aorta by biaxial mechanical testing. *J. Mol.Cell. Cardiol.* 130, 205–215.
- Ferrari, G., Balasubramanian, P., Tubaldi, E., Giovanniello, F., Amabili, M., 2019. Experiments on dynamic behaviour of a Dacron aortic graft in a mock circulatory loop. *J. Biomechanics* 86, 132-140.
- Franchini, G., Breslavsky, I.D., Holzapfel, G.A., Amabili, M., 2021. Viscoelastic characterization of human descending thoracic aortas under cyclic load. *Acta Biomaterialia* 130, 291-307.

- Franchini, G., Breslavsky, I.D., Giovanniello, F., Kassab, A., Holzapfel, G.A., Amabili, M., 2022. Role of smooth muscle activation in the static and dynamic mechanical characterization of human aortas. *PNAS* 119(3), e2117232119.
- Fung, Y. C., 1997. *Biomechanics: Circulation*. Springer, New York, 2nd ed.
- Holzapfel, G.A., Ogden, R.W., Sherifova, S., 2019. On fibre dispersion modelling of soft biological tissues: a review. *Proc. Royal Soc. London A* 475, 20180736.
- Horný, L., Netušil, M., Voňavková, T., 2014. Axial prestretch and circumferential distensibility in biomechanics of abdominal aorta. *Biomech. Model. Mechanobiol.* 13, 783–799.
- Imura, T., Yamamoto, K., Satoh, T., Kanamori, K., Mikami, T., Yasuda, H. 1990. In vivo viscoelastic behavior in the human aorta. *Circ. Res.* 66, 1413–1419.
- International Commission on Radiological Protection, 2009. Adult reference computational phantoms. *ICRP Publication 110, Ann. ICRP* 39(2), 48-51. (see Table A.1. at p. 48)
- Jayendiran, R., Nour, B., Ruimi, A., 2018. Computational fluid–structure interaction analysis of blood flow on patient-specific reconstructed aortic anatomy and aneurysm treatment with Dacron graft. *Journal of Fluids and Structures* 81, 693-711.
- S. Pejčić, S., Najjari, M.R., Bisleri, G., Rival, D.E., 2021. Characterization of the dynamic viscoelastic response of the ascending aorta imposed via pulsatile flow. *J. Mech. Behavior Biomed. Mater.* 118, 104395.
- Safar, M.E., 2018. Arterial stiffness as a risk factor for clinical hypertension. *Nat. Rev. Cardiol.* 15, 97-105.
- Sassani, S.G., Kakisis, J., Tsangaris, S., Sokolis, D.P., 2015. Layer-dependent wall properties of abdominal aortic aneurysms: Experimental study and material characterization. *J. Mech. Behavior Biomed. Mater.* 49 141–161.
- Schaafs, L.-A., Tzschätzsch, H., Reshetnik, A., van der Giet, M., Braun, J., Hamm, B., Sack, I., Elgeti, T., 2019. Ultrasound time-harmonic elastography of the aorta: effect of age and hypertension on aortic stiffness. *Invest. Radiol.* 54, 675-680.
- Valdez-Jasso, D., Bia, D., Zócalo, Y., Armentano, R. L., Haider, M.A., Olufsen, M.S., 2011. Linear and nonlinear viscoelastic modeling of aorta and carotid pressure–area dynamics under in vivo and ex vivo conditions. *Annals Biomed. Eng.* 39, 1438–1456.
- Valdez-Jasso, D., Haider, M.A., Banks, H.T., Santana, D.B., Germán, Y.Z., Armentano, R.L., Olufsen, M.S., 2009. Analysis of viscoelastic wall properties in ovine arteries. *IEEE Trans. Biomed. Eng.* 56, 210–219.
- Weisbecker, H., Pierce, D.M., Regitnig, P., Holzapfel, G.A., 2012. Layer-specific damage experiments and modeling of human thoracic and abdominal aortas with non-atherosclerotic intimal thickening, *J. Mech. Behavior Biomed. Mater.* 12, 93–106.
- Yang, Z., Ma, Z., Liu, S., Li, J., 2021. Tissue adhesion with tough hydrogels: Experiments and modeling. *Mechanics of Materials* 157, 103800.



## **Chapter 4**

# **Role of smooth muscle activation in the static and dynamic mechanical characterization of Human aortas**

Giulio Franchini<sup>1</sup>, Ivan D. Breslavsky<sup>1</sup>, Francesco Giovanniello<sup>1</sup>, Ali Kassab<sup>1,2</sup>, Gerhard A. Holzapfel<sup>3,4</sup>,  
Marco Amabili<sup>1,5</sup>

- (1) Department of Mechanical Engineering, McGill University, Montreal, Canada
- (2) Research Center, Centre Hospitalier Universitaire de Montréal (CHUM), Université de Montréal, Montreal, Canada
- (3) Institute of Biomechanics, Graz University of Technology, Austria
- (4) Department of Structural Engineering, Norwegian University of Science and Technology, Trondheim, Norway
- (5) Dipartimento di Ingegneria e Architettura, University of Parma, Parma, Italy

Keywords: smooth muscle; activation; human aorta; mechanical characterization; experiments.

### **Abstract**

The rupture of aortic aneurysms causes around 10,000 deaths each year in the USA. Surgical repair of aortic aneurysms and aortic dissections absorbs significant healthcare resources. Prosthetic tubes, currently used for aortic repair, present a large mismatch of mechanical properties with the natural aorta, which has negative consequences for perfusion. This motivates research into the mechanical characterization of human aortas in order to develop a new generation of mechanically compatible aortic grafts. Experimental data and a suitable material model for human aortas with smooth muscle activation are not available in the literature despite the need for developing advanced grafts; the present study closes this gap. Mechanical characterization of human descending thoracic aortas was performed with and without vascular smooth muscle (VSM) activation. Specimens were taken from 13 heart-beating donors. The aortic segments were cooled in Belzer UW solution during transport and tested within a few hours after explantation. VSM activation was achieved through the use of potassium depolarization and noradrenaline as vasoactive agents. In addition to isometric activation experiments, the quasi-static passive and active stress-strain curves were obtained for circumferential and longitudinal strips of the aortic material. This characterization made it possible to create an original mechanical model of the

active aortic material that exactly fits the experimental data. The dynamic mechanical characterization was executed using cyclic strain at different frequencies of physiological interest. An initial pre-stretch, which corresponded to the physiological conditions, was applied before cyclic loading. Dynamic tests made it possible to identify the differences in the viscoelastic behavior of the passive and active tissue. This work illustrates the importance of VSM activation for the static and dynamic mechanical response of human aortas. Most importantly, this study provides material data and a material model for the development of a future generation of active aortic grafts that mimic natural behavior and help regulate blood pressure.

## Article

The rupture of aortic aneurysms causes around 10,000 deaths each year in the USA [1]. Surgical repair of aortic aneurysms and aortic dissections absorbs significant healthcare resources [2]. Prosthetic tubes made of polyester (Dacron) or polytetrafluoroethylene (PTFE) are often used for surgical repair of large arteries in aneurysms or acute dissection. Unfortunately, these grafts are so stiff to diameter expansion [3] that they can cause cardiovascular and perfusion problems because they fail to reduce the highly pulsatile nature of the blood flow exiting the heart. This is the reason for an increasing interest in the development of a new generation of grafts [4] in innovative biomaterials or in tissue engineering that mimic the dynamic behavior of the aorta, which is achieved through the correct adjustment of mechanical properties and the introduction of a layered design. Arteries respond to vasoactive chemical stimuli by varying their mechanical properties and diameter due to vascular smooth muscle (VSM) activation; this helps in regulating blood pressure [5]. The present authors envision a future generation of aortic grafts based on tissue engineering that mechanically respond to vasoconstrictors to maintain this function. To achieve this result, it is first necessary to investigate the relationship between VSM activation and the mechanical properties of the aorta and to develop a suitable model of the active mechanical response for the graft design. Since the VSM is mainly located in the tunica media (some cells can infiltrate the intima and adventitia with increasing age), the activation strain can be attributed to this aortic layer. Experimental data and a suitable material model for human aortas with smooth muscle activation are not available in the literature despite the need for the development of advanced grafts. This appears to be due to the difficulty of obtaining suitable human samples. In fact, VSM activation is only possible for a small number of hours after the explantation from a heart-beating donor (i.e. donor in intensive care unit with neurological determination of death) and when the tissue is kept refrigerated in organ preservation solution all the time before testing. Hence, the present study has significant novelty, providing experimental data that has never been obtained before. These data made it possible to create a precise structure-based model of the active aortic tissue and to identify the corresponding material parameters.

The passive (i.e. without VSM activation) quasi-static mechanical properties of the intact wall of the human aorta and its three individual layers have been extensively investigated experimentally. In particular, uniaxial extension tests were carried out on strips (cut in the

circumferential and longitudinal directions) from the intact wall or separated layers [6-9] and biaxial tests on squares and cruciform samples of aortic tissue [10,11] were conducted. The microstructure of the collagen and elastin fiber distributions in the three layers was also examined in detail using second-harmonic generation and two-photon excited fluorescence microscopy [9,10,12]. Along with the progress of experiments, advanced structure-based material models have also been refined. It was assumed that a ground substance/elastin matrix is reinforced by collagen fibers. The orientations and dispersions of the collagen fiber identified from experiments were taken into account in the more advanced models [13-15]. The passive dynamic material properties (also referred to as viscoelastic) of the human aortas, on the other hand, are much less studied. The experiments were performed on a mock circulatory loop under physiological pulsatile pressure and flow [3,16] and on strips of thoracic descending aortas [8,17]. Viscoelastic models have been developed [18,19], but they can only partially describe the experimental results. Experimental data show that the aorta stiffens with increasing age [8,9,11], which favors hypertension [20].

The active (i.e. with VSM activation), quasi-static mechanical characterization of arteries has been less studied than its passive counterpart. The number of studies on human samples is very limited [21, 22] and none have been found on large arteries. Vasoactive agents commonly used to induce VSM contraction are potassium depolarization (KCl) [23], noradrenaline [22], norepinephrine [21], phenylephrine [24]. By using different concentrations of agents, different degrees of activation can be achieved. In previous studies, two methodologies of activation experiments were carried out: (i) pressurization of arterial segments [21, 24-29], and (ii) extension tests on arterial strips and rings [5, 22, 30-32]. Experiments on strips and rings can be isometric, in which the sample is constantly stretched and the increase in force from the passive to the active state is measured [5]; these are the typical experiments that are carried out on a myograph [22]. In isobaric experiments performed on arterial segments, the pressure and axial stretch are fixed; activation of the VSM leads to a reduction in diameter [5]. Approximation formulas allow the change in diameter to be linked to the arterial stiffness. Another type of experiment can be performed to measure the force-displacement curve (then converted to stress-strain) in the case of VSM activation by following a similar procedure used for passive mechanical characterization [6-9]. A comparison of the active and passive curves gives the mechanical characteristics of the VSM activation. Excluding [5, 28, 30], a literature review shows that activation was only measured in the circumferential direction. Indeed, the orientation of VSM cells in arteries has usually been

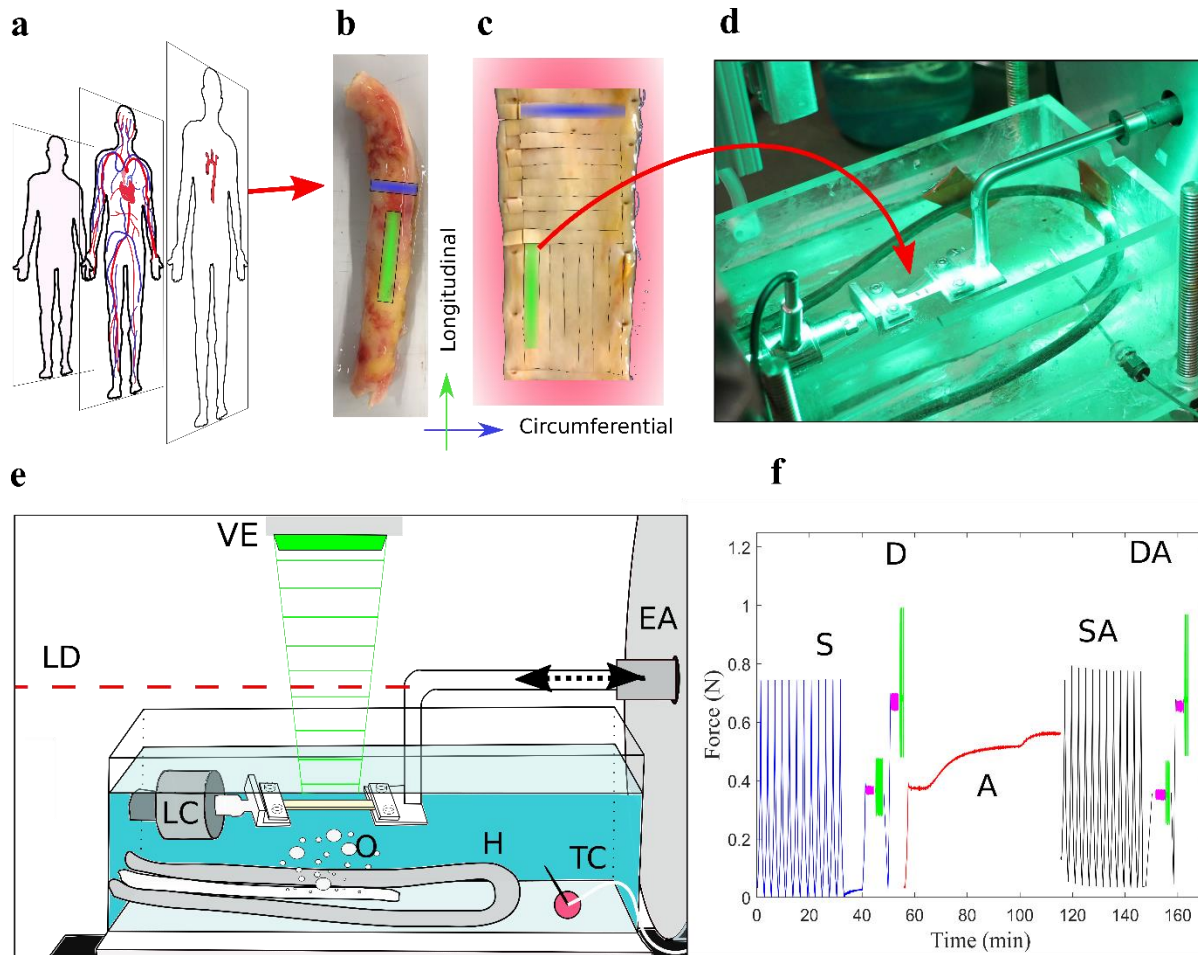


**Figure 4. Specimen preparation and experimental setup.** **a** Position of the thoracic aorta in the human body. **b** Descending thoracic aorta from donor IV with indication of circumferential (blue) and longitudinal (green) strips. **c** Aorta from donor IV opened with a longitudinal cut on the posterior side. Circumferential and longitudinal strips are cut with a punch. **d** Photo of the experimental setup for quasi-static and dynamic uniaxial tensile tests with the thermal control, the strip holders and the aortic strip installed. **e** Scheme of the experimental setup. VE, video extensometer; LD, laser Doppler sensor; EA, electrodynamic actuator; LC, load cell; O, tube carrying oxygen (O<sub>2</sub>) for bubbling the solution; H, heater; TC, temperature control. **f** Typical phases of an experiment on a strip described by the measured force (N) versus time (in minutes). S, quasi-static mechanical characterization of the passive strip reaped several times to achieve pre-conditioning; D, dynamic tests on the passive strip with harmonic loading at two levels of pre-load performed at frequencies from 1 to 5 Hz; A, isometric activation of the strip, first with KCl, followed by noradrenaline; SA, quasi-static mechanical characterization of the active strip; DA, dynamic tests on the active strip with harmonic loading at two levels of pre-load carried out at frequencies from 1 to 5 Hz.

believed to be almost circumferential; the present study shows that this is not the case with the descending thoracic aorta in humans. A detailed literature review on the active mechanical characterization and material modeling of activated arteries is contained in Supplementary Note 1. Mechanical models of the mechanical response of active arteries have been developed [5, 14, 33-39], but generally only consider activation in the circumferential direction. There are two exceptions: the model in [5] introduces independent activation stresses in the circumferential and

axial directions; another study [38] considers two helically arranged symmetric families of VSM without fiber dispersion.

In the present study, the active and passive mechanical characterization of the human descending thoracic aortas was performed on specimens from 13 heart-beating donors. The aortic segments were cooled in Belzer UW solution during transport and tested within a few hours after explantation. VSM activation was achieved through the use of KCl and noradrenaline as vasoactive agents. In addition to isometric activation experiments, the quasi-static passive and active stress-strain curves for circumferential and longitudinal strips of the aortic material were obtained. This characterization made it possible to build an original mechanical model of the active aortic material that exactly matched the experimental data. The dynamic mechanical characterization was also performed using cyclic strain at different frequencies of physiological interest. An initial pre-stretch, which corresponded to the physiological conditions, was applied before the cyclic loading. Dynamic tests allowed to identify the differences in the viscoelastic behavior of the passive and active tissue. The present study illustrates the importance of VSM activation for the static and dynamic mechanical response of human aortas. Most importantly, it provides material data for the development of a future generation of active aortic grafts that mimic the natural behavior.

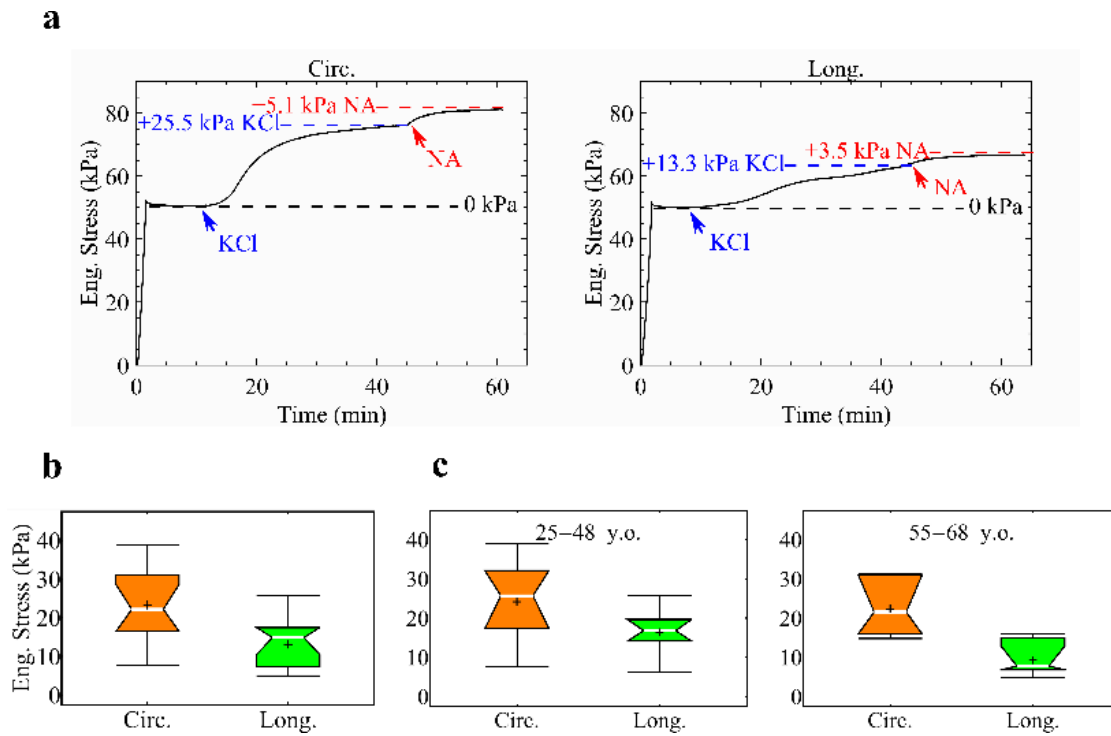


**Figure 2. Isometric activation of aortic strips.** **a** Activation of the circumferential and longitudinal strips from donor VIII as stress developed over time. The time of injection of the vasoactive agent - first KCl, followed by noradrenaline (NA) - is indicated, as well as the corresponding increase in stress. **b** Statistical analysis of the activation stress for the circumferential and longitudinal strips from 13 donors at a pre-stretch corresponding to 50 kPa (engineering stress); maximum, minimum, first quartile, third quartile, median (white horizontal line in the box) and average (+) are reported. **c** Statistical analysis of the activation stress divided into two age groups: 22-48 years (7 donors) and 55-68 years (6 donors)

## Results

Results are presented for 13 descending thoracic aortas from heart-beating donors with 25 to 68 years of age (mean age  $48.6 \pm 14.2$  years). Information on donors can be found in Supplementary Note 2 (Table S1). Figure 1 illustrates the experimental procedure of the mechanical tests. Circumferential and longitudinal strips – about 5 mm wide – were immersed in Krebs-Henseleit buffer solution, bubbled with oxygen and kept at a temperature of 37°C. The time diagram in Figure 1f shows the various phases of each test on a strip that takes just over 2½ hours. First, a passive quasi-static mechanical characterization is carried out, which includes preconditioning, followed by a dynamic characterization with two fixed levels of pre-stress. Isometric VSM activation is then induced at about 50 kPa engineering pre-stress by first using potassium depolarization (KCl, 60 mM), followed by the addition of noradrenaline (18 µM) to achieve the maximum VSM contraction.

A quasi-static mechanical characterization with preconditioning followed by a dynamic characterization at the same two pre-stress levels is carried out on the tissue with VSM activation. The measured stresses versus time corresponding to the isometric activation are presented in Figure 2a for the strips of donor VIII in both directions. The time of insertion of each vasoactive agent is indicated by an arrow. The results for all samples are shown in the Supplementary Note 3. A statistical analysis of the activation stresses for all circumferential and all longitudinal strips together and divided into two age groups (25-48 years; 55-68 years) is presented in Figures 2b,c. While results show larger activation stresses for the circumferential strips (median of all donors 22.2 kPa), the activation stress in the longitudinal direction is also significant (median of all donors 14.9 kPa), which is only 33 % smaller than that in the circumferential direction; this is a novel result. The activation stress seems to decrease with age. The median for the circumferential strips decreases from 25.7 (25-48 years) to 21.6 kPa (55-68 years); for the longitudinal strips the median is reduced from 16.8 (25-48 years) to 7.8 kPa (55-68 years). An ANOVA test indicates a clear statistical difference between the two age groups for the activation stress of the longitudinal strips (p-value 0.0391), while for the circumferential strips likely there is no difference (p-value 0.7274).

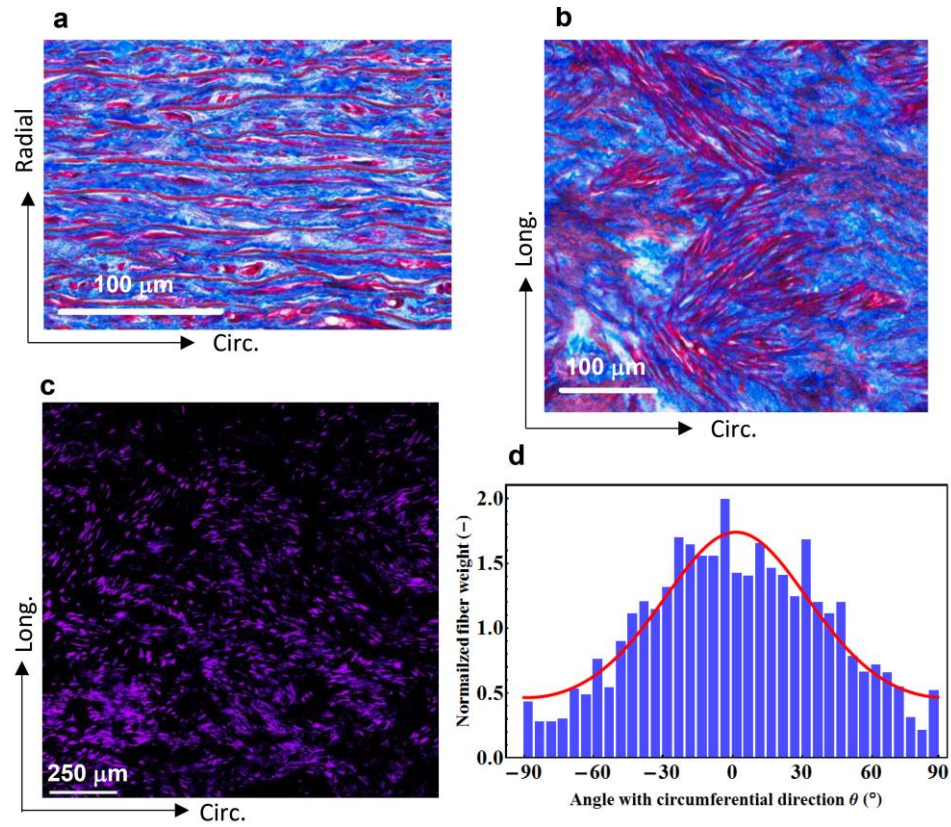


**Figure 3. Microstructural analysis of tunica media.** **a** Cross section (5  $\mu\text{m}$  thick) with Masson trichrome stain (VSM in red) from donor IV. **b** In-plane section (5  $\mu\text{m}$  thick) with Masson trichrome stain (VSM in red) from donor IV. **c** In-plane section with DRAQ5 stain (nuclei of VSM in violet) from donor VIII. **d** Histogram showing the distribution of the VSM directions from image c with the red line of the fitted Poisson distribution; dispersion coefficient  $\kappa_{IP}^{VSM} = 0.343$ .

## **Microstructural characterization.**

In order to elucidate the mechanism of activation both in the circumferential and in the longitudinal direction, the distribution of the VSM cell orientations in the tunica media of donors IV and VIII is examined in Figure 3.

Traditional histology with Masson trichrome stain is shown first in Figure 3a for a cross-section (i.e. through the thickness) and in Figure 3b for an in-plane section (i.e. parallel to the strip surface). While the VSM cells (red in Masson-stained section) appear well organized with parallel fibers in the cross-section, the directional distribution in an in-plane section is quite dispersed. In order to quantify the dispersion of the VSM cell orientation, in-plane sections were stained with DRAQ5 (1/1000, 30 min) in order to make nuclei in VSM cells visible. The tissue was excited by a laser at 638 nm and light was captured above 650 nm with a Leica confocal microscope. The nuclei appear violet in the image in Figure 3c, and since they are elongated, their direction distribution is evaluated by an image-processing code [9], which gives the histogram of the in-plane dispersion. The histogram in Figure 3d shows that the VSM is dispersed, with a peak in the orientation distribution in the circumferential direction. Additional results on the microstructural characterization are presented in the Supplementary Note 4, which shows a larger dispersion of the VSM distribution for a different aorta. The microstructural analysis justifies the observed activation in both directions with a larger force in the circumferential direction.

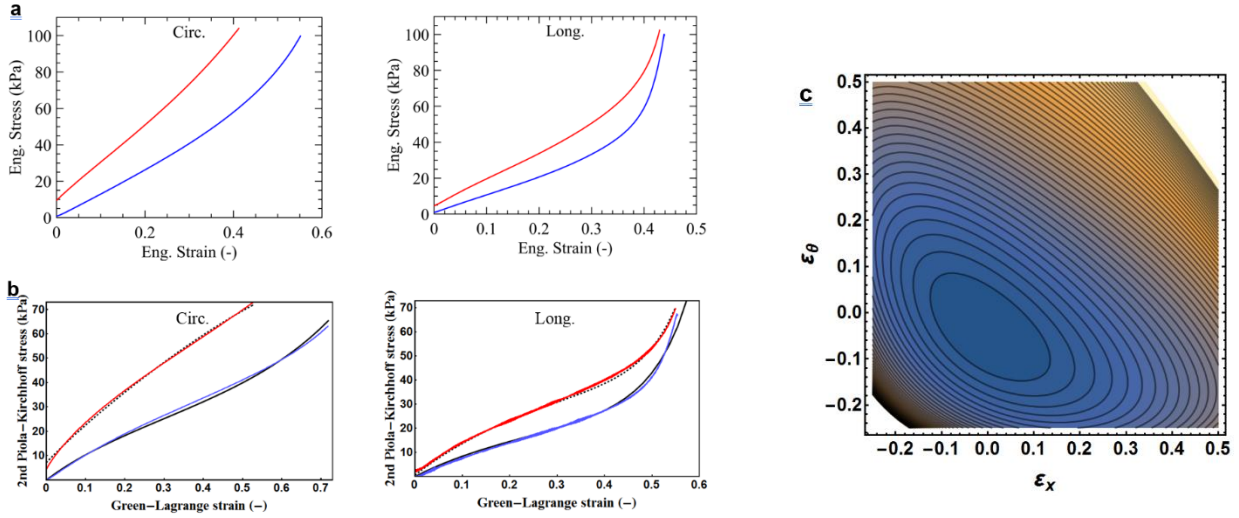


**Figure 4. Quasi-static mechanical characterization and material model.** **a** Stress-strain curves (engineering stress and engineering strain) from quasi-static uniaxial tensile tests on active (red) and passive (blue) circumferential and longitudinal strips from donor VIII. **b** Stress-strain curves (second Piola-Kirchhoff stress and Green-Lagrange strain) from experiments on active (red) and passive (blue) strips from donor VIII and active (black dashed) and passive (black) material model with identified parameters. **c** Contour plot of the strain-energy function  $W$  of the active aortic wall for the case of donor VIII without fiber exclusion; the convex contours represent states of constant energy.

## Quasi-static mechanical characterization.

Uniaxial extension tests were carried out after preconditioning at low strain rate to characterize the active and passive static behavior of aortic strips. Figure 4a shows the passive and active engineering stress-strain behavior for the circumferential and longitudinal strips of donor VIII. While the passive curves start from the origin, both active ones have an initial positive stress at the original zero strain due to the VSM contraction. Other features are that the active curves are above the passive ones (i.e. the material is stiffer) and are significantly less curved (more linear). These stress-strain curves allow material parameters to be identified for the active and passive material once a material model has been built. Material parameters of healthy aortic tissues are necessary to design grafts that mimic the mechanical behavior of the native aorta. The stress-strain curves for all strips tested are given in the Supplementary Note 5.

## Mechanical model of the activated tissue.

The strain-energy function  $W$  of the aortic wall is represented as the sum of the passive and active components

$$W = W^P + W^A, \quad (1)$$

where the passive component  $W^P$  is given in [9] and described in the Supplementary Note 6. It is a microstructurally-based model that presents (i) an isotropic term to describe the elastin network and the ground substance, (ii) one family of collagen fibers taking into account their orientation dispersion and (iii) an orthogonal fiber family to describe the cross-link and lateral interaction of the collagen fibers. The active term refers to the activation of the VSM. It is assumed that the fibers of VSM are not perfectly aligned in the circumferential direction, but rather dispersed around the circumferential direction of the aorta in the plane tangent to the middle surface (in-plane) of the strip. In addition to the main family of dispersed VSM, a second orthogonal family with the same dispersion is considered to describe the lateral interaction between VSM fibers; this is due to the interwoven VSM fibers shown in Figure 3b. This second family is assumed to contribute with a minor active stress than the main family. The proposed active strain-energy function is given by

$$W^A = \tilde{K} \sum_{i=1}^2 K_i \left[ E_i^{VSM} + \frac{a_i}{2} (E_i^{VSM})^2 - \frac{b_i}{m_i + 1} (E_i^{VSM})^{m_i + 1} \right], \quad (2)$$

where  $a_i, b_i > 0$ ,  $m_i$  are integer larger than one and

$$E_1^{VSM} = 2 \left[ \kappa_{IP}^{VSM} (\varepsilon_{xx} + \varepsilon_{\theta\theta}) + (1 - 2\kappa_{IP}^{VSM}) \varepsilon_{\theta\theta} \right], \quad (3a)$$

$$E_2^{VSM} = 2 \left[ \kappa_{IP}^{VSM} (\varepsilon_{xx} + \varepsilon_{\theta\theta}) + (1 - 2\kappa_{IP}^{VSM}) \varepsilon_{xx} \right], \quad (3b)$$

while  $\varepsilon_{xx}$  and  $\varepsilon_{\theta\theta}$  are the longitudinal and circumferential normal Green-Lagrange strains, and  $\tilde{K}$  is the activation level coefficient having a value comprised between zero (no activation) and 1 (maximum activation). Equations (3a,b) are inspired by an expression for the bi-dimensional fiber dispersions proposed in [15]. Expression (2) has nine parameters  $K_i, a_i, b_i, m_i, \kappa_{IP}^{VSM}$ . The first term within the brackets in (2) takes into account the stress value at zero principal strain. In particular,  $K_i$  is a stress-like parameter associated with the initial active stress values. Since the initial stress at zero strain is generally different in the axial and circumferential directions, the model captures this feature through the VSM dispersion parameter  $\kappa_{IP}^{VSM}$ . The second term within the brackets in (2) reflects the relatively slow initial growth of the activation stress with strain, which is controlled by the parameter  $a_i$ . The third term represents the rapid decrease in the activation stress after a certain strain value due to a higher power; the slope of this drop is controlled by the two parameters  $b_i$  and  $m_i$ . The integer power  $m_i$  enables the experimentally observed behavior of the difference between the active and passive mechanical response to be reproduced. The optimization procedure for determining the material parameters is shown in the Supplementary Note 6. The dispersion parameter  $\kappa_{IP}^{VSM}$  is obtained by fitting a von Mises probability distribution [9, 15], i.e.

$$\rho_{IP}(\theta) = \frac{\exp[c \cos(2\theta)]}{I_0(c)} \quad (4)$$

to the experimental histogram of the VSM distribution in Figure 3d to obtain the concentration parameter  $c$ ;  $I_0$  is the modified Bessel function of the first kind of order zero. Once a normalization of the area under the distribution (4) is introduced, the dispersion parameter  $\kappa_{IP}^{VSM}$  is given by [9, 15]

$$\kappa_{IP}^{VSM} = \frac{1}{2} - \frac{I_1(c)}{2I_0(c)}, \quad (5)$$

where  $I_1$  is the modified Bessel function of the first kind of order one.  $\kappa_{IP}^{VSM}$  takes on values between 0 for perfectly aligned VSM fibers in the circumferential direction and 0.5 for an isotropic response (*i.e.* identical response in the circumferential and longitudinal directions) of the VSM.

The second Piola-Kirchhoff stresses in the longitudinal and circumferential directions are obtained by

$$S_{xx} = \frac{\partial \hat{W}}{\partial \varepsilon_{xx}}, \quad S_{\theta\theta} = \frac{\partial \hat{W}}{\partial \varepsilon_{\theta\theta}}, \quad (6a,b)$$

where  $\hat{W}$  is the function  $W$  given in (1), in which the incompressibility condition was inserted. In fact, the aortic tissue is generally considered incompressible [40]. One of the two stresses in equations (6a,b) is zero in uniaxial extension tests. This introduces a relationship that is used to link the strains. It is important to note that because of this link, the active term  $W^A$  depends on the passive one  $W^P$ . This means that the model takes into account the passive mechanical response of the tissue in order to obtain the activation stress. Fibers that are under compression must be excluded in equations (6,a,b) [41].

The parameters of the active and passive material model of all the tested aortas are given in the Supplementary Note 6 (Tables S2 and S3). It is interesting that these material parameters were obtained from experiments with maximum activation of the VSM, i.e. with  $\tilde{K} = 1$ . To obtain lower levels of activation corresponding to lower concentrations of vasoactive agents, reduced values of  $\tilde{K}$  should be used while maintaining the same material parameters.

The comparison between the material model and the experimental characterization of the aortic tissue of donor VIII is presented in Figure 4b (note the change in the shape of the curves with respect to 4a due to different stress and strain definitions), where the VSM dispersion parameter  $\kappa_{IP}^{VSM} = 0.343$  was obtained from Figure 3d. The comparison of the experimental results and the model (with the identified material parameters) in Figure 4b is very satisfactory for both passive and active behavior. The convexity of the strain-energy function (1) has been verified numerically for the studied cases. The contour plots of  $W$  are presented in Figure 4c for the active case of donor VIII and they are convex.

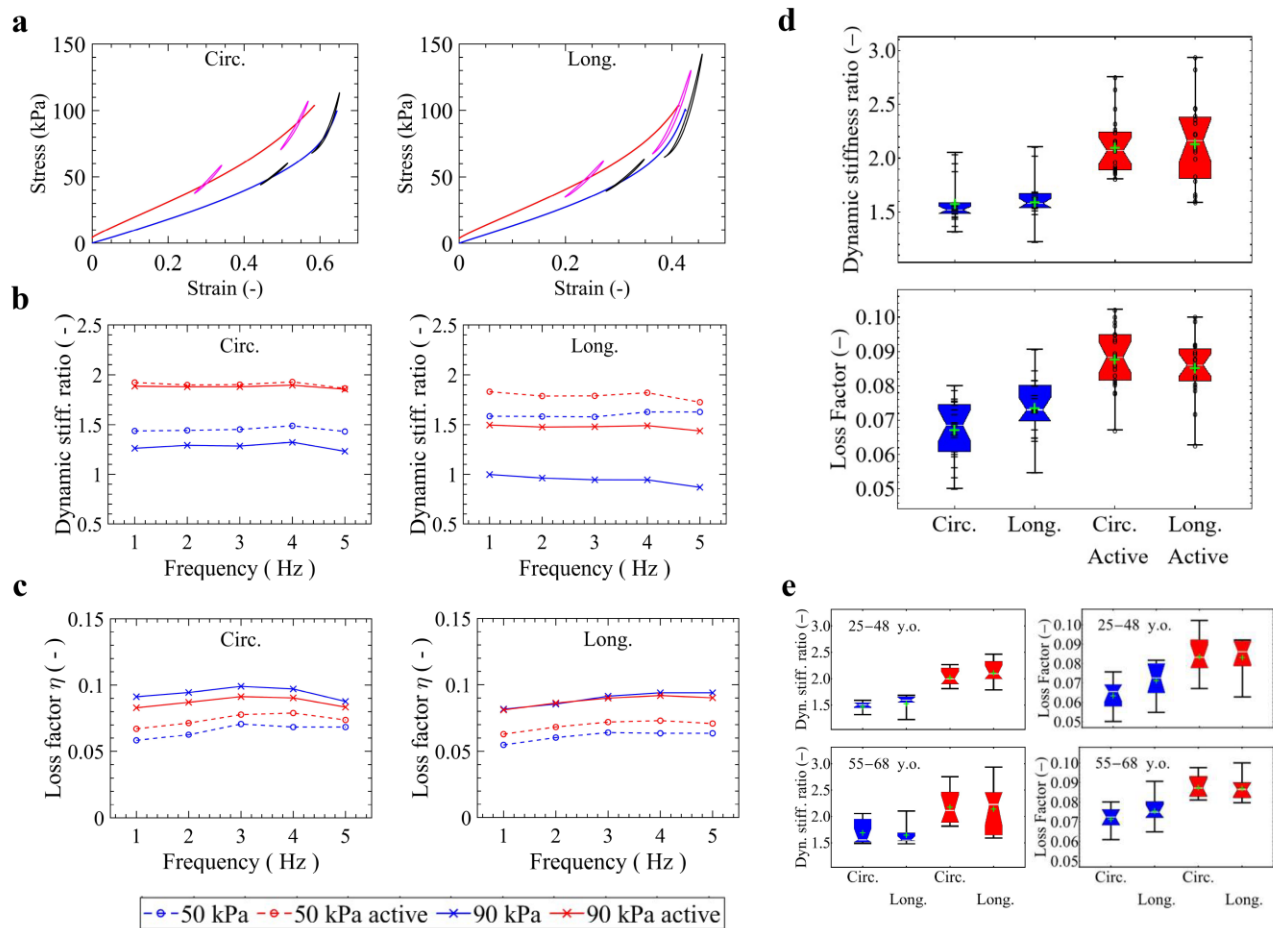


**Figure 5. Dynamic characterization of active and passive aortic strips.** **a** Hysteresis loops at 1 Hz (active = magenta; passive = black) superimposed to the quasi-static uniaxial tensile tests (active = red; passive = blue) of the circumferential and longitudinal strips from donor IV. Engineering stress versus engineering strain is given. Two cycles at different initial pre-stretches corresponding to about 50 and 90 kPa for the midpoint of the loop were measured. The amplitude of each cycle was about 0.07 in strain. **b** Dynamic stiffness ratio versus frequency for the circumferential and longitudinal strips from donor IV for the two pre-stress levels (1<sup>st</sup> level 50 kPa; 2<sup>nd</sup> level 90 kPa). Active = red; passive = blue. **c** Loss factor versus frequency. **d** Statistical analysis of the dynamic stiffness ratio and loss factor at 1 and 3 Hz for the active (red) and passive (blue) circumferential and longitudinal strips from 11 donors at a pre-stretch corresponding to 50 kPa (engineering stress); maximum, minimum, first quartile, third quartile, median (white horizontal line in the box) and average (+) are reported. **e** Statistical analysis of the dynamic stiffness ratio and loss factor at 1 and 3 Hz for the circumferential and longitudinal strips from the donors, divided into two age groups (25-48 years and 55-68 years) at a pre-stretch corresponding to 50 kPa; active (red), passive (blue).

## Dynamic mechanical characterization.

Due to the viscoelastic behavior, the mechanical response of the aortic tissue to dynamic loading is different than to quasi-static loading. The aorta is subjected to cyclic pulsatile pressure at a frequency in the range of 1 to about 3 Hz (i.e. 60 to 180 beats per minute). The pulsatile pressure is not harmonic [3], but can be expanded in a Fourier series with harmonic components. In this study, the strips were loaded by a harmonic cyclic strain with an amplitude of 7 % of their length. The loading frequencies used in the tests were set from 1 to 5 Hz in 1 Hz steps. Two dimensionless parameters are introduced to describe the viscoelastic behavior: (i) the dynamic stiffness ratio, which describes the stiffness increase of the tissue under harmonic loading in relation to quasi-static loading; (ii) the loss factor, which is the percentage of energy loss in a cycle with respect to the elastic energy stored in a quarter of the cycle. Mathematical definitions are given in the Supplementary Note 7.

Figure 5a shows the hysteresis loops at 1 Hz superimposed on the quasi-static uniaxial extension tests of the active and passive circumferential and longitudinal strips of donor IV. Cycles were performed at two different initial pre-stress levels, 50 and 90 kPa (engineering stress) for the center of the loop of each strip. The dynamic stiffness ratio and loss factor versus frequency for the active and passive circumferential and longitudinal strips of donor IV for the two pre-stress levels are given in Figures 5b,c. The results show that both viscoelastic parameters are hardly influenced by the frequency in the studied range. The dynamic stiffness ratio increases significantly for the active strips for both pre-stress levels, while the loss factor increases for the two active strips for the first pre-stress level (50 kPa). This level is a good representation of the physiological condition, as described in the Supplementary Note 8; therefore this level is chosen to present a statistical analysis for all strips tested (11 of the 13 aortas were also tested dynamically; the results are presented in Tables S3 and S4 in the Supplementary Note 8).

Figure 5d shows a statistical analysis of the dynamic stiffness ratio and the loss factor at 1 and 3 Hz (combined) for the circumferential and longitudinal strips from 11 donors at 50 kPa pre-stress. The median of the dynamic stiffness ratio increases from 1.52 (passive) to 2.07 (active) in the circumferential direction (36 % increase); it increases from 1.58 (passive) to 2.16 (active) in the longitudinal direction (37 % increase). This shows that the increase in both directions is significant and almost identical, which in turn confirms that the activation in the longitudinal direction is very relevant. The median of the loss factor increases from 0.0686 (passive) to 0.0883

(active) in the circumferential direction (29% increase) and from 0.0730 (passive) to 0.0861 (active) in the longitudinal direction (18% increase). ANOVA tests strongly confirm that dynamic stiffness ratio and loss factor are statistically different before and after activation for both directions ( $p < 3.910^{-5}$  in the four tests, rejecting the hypothesis of no difference). Figure 5e presents a statistical analysis of the viscoelastic parameters that divide the donors into two age groups: 25-48 and 55-68 years. Both age groups show a significant increase in both viscoelastic parameters with active strips. ANOVA tests suggest that likely there are no age-associated differences for the active viscoelastic parameters.

## **Discussion**

In summary, the results show that VSM activation has a significant quasi-static stiffness increase of the descending thoracic aortic tissue in both the circumferential and longitudinal directions. This effect diminishes with age in longitudinal direction. A microstructural analysis of the VSM cells in the tunica media confirms their dispersion in the plane parallel to the aortic surface, while in a section through the thickness of the aortic wall they are well organized and parallel to the surface. An accurate material model was developed for the active tissue and the material parameters were identified from experiments. Harmonic cyclic loading show that the viscoelastic material properties of the aortic tissue increase significantly with the VSM activation. Since activation of the VSM is relevant to the mechanics and physiology of the aorta [5, 42], the experimental data and material model presented in this study could be used to design and develop a mechanically compatible active aortic graft.

## **Methods**

### **Ethics.**

This research on human samples has been approved by the Ethics Committee of McGill University.

### **Sample preparation.**

Descending thoracic aortas from 13 heart-beating donors, with age from 25 to 68 years (mean age  $48.6 \pm 14.2$  years) were studied. They were collected during a transplant organ donation under a research agreement with *Transplant Québec*, which is the transplant coordinator agency in Québec, Canada. The donors were maintained heart-beating after neurological determination of death. All aortas were maintained in Belzer UW organ preservation solution at 4°C prior to testing. The tissue preparation for experiments consisted of: (i) removal of the periaortic connective tissue and arterial branches; (ii) excising the aorta longitudinally at the posterior part between the pair of tiny holes that remain after the intercostal arteries are removed; (iii) obtaining longitudinal and circumferential strips of approximate dimensions  $5 \times 35$  mm with a punch of 5 mm wide. The thickness and width of the strips were measured with a Micro-Epsilon triangulation laser sensor

(model optoNCDT1402) and caliper at five different locations in order to obtain the cross-sectional area.

Histological analysis was performed on the same strips used in mechanical experiments after discharging the parts in contact with the grips. Samples were processed at the GCRC histology core of McGill University. The tissues were dehydrated in 70% ethanol, processed in a Sakura Tissue-Tek vacuum infiltration processor model VIP 6-AI by treating with ethanol, xylene and paraffin according to a specific protocol. A Leica EG1150 was used for the embedding process. A Leica RM2255 microtome picked up 5  $\mu\text{m}$ , 10  $\mu\text{m}$  and 20  $\mu\text{m}$  thick sections which were placed on charged slides (Epic scientific charged white frosted slides). The slides were placed at 36°C to remove folds and excess moisture. Paraffin was removed in a Leica ST5020 automatic stainer using a de-waxing protocol. This procedure was performed with the samples already on the slides. Some sections were stained with Masson trichrome using an automatic stainer Leica ST5020. The images were obtained using a Leica Aperio AT Turbo digital pathology scanner. Other sections were stained with DRAQ5 (1/1000, 30 min) to visualize nuclei in VSM cells.

### **Mechanical tests.**

The experiments were completed within 8-10 hours of explanting the aorta from the donor's body, which is the time window to obtain proper VSM activation. Since organ explantation are planned only a few hours in advance and are often linked to accidents, the testing team had to be ready for testing any day and at any time not to lose any specimen.

Definitions: engineering stress = force/undeformed area; engineering strain = elongation/original length.

Quasi-static and dynamic uniaxial extension tests were carried out on a device that was developed for aortic tissue and controlled by a dSPACE hardware with a Simulink code. An Epsilon ONE-52PT video extensometer equipped with a telecentric lens (approximate 5 mm distance between the markers on the strip; absolute error no greater than  $\pm 5 \mu\text{m}$ ) measured the strain in the strip direction and an Interface model WMCFP-1000g load cell obtained the force.

The tested strip was immersed in bubbled ( $\text{O}_2$ ) Krebs-Henseleit buffer solution (D-glucose 2.0 g/L; magnesium sulfate 0.141 g/L; potassium phosphate monobasic 0.16 g/L; potassium chloride 0.35 g/L; sodium chloride 6.9 g/L; calcium chloride 0.373 g/L; sodium bicarbonate 2.1 g/L) at

37°C. The distance between the grips had an accuracy of  $\pm 1 \mu\text{m}$  and the tensile force measurement had an accuracy of  $\pm 0.01 \text{ N}$ .

The mechanical characterization took place after eight preconditioning cycles with a displacement rate of 0.05 mm/s. It has been verified that this rate is suitable for minimizing viscoelastic effects. Forces were converted into engineering stresses using the cross-sectional area of the strip. The grip distance was adjusted to have an initial load-free position with no sagging of the strip. If necessary, this position was adjusted after preconditioning without a test stop and the corresponding strain was set to zero.

### **Data availability**

The experimental and numerical data to support the results of this study are available on request from the corresponding author.

### **Code availability**

All numerical codes for image analysis and modeling the active and passive mechanical behavior of the aortic tissue are available on request from the corresponding author.

## References

1. Centers for Disease Control and Prevention, National Center for Health Statistics. Underlying cause of death 1999–2018 on CDC WONDER database website. <http://wonder.cdc.gov/icd10.html>.
2. McClure, R.S., Brogly, S.B., Lajkosz, K., McClintock, C., Payne, D., Smith, H.N., Johnson, A.P., Economic burden and healthcare resource use for thoracic aortic dissections and thoracic aortic aneurysms – A population-based cost-of-illness analysis. *J. Am. Heart Assoc.* **9**, 014981 (2020).
3. Amabili, M., Balasubramanian, P., Bozzo, I., Breslavsky, I.D., Ferrari, G., Franchini, G., Giovanniello, F., Pogue, C., Nonlinear dynamics of human aortas for material characterization. *Phys. Rev. X* **10**, 011015 (2020).
4. Akentjew, T.L., Terraza, C., Suazo, C., Maksimcuka, J., Wilkens, C.A., Vargas, F., Zavala, G., Ocaña, M., Enrione, J., García-Herrera, C.M., Valenzuela, L.M., Blaker, J.J., Khoury, M., Acevedo, J.P., Rapid fabrication of reinforced and cell-laden vascular grafts structurally inspired by human coronary arteries. *Nat. Commun.* **10**, 3098 (2019).
5. Caulk, A.W., Humphrey, J.D., Murtada, S.-I., Fundamental roles of axial stretch in isometric and isobaric evaluations of vascular contractility. *J. Biomech. Eng.* **141**, 031008 (2019).
6. Weisbecker, H., Pierce, D.M., Regitnig, P., Holzapfel, G.A., Layer-specific damage experiments and modeling of human thoracic and abdominal aortas with non-atherosclerotic intimal thickening. *J. Mech. Behav. Biomed. Mater.* **12**, 93-106 (2012).
7. Sassani, S.G., Kakisis, J., Tsangaris, S., Sokolis, D.P., Layer-dependent wall properties of abdominal aortic aneurysms: Experimental study and material characterization. *J. Mech. Behav. Biomed. Mater.* **49**, 141-161 (2015).
8. Amabili, M., Balasubramanian, P., Bozzo, I., Breslavsky, I.D., Ferrari, G., Layer-specific hyperelastic and viscoelastic characterization of human descending thoracic aortas. *J. Mech. Behav. Biomed. Mater.* **99**, 27-46 (2019).
9. Amabili, M., Asgari, M., Breslavsky, I.D., Franchini, G., Giovanniello, F., Holzapfel, G.A., Microstructural and mechanical characterization of the layers of human descending thoracic aortas. *Acta Biomaterialia* in press (2021). <https://doi.org/10.1016/j.actbio.2021.07.036>
10. Niestrawska, J.A., Viertler, C., Regitnig, P., Cohnert, T.U., Sommer, G., Holzapfel, G.A., Microstructure and mechanics of healthy and aneurysmatic abdominal aortas: experimental analysis and modelling. *J. R. Soc. Interface* **13**, 20160620 (2016).
11. Jadidi, M., Habibnezhad, M., Anttila, E., Maleckis, K., Desyatova, A., MacTaggart, J., Kamenskiy, A., Mechanical and structural changes in human thoracic aortas with age. *Acta Biomater.* **103**, 172-188 (2020).
12. Koch, R.G., Tsamis, A., D'Amore, A., Wagner, W.R., Watkins, S.C., Gleason, T.G., Vorp, D.A., A custom image-based analysis tool for quantifying elastin and collagen micro-architecture in the wall of the human aorta from multi-photon microscopy. *J. Biomech.* **47**, 935-943 (2014).
13. Gasser, T.C., Ogden, R.W., Holzapfel, G.A., Hyperelastic modelling of arterial layers with distributed collagen fibre orientations. *J. R. Soc. Interface* **3**, 15-35 (2006).
14. Baek, S., Gleason, R.L., Rajagopal, K.R., Humphrey, J.D., Theory of small on large: Potential utility in computations of fluid–solid interactions in arteries. *Comput. Methods Appl. Mech. Engrg.* **196**, 3070–3078 (2007).

15. Holzapfel, G.A., Niestrawska, J.A., Ogden, R.W., Reinisch, A.J., Schriefl, A.J., Modelling non-symmetric collagen fibre dispersion in arterial walls. *J. R. Soc. Interface* **12**, 20150188 (2015).
16. Valdez-Jasso, D., Haider, M.A., Banks, H.T., Bia, S.D., Zocalo, G.Y., Armentano, R.L., Olufsen, M.S., Analysis of viscoelastic wall properties in ovine arteries. *IEEE Trans. Biomed. Eng.* **56**, 210-219 (2009).
17. Franchini, G., Breslavsky, I.D., Holzapfel, G.A., Amabili, M., Viscoelastic characterization of human descending thoracic aortas under cyclic load. *Acta Biomater.* **130**, 291-307 (2021).
18. Holzapfel, G.A., Gasser, T.C., Stadler, M., A structural model for the viscoelastic behavior of arterial walls: continuum formulation and finite element analysis. *European J. Mech. A/Solids* **21**, 441-463 (2002).
19. Amabili, M., Balasubramanian, P., Breslavsky, I.D., Anisotropic fractional viscoelastic constitutive models for human descending thoracic aortas. *J. Mech. Behav. Biomed. Mater.* **99**, 186-197 (2019).
20. Safar, M.E., Arterial stiffness as a risk factor for clinical hypertension. *Nat. Rev. Cardiol.* **15**, 97-105 (2018).
21. Bank, A.J., Wang, H., Holte, J.E., Mullen, K., Shammass, R., Kubo, S.H., Contribution of collagen, elastin, and smooth muscle to in vivo human brachial artery wall stress and elastic modulus. *Circulation* **94**, 3263–3270 (1996).
22. Betrie, A.H., Brock, J.A., Harraz O.F., Bush, A.I., He, G.-W., Nelson, M.T., Angus, J.A., Wright, C.E., Ayton, S., Zinc drives vasorelaxation by acting in sensory nerves, endothelium and smooth muscle. *Nat. Commun.* **12**, 3296 (2021).
23. Ratz, P.H., Berg, K.M., Urban, N.H., Miner, A.S., Regulation of smooth muscle calcium sensitivity: KCl as a calcium sensitizing stimulus. *Am. J. Physiol. Cell. Physiol.* **288**, C769–C783 (2005).
24. Armentano, R.L., Barra, J.G., Levenson, J., Simon, A., Pichel, R.H., Arterial wall mechanics in conscious dogs. Assessment of viscous, inertial, and elastic moduli to characterize aortic wall behavior. *Circ. Res.* **76**, 468-478 (1995).
25. Dobrin, P.B., Rovick, A.A., Influence of vascular smooth muscle on contractile mechanics and elasticity of arteries. *Am. J. Physiol.* **217**, 1644-1651 (1969).
26. Dobrin, P.B., Mechanical behavior of vascular smooth muscle in cylindrical segments of arteries in vitro. *Ann. Biomed. Eng.* **12**, 497–510 (1984).
27. Cox, R.H., Effects of norepinephrine on mechanics of arteries in vitro. *Am. J. Physiol.* **231**, 420-425 (1976).
28. Gaballa, M.A., Jacob, C.T., Raya, T.E., Liu, J., Simon, B., Goldman, S., Large artery remodeling during aging: biaxial passive and active stiffness. *Hypertension* **32**, 437–443 (1998).
29. Fridez, P., Makino, A., Kakoi, D., Miyazaki, H., Meister, J.J., Hayashi, K., Stergiopoulos, N., Adaptation of conduit artery vascular smooth muscle tone to induced hypertension. *Ann. Biomed. Eng.* **30**, 905–916 (2002).
30. Attinger, F.M.L., Two-dimensional in-vitro studies of femoral arterial walls of the dog. *Circ. Res.* **22**, 829-840 (1968).
31. Herlihy, J.T., Murphy, R.A., Length-tension relationship of smooth muscle of the hog carotid artery. *Circ. Res.* **33**, 275-283 (1973).

32. Yang, S., Wu, Q., Huang, S., Wang, Z., Qi, F., Sevoflurane and isoflurane inhibit KCl induced Class II phosphoinositide 3-kinase  $\alpha$  subunit mediated vasoconstriction in rat aorta. *BMC Anesthesiol.* **16**, 63 (2016).
33. Rachev, A., Hayashi, K., Theoretical study of the effects of vascular smooth muscle contraction on strain and stress distributions in arteries. *Ann. Biomed. Eng.* **27**, 459–468 (1999).
34. Zulliger, M.A., Rachev, A., Stergiopoulos, N., A constitutive formulation of arterial mechanics including vascular smooth muscle tone. *Am. J. Physiol. Heart Circ. Physiol.* **287**, H1335–H1343 (2004).
35. Wagner, H.P., Humphrey, J.D., Differential passive and active biaxial mechanical behaviors of muscular and elastic arteries: basilar versus common carotid. *J. Biomech. Eng.* **133**, 051009 (2011).
36. Murtada, S.C., Arner, A., Holzapfel, G.A., Experiments and mechanochemical modeling of smooth muscle contraction: significance of filament overlap. *J. Theor. Biol.* **297**, 176–186 (2012).
37. Murtada, S.-I., Lewin, S., Arner, A., Humphrey, J.D., Adaptation of active tone in the mouse descending thoracic aorta under acute changes in loading. *Biomech. Model. Mechanobiol.* **15**, 579–592 (2016).
38. Haspinger, D.C., Murtada, S.-I., Niestrawska, J.A., Holzapfel, G.A., Numerical analyses of the interrelation between extracellular smooth muscle orientation and intracellular filament overlap in the human abdominal aorta. *Z. Angew. Math. Mech.* **98**, 2198–2221 (2018).
39. Gade, J.-L., Thore, C.-J., Sonesson, B., Stålhand, J., In vivo parameter identification method for arteries is extended to account for smooth muscle activity. *Biomech. Model. Mechanobiol.* in press (2021). <https://doi.org/10.1007/s10237-021-01462-4>.
40. Holzapfel, G.A., Gasser, T.C., Ogden, R.W., A new constitutive framework for arterial wall mechanics and a comparative study of material models. *J. Elasticity* **61**, 1–48 (2000).
41. Breslavsky, I.D., Franchini, G., Amabili, M., Effect of fiber exclusion in uniaxial tensile tests of soft biological tissues. *J. Mech. Behav. Biomed. Mater.* **112**, 104079 (2020).
42. Lacolley, P., Regnault, V., Segers, P., Laurent, S., Vascular smooth muscle cells and arterial stiffening: relevance in development, aging, and disease. *Physiol. Rev.* **97**, 1555–1617 (2017).

### Acknowledgments

M.A. acknowledges financial support from the NSERC Discovery Grant and the NSERC RTI Grant. Prabakaran Balasubramanian and Giovanni Ferrari assisted with experiments. Nicolas Audet of the Imaging and Molecular Biology Platform of McGill University helped with the imaging. The GCRC histology core of McGill University prepared the samples for histology.

### Author Contributions

G.F. carried out the mechanical tests, analyzed the test results, prepared figures and contributed to writing the paper; I.B. developed the active tissue model, produced numerical results and contributed to writing the paper; F.G. produced the microscopy images and their analysis; A.K. retrieved the samples, prepared them for experiments and took photos; G.A.H. contributed to the model development and to writing the paper; M.A. conceived the research and experiments, supervised the work, contributed to model development and data analysis, organized the sample delivery and wrote the paper.

**Competing interests**

The authors declare no competing interests.

**Additional information**

Supplementary information is available for this paper at the following subchapter.

## Supplementary Note 1 - Literature review on the mechanical characterization of active vascular tissue

According to the literature, the mechanical properties of the aorta with vascular smooth muscle (VSM) activation were only studied in animals. In the available studies, the orientation of the VSM cells in arteries was mostly assumed to be circumferential [1], which is not the case in the human aorta. Two methodologies of activation experiments were conducted: (i) pressurization of arterial segments, and (ii) extension tests on arterial strips and rings. By exploring the first methodology, Dobrin and Rovick [2] determined the circumferential stress as a function of arterial diameter for both passive and norepinephrine-stimulated excised and inflated carotid arteries of dogs. Some approximate formulas were used and an active peak stress value of 88 kPa (average over 17 arteries) based on the entire wall was obtained. Dobrin [3] continued this research. A similar approach was used by Cox [4] to investigate the active mechanical response of canine iliac and carotid arteries. Experiments on canine descending thoracic aortas exposed to a vasoactive agent (phenylephrine) to activate VSM have been conducted by Armentano et al. [5] under dynamic pressure. The stress-strain curve was only obtained for measuring the change in diameter of vessels in the circumferential direction. An intravascular ultrasound technique was used to indirectly measure (true approximate formulas) the total brachial artery (this is a muscular artery) wall stress and the incremental elastic modulus in seven normal human subjects at the baseline and after intra-arterial norepinephrine (1.2  $\mu\text{g}$ ) and nitroglycerin (100  $\mu\text{g}$ ) by Bank et al. [6]. Gaballa et al. [7] measured *in vivo* pressure-radius and axial force-radius curves in carotid arteries of rats with and without VSM activation (norepinephrine). Fridez et al. [8] obtained a complete tracing of VSM tone adaptation in the rat common carotid arteries subjected to sustained step pressure change *in vivo*; norepinephrine ( $5 \times 10^{-7}$  mol/L) was used as a vasoactive agent.

For the second methodology, Attinger [9] performed tests on the activation (norepinephrine) of circumferential rings and longitudinal strips of femoral arteries (a muscular artery) in dogs. He found that the longitudinal stress-strain relation was not altered by the constriction of the vascular smooth muscle. The length-tension relationships for arterial smooth muscles were determined by Herlihy and Murphy [10] using vascular strips from the media of dog carotid arteries, taken in helicoidal direction ( $4.5^\circ$  with respect to the circumferential direction). Potassium depolarization (KCl), used as a vasoactive agent, produced an active stress of 222 kPa. The KCl-induced

contraction of aortic rings and strips of rat aortic tissue has been reported by Yang et al. [11]. Caulk et al. [12] evaluated effects of uniaxial versus biaxial deformations on smooth muscle contractility by stimulating two regions of the mouse aorta with different vasoconstrictors (KCl and phenylephrine) using one of three test protocols on aortic ring segments: (i) uniaxial isometric testing with arterial rings mounted on a myograph, (ii) biaxial isometric testing, and (iii) axially isometric plus isobaric testing. Betrie et al. [13] demonstrated a role of zinc in the vascular tone regulation (vasorelaxation). *Ex vivo*, 2 mm wide ring segments of arteries (mostly rats, but also human internal mammary arteries) were mounted in myograph chambers for isometric force measurement. The activation of smooth muscles was achieved by a potassium depolarizing solution (124 mM K<sup>+</sup> replacing Na<sup>+</sup> in physiological salt solution), noradrenaline (10 μM) or electric stimulus. Only some of these studies provide the stress-strain curves of the passive and active arterial tissue.

The effect of smooth muscle activation (norepinephrine) on the circumferential residual strain of rat aortas has been studied by Matsumoto et al. [14]. Driska [1] has compiled an overview of the early research on both methodologies. A review of vascular smooth muscle cells and arterial stiffening was provided by Lacolley et al. [15]. The mechanism of VSM activation by KCl was described in [16] and the force produced was compared to different concentrations of phenylephrine.

Theoretical studies on the effect of smooth muscle activation on the mechanical response of arteries are available. Rachev and Hayashi [17] modeled the effect of the vascular smooth muscle contraction, which is assumed to only occur in the circumferential direction, on the strain and stress distributions in arteries with a particular focus on residual strains. A pseudo strain-energy function describing the biomechanical properties of large conduit arteries under the influence of the vascular VSM tone was proposed by Zulliger et al. [18]. This energy does not depend on the deformation in the longitudinal direction. A strain-energy function taking smooth muscle activation into account has been published by Baek et al. [19]. The contribution of the active term is only circumferential and is described by a ratio of polynomial functions in the stretch. Wagner and Humphrey [20] developed a model that takes into account the generation of both circumferential and longitudinal stresses due to the activation of the smooth muscles. This model was based on the simplification that the stresses due to the activation in the two directions were separable (i.e. independent). A mathematical mechanochemical model for the smooth muscle

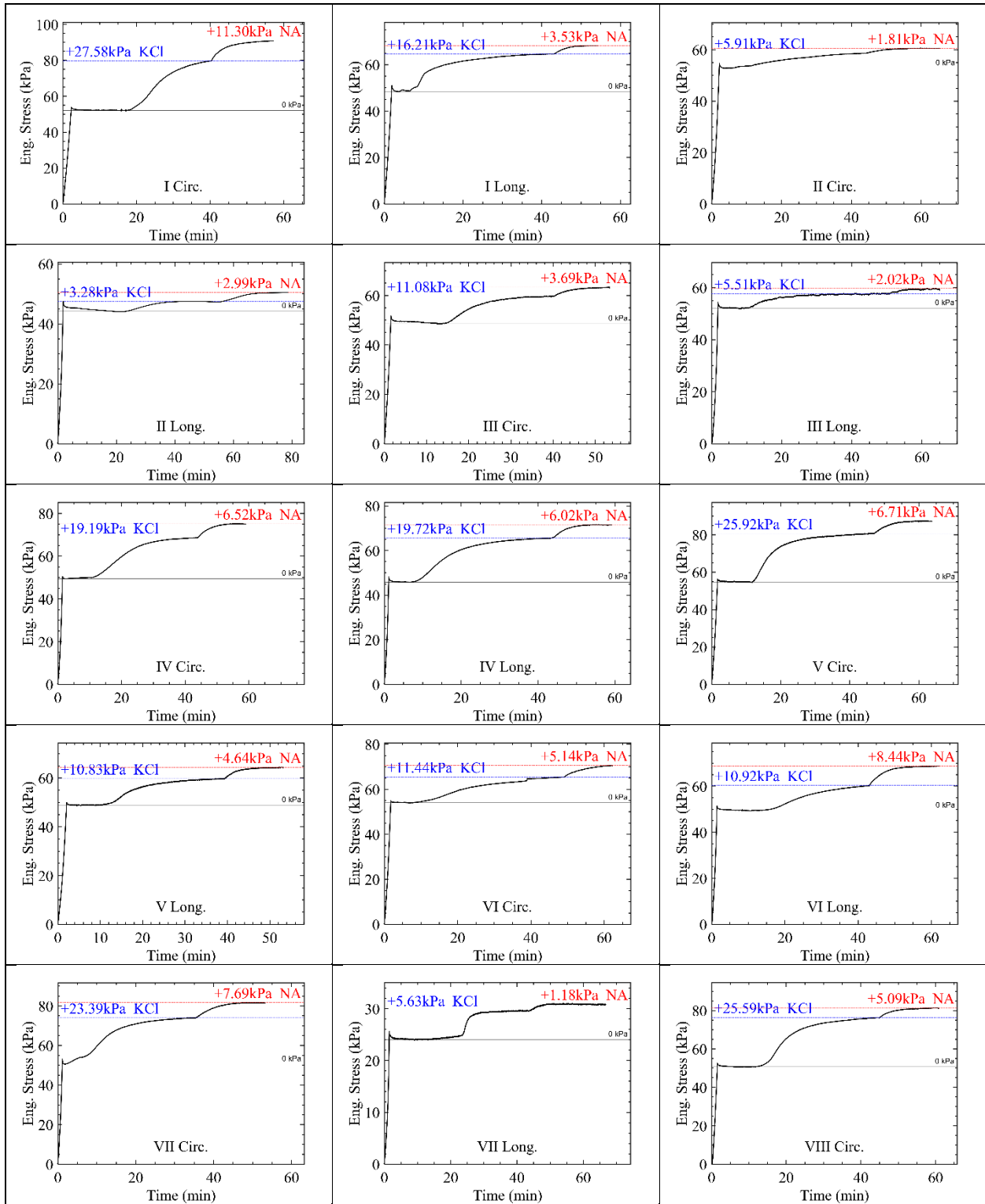
contractile unit was developed by Murtada et al. [21]. Murtada et al. [22] studied experimentally and computationally the adaptive functions of active VSM in arterial rings that were excised from descending thoracic aortas of mice stimulated by various agonists. The model developed was for activation in the circumferential direction. Haspinger et al. [23] assumed activation of the medial layer caused by VSM cells, which are oriented as two helically arranged symmetric families without fiber dispersion. Each of the two families was modeled using the contractile unit proposed in [21]. Gade et al. [24] extended an *in vivo* parameter identification method for arteries to account for smooth muscle activity.

## Supplementary Note 2 - Information on donors

**Table S1.** Information on donors with the following abbreviations: M = male; F = female; TBI = traumatic brain injury; HAI = hypoxic-anoxic injury; CVA = cerebrovascular accident.

Donor	I	II	III	IV	V	VI	VII	VII	IX	X	XI	XII	XIII
	I	II	III	IV	V	VI	VII	I	IX	X	XI	XII	XIII
Age	32	48	55	40	25	30	68	42	68	58	47	59	60
Gender	F	M	F	F	F	M	F	M	F	M	M	F	M
Weight (kg)	105	81	59	65	75	72	80.6	80	56	70	115	76.4	72.6
Height (cm)	175	175	175	173	159	158	165	175	163	168	187	165	171
Cause of death	HA	CV				HA	CV	HA	CV	CV	HA	CV	CV
	I	A	TBI	TBI	TBI	I	A	I	A	A	I	A	A

### Supplementary Note 3 - Isometric experiments on activation



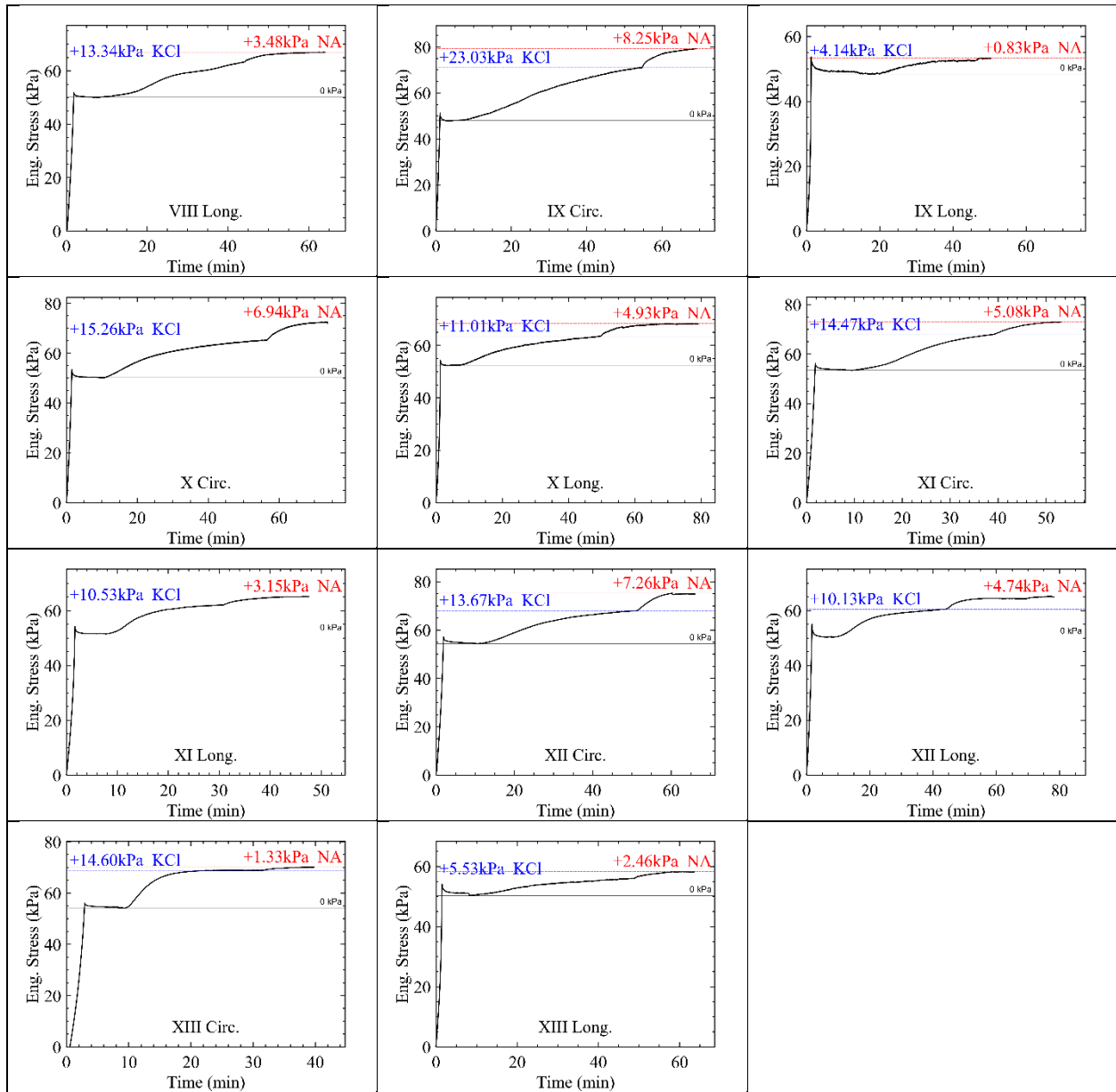
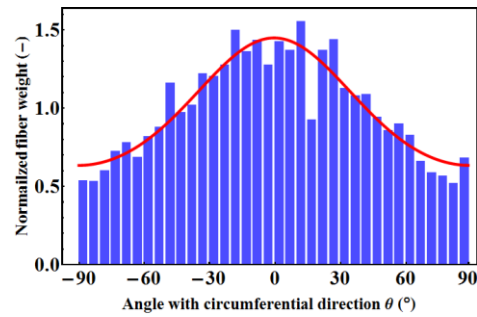
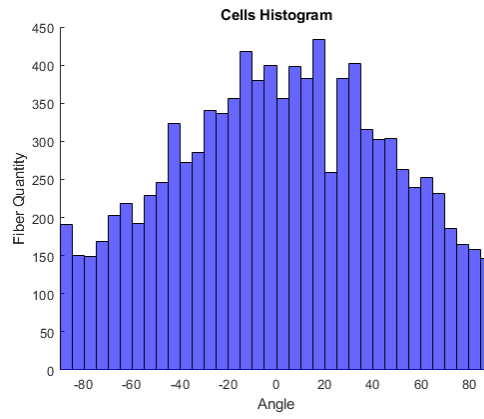
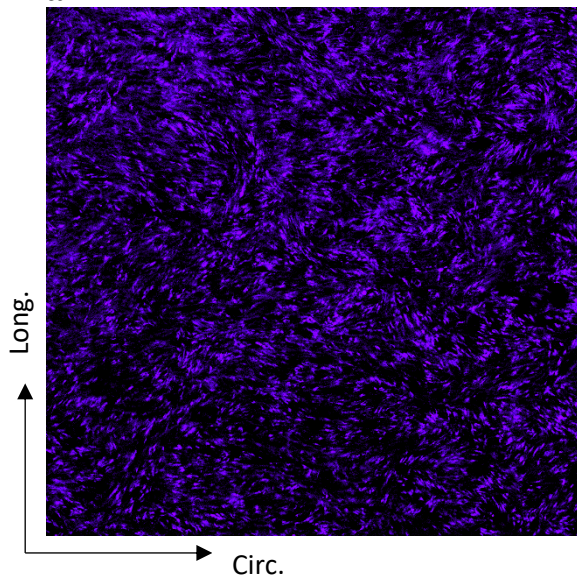


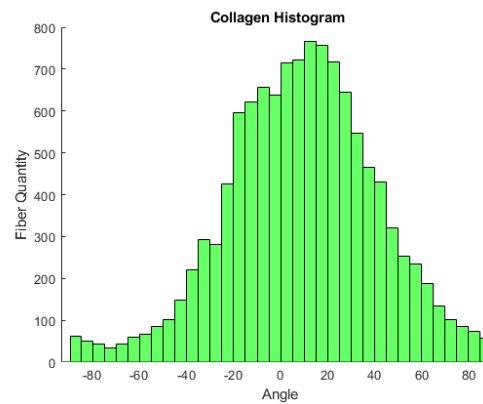
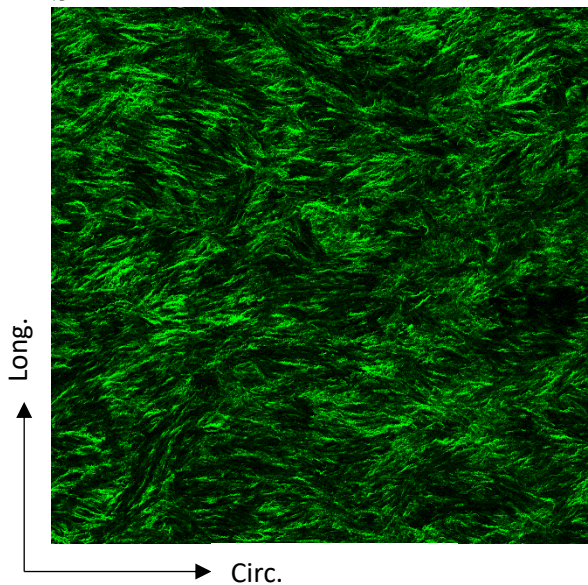
**Figure S1.** Isometric activation of circumferential and longitudinal strips versus time from 13 descending thoracic aortas (identified by the roman number). Pre-stress around 50 kPa. First vasoactive agent, KCl; second vasoactive agent, noradrenaline (NA). Circ. = circumferential strip; Long. = longitudinal strip.

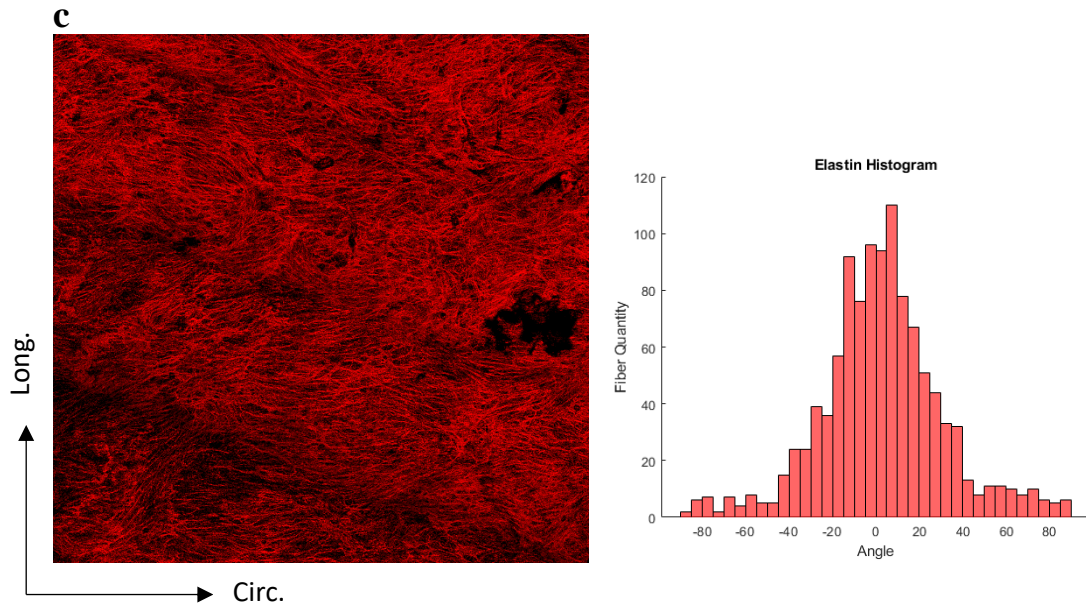
# Supplementary Note 4 - Additional results for microstructural characterization

**a**



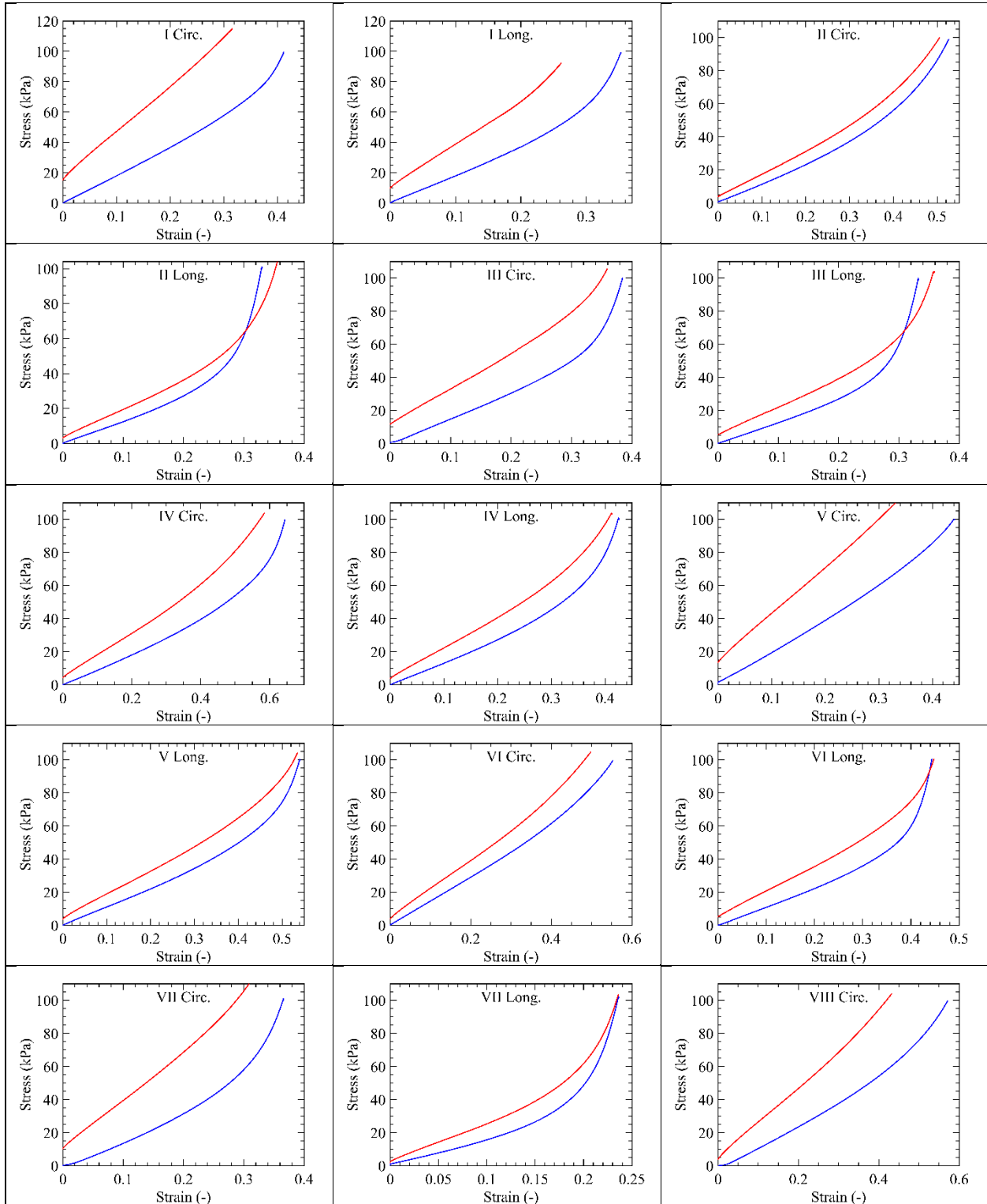
**b**





**Figure S2.** Microstructural analysis of an in-plane section from the tunica media of donor XII. The three images show the same area of the tissue measuring  $1600 \times 1600 \mu\text{m}$ . **a** VSM cell orientation using DRAQ5 staining; distribution of the orientation and fitted Poisson distribution; dispersion coefficient  $\kappa_{IP}^{VSM} = 0.399$ . **b** Collagen distribution by second harmonic generation microscopy. **c** Elastin distribution by two-photon microscopy. Angle  $0^\circ$  indicates the circumferential direction.

### Supplementary Note 5 - Active and passive quasi-static extension tests



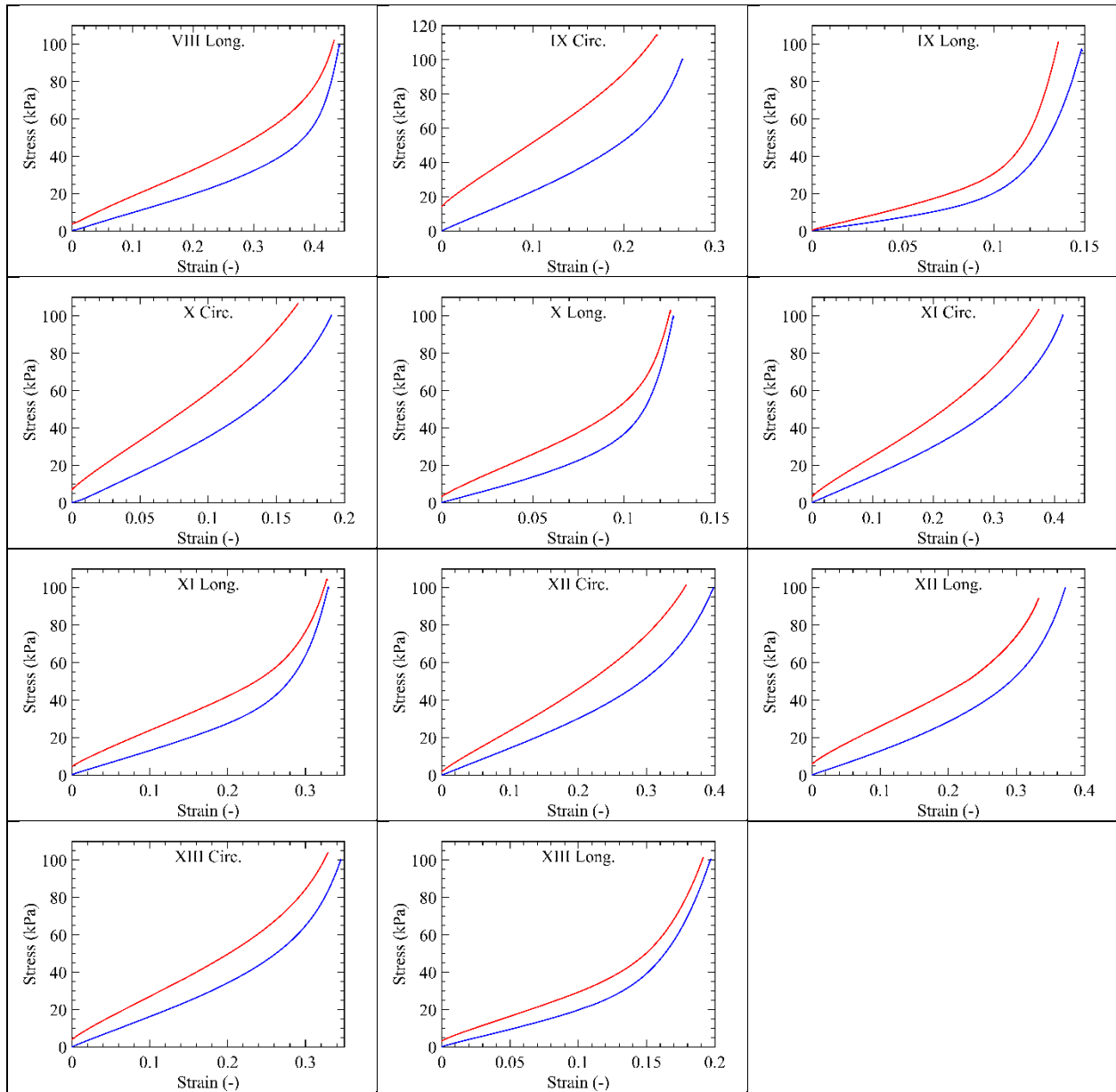


**Figure S3.** Engineering stress versus engineering strain: quasi-static curves of circumferential and longitudinal strips of 13 descending thoracic aortas (identified by the roman number). Maximum activation after KCl and noradrenaline. Activation of the VSM = red curve; passive behavior = blue curve; Circ. = circumferential strip; Long. = longitudinal strip.

## Supplementary Note 6 - Details on the material model of the passive and active aortic tissue

The strain-energy function  $W$  of the aortic wall is represented as the sum of passive and active components

$$W = W^P + W^A, \quad (6.1)$$

where the passive component  $W^P$  is given by

$$W^P = W_{ISO}^P + W_{ANISO}^P. \quad (6.2)$$

$W_{ISO}^P$  accounts for the passive hyperelastic response of the ground matrix and the elastin network and is assumed in the form of an isotropic neo-Hookean strain-energy function;  $W_{ANISO}^P$  accounts for the anisotropic passive response due to collagen fibers;  $W^A$  represents the contribution of the activated smooth muscles, which is mainly present in the tunica media. In particular,

$$W_{ISO} = \frac{\mu}{2}(I_1 - 3), \quad (6.3)$$

where  $\mu$  is a material parameter,  $I_1$  is the first invariant of the right Cauchy-Green tensor, here given in matrix form as

$$\mathbf{C} = \begin{pmatrix} 2\varepsilon_{xx} + 1 & \gamma_{x\theta} & \gamma_{xz} \\ \gamma_{x\theta} & 2\varepsilon_{\theta\theta} + 1 & \gamma_{\theta z} \\ \gamma_{xz} & \gamma_{\theta z} & 2\varepsilon_{zz} + 1 \end{pmatrix},$$

where  $\varepsilon$  and  $\gamma$  indicate the normal and shear Green-Lagrange strain components;  $x, \theta, z$  are the three orthogonal coordinates in the longitudinal, circumferential and radial directions, respectively.

The first invariant of the tensor  $\mathbf{C}$  is [25]

$$I_1 = \text{tr}(\mathbf{C}) = 2(\varepsilon_{xx} + \varepsilon_{\theta\theta} + \varepsilon_{zz}) + 3. \quad (6.4)$$

Two families of fibers are used in  $W_{ANISO}^P$ . One represents the effect of collagen fibers, which are mainly oriented in the circumferential or longitudinal direction, and an orthogonal family represents the cross-link and lateral interaction of collagen

$$W_{ANISO}^P = \sum_{i=1}^2 C^{(i)} W_F^{(i)}(\alpha^{(i)}), \quad (6.5)$$

where the coefficients  $C^{(i)}$  with a value between 0 and 1 describe the portion of active fibers (i.e. the uncompressed), as introduced in [26]. In eq. (6.5) the strain-energy function of a fiber family is represented by

$$W_F^{(i)} = \frac{\mu_1^{(i)}}{\mu_2^{(i)}} \left\{ \exp \left[ \mu_2^{(i)} \left( E^{(i)} \right)^2 \right] - 1 \right\}, \quad (6.6)$$

$$E^{(i)} = 2\kappa_{OP}^{(i)}\kappa_{IP}^{(i)}I_1 + 2\kappa_{OP}^{(i)}(1-2\kappa_{IP}^{(i)})I_4^{(i)} + \left(1-2\kappa_{OP}^{(i)}(\kappa_{IP}^{(i)}+1)\right)I_n - 1, \quad (6.7)$$

where  $\mu_1^{(i)}, \mu_2^{(i)}$  are parameters describing the fiber material,  $\kappa_{IP}^{(i)}$  is the in-plane dispersion parameter, which varies from 0 (perfectly aligned fibers) to 1/2 (in-plane isotropy),  $\kappa_{OP}^{(i)}$  is the out-of-plane dispersion parameter, which can take on values between 1/3 (out-of-plane isotropy) and 1/2 (perfectly in-plane fibers). It is assumed that the mean direction of the fiber family forms the angle  $\alpha^{(i)} = 0$  (circumferential) or  $\pi/2$  (longitudinal) with the circumferential direction of the aorta in the plane tangential to the middle surface (in-plane). The unit vector of the mean direction is  $\{\mathbf{M}_{(i)}\}^T = \{\sin \alpha^{(i)}, \cos \alpha^{(i)}, 0\}$  in the coordinates  $\{x, \theta, z\}$ . Using the introduced notation, it is convenient to represent the pseudo-invariants  $I_4^{(i)}$  and  $I_n$  as [25, 27]

$$I_4^{(i)} = \mathbf{C} : \mathbf{M}_{(i)} \otimes \mathbf{M}_{(i)} = 1 + 2(\varepsilon_{xx} \sin^2 \alpha^{(i)} + \varepsilon_{\theta\theta} \cos^2 \alpha^{(i)} + \gamma_{x\theta} \sin \alpha^{(i)} \cos \alpha^{(i)}), \quad (6.8)$$

$$I_n = \mathbf{C} : \mathbf{e}_z \otimes \mathbf{e}_z = 2\varepsilon_{zz} + 1, \quad (6.9)$$

where  $\{\mathbf{e}_z\}^T = \{0, 0, 1\}$  is the unit vector in the radial direction, the operation  $:$  denotes the double contraction of tensors, and  $\otimes$  is the outer product of vectors. The pseudo-invariants  $I_4^{(i)}$  and  $I_n$  measure the squares of the fiber stretches in the directions  $\mathbf{M}_{(i)}$  and  $\mathbf{e}_z$ , respectively.

The change in volume during the deformation is related to the third invariant of  $\mathbf{C}$ , i.e.

$$I_3 = \det(\mathbf{C}) = (2\varepsilon_{xx} + 1)(2\varepsilon_{\theta\theta} + 1)(2\varepsilon_{zz} + 1) - (2\varepsilon_{xx} + 1)\gamma_{\theta z}^2 - (2\varepsilon_{\theta\theta} + 1)\gamma_{xz}^2 - (2\varepsilon_{zz} + 1)\gamma_{x\theta}^2 + 2\gamma_{x\theta}\gamma_{xz}\gamma_{\theta z}. \quad (6.10)$$

Aortic tissue is considered incompressible (see, e.g., [28]), which gives

$$I_3 = 1. \quad (6.11)$$

Equations (6.10) and (6.11) allow to obtain  $\varepsilon_{zz}$  as a function of the other strains

$$\varepsilon_{zz} = \frac{\gamma_{x\theta}^2 + \gamma_{xz}^2 + \gamma_{\theta z}^2 - 2(\varepsilon_{xx} + \varepsilon_{\theta\theta}) - 4\varepsilon_{xx}\varepsilon_{\theta\theta} + 2\varepsilon_{xx}\gamma_{\theta z}^2 + 2\varepsilon_{\theta\theta}\gamma_{xz}^2 - 2\gamma_{x\theta}\gamma_{xz}\gamma_{\theta z}}{2\left((2\varepsilon_{xx} + 1)(2\varepsilon_{\theta\theta} + 1) - \gamma_{x\theta}^2\right)}. \quad (6.12)$$

Expression (6.12) is inserted into  $W$ , and the resulting equation, which does not depend on  $\varepsilon_{zz}$ , is denoted as

$$\hat{W} = \hat{W}^P + \hat{W}^A.$$

Initially the parameters of the passive hyperelastic model are determined by simultaneously fitting the stress-strain curves of the longitudinal and circumferential aortic strips. The minimization functional for this case has the form

$$f^P = \frac{1}{2} \left\{ \frac{1}{N_{axial}^P} \sum_{i=1}^{N_{axial}^P} \left( \bar{S}_{xx}^P(\varepsilon_{xx}^{P,(i)}) - S_{xx}^{P,(i)} \right)^2 + \frac{1}{N_{circ}^P} \sum_{i=1}^{N_{circ}^P} \left( \bar{S}_{\theta\theta}^P(\varepsilon_{\theta\theta}^{P,(i)}) - S_{\theta\theta}^{P,(i)} \right)^2 \right\}, \quad (6.13)$$

where  $(\varepsilon_{xx}^{P,(i)}, S_{xx}^{P,(i)})$  and  $(\varepsilon_{\theta\theta}^{P,(i)}, S_{\theta\theta}^{P,(i)})$  are the experimentally obtained points on the stress-strain curves (second Piola-Kirchhoff stress and Green-Lagrange strain) of the non-activated longitudinal and circumferential strips, respectively, and  $N_{axial}^P, N_{circ}^P$  are the numbers of experimental points in the curves for the axial and circumferential strips, respectively. The passive second Piola-Kirchhoff stresses are determined as

$$\begin{aligned} \bar{S}_{xx}^P(\varepsilon_{xx}) &= S_{xx}^P(\varepsilon_{xx}, \varepsilon_{\theta\theta}^P(\varepsilon_{xx})), \\ \bar{S}_{\theta\theta}^P(\varepsilon_{xx}) &= S_{\theta\theta}^P(\varepsilon_{xx}^P(\varepsilon_{\theta\theta}), \varepsilon_{\theta\theta}), \end{aligned}$$

where

$$S_{xx}^P = \frac{\partial \hat{W}^P}{\partial \varepsilon_{xx}}, \quad S_{\theta\theta}^P = \frac{\partial \hat{W}^P}{\partial \varepsilon_{\theta\theta}}.$$

The functions  $\varepsilon_{xx}^P(\varepsilon_{\theta\theta})$ ,  $\varepsilon_{\theta\theta}^P(\varepsilon_{xx})$  are determined from the conditions of absence of transverse normal stresses

$$\varepsilon_{xx}^P(\varepsilon_{\theta\theta}): S_{xx}^P(\varepsilon_{xx}, \varepsilon_{\theta\theta}) = 0, \quad \varepsilon_{\theta\theta}^P(\varepsilon_{xx}): S_{\theta\theta}^P(\varepsilon_{xx}, \varepsilon_{\theta\theta}) = 0. \quad (6.14)$$

The functional (6.14) is minimized by using a genetic algorithm described in [29].

## Mechanical response of the activated tissue

Experimental observations show that the difference between passive and active responses with increasing strain initially increases up to a certain strain value and then it decreases. In earlier studies [19-23] this observation led to the assumption of a parabolic term in stress to describe the difference between active and passive responses. Thus, the corresponding active term in the strain-energy function was of cubic order in strain. The experiments presented in this study show that the absolute value of the tangent of the difference between passive and active responses is often much lower in the ascending part than in the descending part. Typical curves are shown in Figure S4.

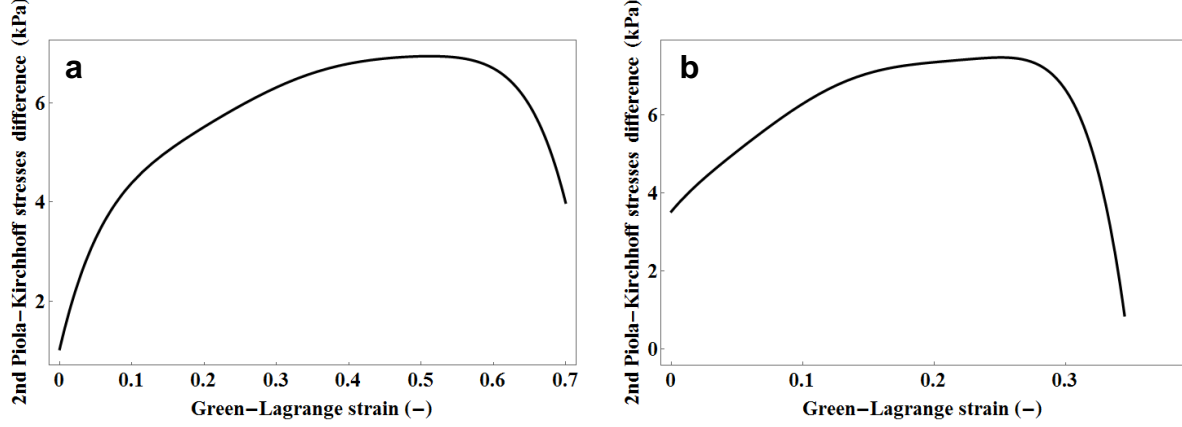


**Figure S4.** Experimentally observed difference between active and passive curves from quasi-static uniaxial extension tests on the aorta from donor II. **a** circumferential strip; **b** longitudinal strip.

This non-symmetric character of the curves can be better described by a function of the power higher than two under stress. In addition, in contrast to previous studies [19], it is assumed that the smooth muscle fibers are not perfectly aligned in the circumferential direction, but rather dispersed around the circumferential direction of the aorta in the plane tangential to the middle surface (in-plane) of the strip. In addition to the main family of dispersed VSMs with the dispersion parameter  $\kappa_{IP}^{VSM}$ , a second orthogonal family with the same dispersion is considered to describe the lateral interaction between VSM fibers; this is justified by the mutual winding of the VSM fibers shown in Figure 3(b). This second family introduces a minor active stress that is the main one. The proposed active strain-energy function is given by

$$W^A = \tilde{K} \sum_{i=1}^2 K_i \left( E_i^{VSM} + \frac{a_i}{2} (E_i^{VSM})^2 - \frac{b_i}{m_i + 1} (E_i^{VSM})^{m_i + 1} \right), \quad a_i, b_i > 0, \quad (6.15)$$

where  $m_i$  is an integer larger than one and

$$E_1^{VSM} = 2 \left[ \kappa_{IP}^{VSM} (\varepsilon_{xx} + \varepsilon_{\theta\theta}) + (1 - 2\kappa_{IP}^{VSM}) \varepsilon_{\theta\theta} \right], \quad (6.16a)$$

$$E_2^{VSM} = 2 \left[ \kappa_{IP}^{VSM} (\varepsilon_{xx} + \varepsilon_{\theta\theta}) + (1 - 2\kappa_{IP}^{VSM}) \varepsilon_{xx} \right]. \quad (6.16b)$$

$\tilde{K}$  is the activation level coefficient with a value between zero (no activation) and 1 (maximum activation). Equations (6.16a,b) are inspired by an expression proposed in [30] for the bi-dimensional fiber dispersions. In (6.15) it is assumed that all smooth muscle fibers lie perfectly in-plane, as the experimental observations suggest. Expression (6.15) has nine parameters  $K_i, a_i, b_i, m_i, \kappa_{IP}^{VSM}$ . The convexity of the strain-energy function (6.1) has been verified

numerically for the studied cases. The contour plots of  $W$  are presented in Figure 4c for the case of donor VIII and they are convex. The first summand in (6.15) take into account the stress value at zero principal strain. In particular,  $K_i$  is a stress-like parameter that represents the initial active stress values. These values in the axial and circumferential directions can be different, and the model captures this feature through the VSM dispersion parameter  $\kappa_{IP}^{VSM}$ . The second summand in (6.15) reflects the relatively slow initial increase of the stress difference, which is controlled by the parameter  $a_i$ . The third summand in (6.15), because of its higher power, represents the rapid decrease in the difference after a certain strain value. The slope of this decrease is controlled by the two parameters  $b_i$  and  $m_i$ . The dispersion parameter  $\kappa_{IP}^{VSM}$  is obtained by fitting a von Mises probability distribution [27, 30], i.e.

$$\rho_{IP}(\theta) = \frac{\exp[c \cos(2\theta)]}{I_0(c)}, \quad (6.17)$$

to the experimental histogram of the VSM distribution in Figure 3(d) to obtain the concentration parameter  $c$ ;  $I_0$  is the modified Bessel function of the first kind of order zero. The following normalization condition is also introduced, i.e.

$$\frac{1}{2\pi} \int_0^{2\pi} \rho_{IP}(\theta) d\theta = 1.$$

The dispersion parameters  $\kappa_{IP}^{VSM}$  is given by [27, 30]

$$\kappa_{IP}^{VSM} = \frac{1}{2} - \frac{I_1(c)}{2I_0(c)}, \quad (6.18)$$

where  $I_1$  is the modified Bessel function of the first kind of order one, whereas  $\kappa_{IP}^{VSM}$  takes on values between 0 for perfectly aligned VSM fibers in the circumferential direction and 0.5 for isotropic response of the VSM.

### Identification of the material parameters for the activated tissue

Fitting the results of uniaxial extension tests on the activated tissue to the active material model takes place after the material parameters of the passive tissue have been identified. All material parameters determined by minimizing the functional (6.13) for the passive behavior remain the same. The parameters identified at this stage are  $K_i, a_i, b_i, m_i$ . Although active and passive

components in (6.1) are independent and the total strain-energy function is their sum, the resulting stresses do not add up. The stresses are coupled by the equation for the orthogonal stress. Here the case of the axial strip in the uniaxial extension test is considered. The stress in the circumferential direction is zero during the test. In case of a passive response, the corresponding equation reads

$$S_{\theta\theta}^P(\varepsilon_{xx}, \varepsilon_{\theta\theta}) = 0,$$

which allows to obtain  $\varepsilon_{\theta\theta}^P(\varepsilon_{xx})$ . In the case of VSM activation, we have

$$S_{\theta\theta}^P(\varepsilon_{xx}, \varepsilon_{\theta\theta}) + S_{\theta\theta}^A(\varepsilon_{xx}, \varepsilon_{\theta\theta}) = 0, \quad (6.19)$$

where

$$S_{\theta\theta}^A = \frac{\partial \hat{W}^A}{\partial \varepsilon_{\theta\theta}}.$$

Equation (6.19) allows to obtain  $\varepsilon_{\theta\theta}(\varepsilon_{xx})$ . In general,  $\varepsilon_{\theta\theta}(\varepsilon_{xx}) \neq \varepsilon_{\theta\theta}^P(\varepsilon_{xx})$ . This means that

$$S_{xx}^P(\varepsilon_{xx}, \varepsilon_{\theta\theta}^P(\varepsilon_{xx})) \neq S_{xx}^P(\varepsilon_{xx}, \varepsilon_{\theta\theta}(\varepsilon_{xx})).$$

Therefore, the total mechanical response must be fitted by varying the parameters  $K_i, a_i, b_i, m_i$  of the active components and leaving the previously identified passive hyperelastic coefficients unchanged.

The minimization functional  $f^A$  in this case has a form similar to (6.13)

$$f^A = \frac{1}{2} \left\{ \frac{1}{N_{axial}^A} \sum_{i=1}^{N_{axial}^A} \left( \bar{S}_{xx}(\varepsilon_{xx}^{A,(i)}) - S_{xx}^{A,(i)} \right)^2 + \frac{1}{N_{circ}^A} \sum_{i=1}^{N_{circ}^A} \left( \bar{S}_{\theta\theta}(\varepsilon_{\theta\theta}^{A,(i)}) - S_{\theta\theta}^{A,(i)} \right)^2 \right\}, \quad (6.20)$$

where  $(\varepsilon_{xx}^{A,(i)}, S_{xx}^{A,(i)})$  and  $(\varepsilon_{\theta\theta}^{A,(i)}, S_{\theta\theta}^{A,(i)})$  are the experimental points of the stress-strain curves of the activated longitudinal and circumferential strips, respectively, and  $N_{axial}^A, N_{circ}^A$  are the numbers of experimental points for the axial and circumferential strips, respectively. The second Piola-Kirchhoff stresses of the activated tissue are obtained in a similar way to the passive case, but with the total strain-energy function (6.1) instead of just the passive component

$$\bar{S}_{xx}(\varepsilon_{xx}) = S_{xx}(\varepsilon_{xx}, \varepsilon_{\theta\theta}(\varepsilon_{xx})),$$

$$\bar{S}_{\theta\theta}(\varepsilon_{xx}) = S_{\theta\theta}(\varepsilon_{xx}(\varepsilon_{\theta\theta}), \varepsilon_{\theta\theta}),$$

where

$$S_{xx} = \frac{\partial \hat{W}}{\partial \varepsilon_{xx}}, \quad S_{\theta\theta} = \frac{\partial \hat{W}}{\partial \varepsilon_{\theta\theta}}.$$

The functions  $\varepsilon_{xx}(\varepsilon_{\theta\theta})$  and  $\varepsilon_{\theta\theta}(\varepsilon_{xx})$  are determined from the conditions of absence of the transverse normal stress (6.19) and its counterpart for the case of the circumferential strip, i.e.

$$S_{.xx}^P(\boldsymbol{\varepsilon}_{.xx}, \boldsymbol{\varepsilon}_{\theta\theta}) + S_{.xx}^A(\boldsymbol{\varepsilon}_{.xx}, \boldsymbol{\varepsilon}_{\theta\theta}) = 0.$$

**Table S2.** Parameters of the passive aortic material model identified from the experiments.  $R^2$  indicates the accuracy of the model with respect to the experimental data.

Donor	$\mu$ (kPa)	$\alpha^{(1)}$	$\mu_1^{(1)}$ (kPa)	$\mu_2^{(1)}$ (-)	$\kappa_{OP}$ (-)	$\kappa_{IP}$ (-)	$\mu_1^{(2)}$ (kPa)	$\mu_2^{(2)}$ (-)	$R^2$ (-)
I	50.21	0	16.41	2.327	0.3473	0.0490	4.400	1.366	0.997
II	23.90	0	14.93	2.140	0.4534	0.3568	4.957	2.050	0.987
III	13.54	0	22.88	1.714	0.4688	0.2668	6.726	1.675	0.982
IV	32.57	$\pi/2$	5.214	1.411	0.4951	0.1158	1.130	0.503	0.997
V	53.25	$\pi/2$	9.040	1.475	0.3463	0.0295	3.835	0.720	0.989
VI	41.51	$\pi/2$	63.33	15.89	0.2387	0.1521	2.232	0.563	0.987
VII	19.31	0	26.46	4.133	0.4155	0.2064	3.638	4.106	0.975
VIII	32.53	$\pi/2$	29.91	27.07	0.3442	0.4123	3.143	0.363	0.995
IX	39.05	$\pi/2$	14.79	98.60	0.3927	0.1438	7.050	3.501	0.982
X	18.19	0	857.4	37.26	0.3792	0.4516	14.55	21.00	0.979
XI	22.67	$\pi/2$	70.88	22.00	0.3405	0.2877	4.323	1.273	0.966
XII	28.21	$\pi/2$	36.72	5.100	0.3967	0.2761	5.473	1.009	0.995
XIII	26.89	0	75.47	16.32	0.3973	0.4205	9.379	7.188	0.979

**Table S3.** Parameters of the active aortic material model identified from the experiments.  $R^2$  indicates the accuracy of the model with respect to the experimental data.

Donor	$K_1$ (kPa)	$a_1$ (-)	$b_1$ (-)	$m_1$ (-)	$\kappa_{IP}^{VSM}$ (-)	$K_2$ (kPa)	$a_2$ (-)	$b_2$ (-)	$m_2$ (-)	$R^2$ (-)
I	7.486	20.20	34.59	2	0.2960	4.674	30.44	63.36	2	0.962
II	0.943	31.16	30.12	2	0.3007	1.589	34.11	93.88	2	0.996
III	4.151	18.08	47.48	3	0.2807	1.540	24.50	57.54	2	0.941
IV	1.249	31.66	71.27	3	0.4988	10.05	$1 \times 10^{-5}$	4.328	4	0.994
V	2.901	39.83	54.09	2	0.2410	1.052	39.68	47.60	2	0.957
VI	5.277	35.51	22.44	2	0.4539	5.981	0.022	49.47	2	0.894
VII	5.186	17.26	49.23	3	0.2286	1.117	21.73	56.94	2	0.974
VIII	8.251	5.695	8.363	3	0.3433	0.942	40.15	73.28	2	0.998
IX	5.470	16.05	57.32	3	0.1576	0.649	66.17	48.14	2	0.969
X	22.00	6.075	52.51	2	0.4325	19.40	2.737	52.64	3	0.958
XI	6.637	5.622	3.121	2	0.3814	1.450	27.78	118.8	2	0.945
XII	4.033	19.50	59.45	3	0.3989	2.876	20.09	36.28	2	0.958
XIII	3.294	27.97	45.61	2	0.3188	3.665	18.73	49.46	2	0.992

## Supplementary Note 7 - Dynamic characterization: dynamic stiffness ratio and loss factor

A hysteresis loop of the cyclic strain is shown in Figure S5; the quasi-static stress-strain curve is also displayed in the figure. The middle curve of the loop is calculated as the mean of the upper and lower curves that make up the loop. The center of the loop is placed on this middle curve. The point on the quasi-static stress-strain curve corresponding to the center of the loop is shown in Figure S5 as the intersection of the static curve and the minimal distance line. The center of the loop should be placed on the static curve, but there may be small differences due to relaxation, creep and inelasticity that occur in the time between the quasi-static test and the dynamic test.

The tangent to the middle curve of the loop (in the middle of the loop) has the slope  $\alpha_L$ ; then  $\tan(\alpha_L)$  is proportional to the storage modulus. The slope of the tangent to the static curve at the point corresponding to the center of the loop is  $\alpha_s$ ; then  $\tan(\alpha_s)$  is proportional to the static modulus. The dynamic stiffness ratio  $\delta$  is defined [29] as the ratio between the storage modulus and the corresponding static modulus.  $\delta$  indicates the stiffness increase of the aortic strip with dynamic loading compared to a quasi-static loading and it depends on the amount of pre-stress (or pre-stretch), on the amplitude of the harmonic cyclic strain and on the frequency of the cyclic loading.

The loss factor  $\eta$  can be determined from the hysteresis loop in Figure S5. For a loading cycle, the energy  $\Delta W_d$  dissipated per unit volume by the cyclically loaded aortic strip is [25]

$$\Delta W_d = \int_{cycle} \sigma d\varepsilon, \quad (7.1)$$

where  $\sigma$  is the dynamic stress and  $\varepsilon$  is the dynamic strain. The integral in eq. (7.1) returns the area contained within the hysteresis loop. The hysteresis loop shown in Figure S5 can be divided into two parts: the upper half corresponds to the loading and the lower half to the unloading. They connect at the two extreme strain values of the loop,  $\varepsilon_{min}$  and  $\varepsilon_{max}$ . The elastic relationship, which describes the dynamic stress-strain curve of the viscoelastic aorta under dynamic strain, is taken as the average of the upper and lower halves of the loop. This is the backbone of the loop drawn in red in Figure S5. The storage energy  $W_s$  per unit volume for a quarter of cycle [25] results as

$$W_s = \frac{A_1 + A_2}{2}, \quad (7.2)$$

where  $A_1$  and  $A_2$  are the areas of the two curvilinear triangles under the middle curve of the loop

in Figure S5. Since the dynamic elastic relationship is nonlinear, the areas  $A_1$  and  $A_2$  are different and an average of the two is introduced in eq. (7.2). The loss factor  $\eta$  is given by [25, 31]

$$\eta = \frac{\Delta W_d}{2\pi W_s} = \frac{\Delta W_d}{\pi(A_1 + A_2)}, \quad (7.3)$$

which is a ratio of two areas in Figure S5; therefore, it is dimensionless and does not depend on the scale of the axes.

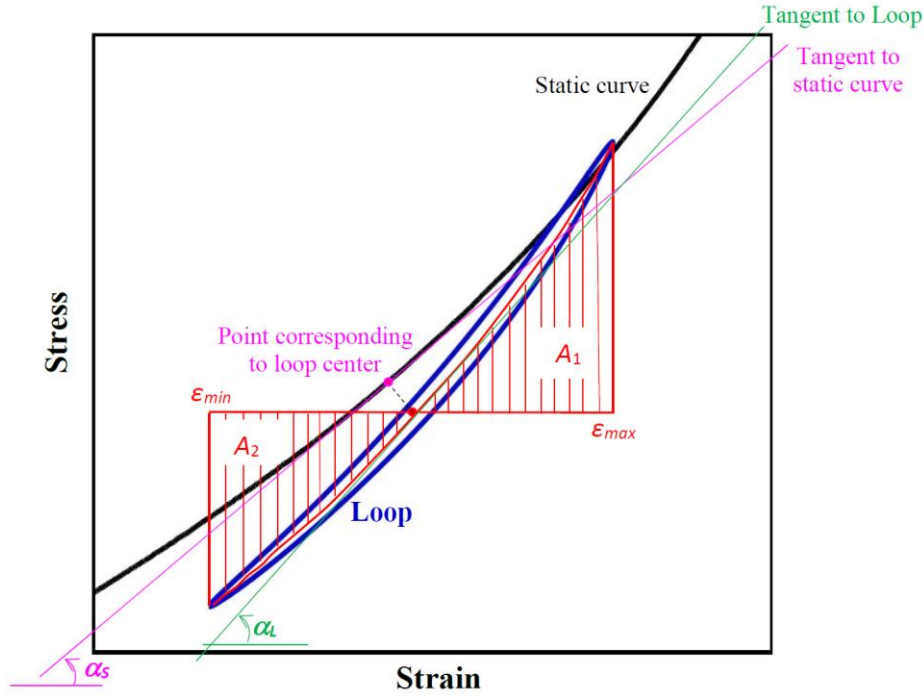


**Figure S5.** Hysteresis loop (—) and quasi-static curve (—) of a strip under harmonic load in the stress-strain diagram. The energy loss in one cycle is proportional to the area inside the loop. The mean of the areas  $A_1$  and  $A_2$ , determined from the middle curve of the loop (—) and the horizontal line passing through the middle of the loop, is proportional to the storage energy. The slope of the tangent to the middle line of the loop (—) at the loop center is  $\alpha_L$ ;  $\tan(\alpha_L)$  is proportional to the storage modulus; the slope of the tangent to the static curve (—) at the point corresponding to the loop center is  $\alpha_s$  and  $\tan(\alpha_s)$  is proportional to the corresponding static module.

## Supplementary Note 8 - Dynamic characterization: additional data

Among the two pre-stress levels, 50 and 90 kPa, the 50 kPa (first level) is a good choice to represent the physiological condition. An approximate formula for a thin cylindrical shell under pressure gives a stress  $S = pR/h$ ; for a mean blood pressure  $p = 93.3$  mmHg (obtained with a pulsatile pressure between 80 and 120 mmHg as  $80+40/3$  mmHg), mean aortic radius  $R = 10$  mm and wall thickness  $h = 2$  mm, results in 62 kPa, which is not far from 50 kPa.

**Table S3.** Dynamic stiffness ratio and loss factor of active and passive circumferential and longitudinal strips. 1<sup>st</sup> level pre-stress, 50 kPa; frequencies 1 and 3 Hz. N.A., not available.

		Dynamic stiffness ratio				Loss factor			
		Passive		Active		Passive		Active	
		1 Hz	3 Hz	1 Hz	3 Hz	1 Hz	3 Hz	1 Hz	3 Hz
II	Circ.	1.52	1.52	1.90	1.89	0.0694	0.0754	0.0781	0.086
	Long.	1.22	1.23	2.06	2.10	0.0731	0.0817	0.0787	0.0865
III	Circ.	1.49	1.51	1.81	1.86	0.0731	0.0787	0.0885	0.083
	Long.	1.55	1.54	2.22	2.23	0.0673	0.0764	0.0828	0.0899
IV	Circ.	1.44	1.45	1.92	1.90	0.0595	0.0689	0.0671	0.0778
	Long.	1.58	1.58	1.83	1.79	0.0548	0.064	0.0628	0.0719
V	Circ.	1.58	1.49	2.14	2.25	0.0563	0.0651	0.0936	0.0987
	Long.	N.A.	N.A.	N.A.	N.A.	N.A.	N.A.	N.A.	N.A.
VI	Circ.	1.32	1.37	1.81	1.87	0.0501	0.0534	0.0803	0.0881
	Long.	1.55	1.62	2.33	2.46	0.0725	0.0816	0.0856	0.0894
VIII	Circ.	1.46	1.54	2.24	2.27	0.0602	0.0660	0.1000	0.1022
	Long.	1.60	1.68	2.22	2.36	0.0649	0.0723	0.0854	0.0916
IX	Circ.	2.06	2.04	2.32	2.46	0.0745	0.0801	0.0952	0.0976
	Long.	1.55	1.55	1.61	1.67	0.0729	0.0802	0.0806	0.0877
X	Circ.	1.88	1.95	2.64	2.75	0.0688	0.0763	0.0889	0.0931
	Long.	1.64	1.69	2.39	2.46	0.0649	0.0722	0.0823	0.0878
XI	Circ.	1.56	1.59	2.07	2.16	0.0667	0.0757	0.0896	0.0949
	Long.	1.66	1.68	2.00	2.08	0.0726	0.08	0.0921	0.092
XII	Circ.	1.52	1.56	1.88	1.96	0.0658	0.0717	0.0811	0.0850
	Long.	2.02	2.11	2.83	2.94	0.0845	0.0906	0.1000	0.0988
XIII	Circ.	1.51	1.55	2.07	2.16	0.0609	0.0683	0.0816	0.0859
	Long.	1.48	1.51	1.59	1.65	0.0733	0.0773	0.0797	0.0852

**Table S4.** Medians of dynamic stiffness ratio and loss factor of active and passive circumferential and longitudinal strips. 1<sup>st</sup> level pre-stress, 50 kPa; frequencies 1 and 3 Hz.

		Dynamic stiffness ratio			Loss factor		
		All	25-48 y.	55-68 y.	All	25-48 y.	55-68 y.
Passive	Circ.	1.52	1.51	1.56	0.0686	0.0656	0.0724
	Long.	1.58	1.59	1.55	0.0730	0.0725	0.0748
Active	Circ.	2.07	1.99	2.11	0.0883	0.0832	0.0872
	Long.	2.16	2.09	2.23	0.0861	0.0861	0.0865

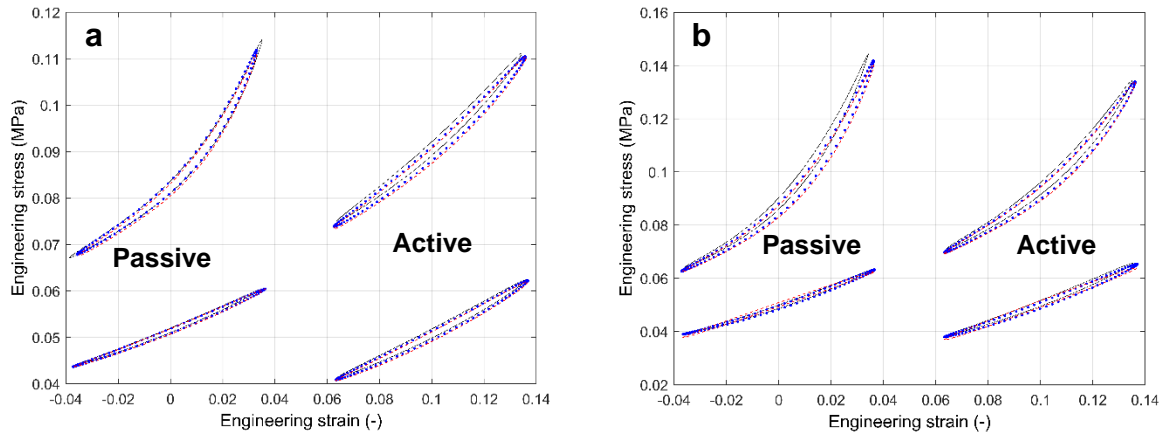


**Figure S6.** Effect of frequency on the experimentally measured hysteresis loops; 1 Hz (black), 2 Hz (blue) and 3 Hz (red) for the circumferential and longitudinal strips from donor IV. Cycles at different initial pre-stretches, corresponding to about 50 and 90 kPa for the midpoint of the loop, were measured. The amplitude of each loop was about 0.07 in engineering strain. Just for representation purposes, the passive loops are centered at 0 strain, while the active loops are centered at 0.1. **a** circumferential strip; **b** longitudinal strip.

## References

1. Driska, S.P., Mechanical properties and regulation of vascular smooth muscle contraction. In *Physiology and Patophysiology of the Heart* (2<sup>nd</sup> ed.), edited by N. Sperelakis, Kluwer, 879-898 (1989).
2. Dobrin, P.B., Rovick, A.A., Influence of vascular smooth muscle on contractile mechanics and elasticity of arteries. *Am. J. Physiol.* **217**, 1644-1651 (1969).
3. Dobrin, P.B., Mechanical behavior of vascular smooth muscle in cylindrical segments of arteries in vitro. *Ann. Biomed. Eng.* **12**, 497-510 (1984).
4. Cox, R.H., Effects of norepinephrine on mechanics of arteries in vitro. *Am. J. Physiol.* **231**, 420-425 (1976).
5. Armentano, R.L., Barra, J.G., Levenson, J., Simon, A., Pichel, R.H., Arterial wall mechanics in conscious dogs. Assessment of viscous, inertial, and elastic moduli to characterize aortic wall behavior. *Circ. Res.* **76**, 468-478 (1995).
6. Bank, A.J., Wang, H., Holte, J.E., Mullen, K., Shammas, R., Kubo, S.H., Contribution of collagen, elastin, and smooth muscle to in vivo human brachial artery wall stress and elastic modulus. *Circulation* **94**, 3263-3270 (1996).
7. Gaballa, M.A., Jacob, C.T., Raya, T.E., Liu, J., Simon, B., Goldman, S., Large artery remodeling during aging: biaxial passive and active stiffness. *Hypertension* **32**, 437-443 (1998).
8. Fridez, P., Makino, A., Kakoi, D., Miyazaki, H., Meister, J.J., Hayashi, K., Stergiopoulos, N., Adaptation of conduit artery vascular smooth muscle tone to induced hypertension. *Ann. Biomed. Eng.* **30**, 905-916 (2002).
9. Attinger, F.M.L., Two-dimensional in-vitro studies of femoral arterial walls of the dog. *Circ. Res.* **22**, 829-840 (1968).
10. Herlihy, J.T., Murphy, R.A., Length-tension relationship of smooth muscle of the hog carotid artery. *Circ. Res.* **33**, 275-283 (1973).
11. Yang, S., Wu, Q., Huang, S., Wang, Z., Qi, F., Sevoflurane and isoflurane inhibit KCl induced Class II phosphoinositide 3-kinase  $\alpha$  subunit mediated vasoconstriction in rat aorta. *BMC Anesthesiol.* **16**, 63 (2016).
12. Caulk, A.W., Humphrey, J.D., Murtada, S.-I., Fundamental roles of axial stretch in isometric and isobaric evaluations of vascular contractility. *J. Biomech. Eng.* **141**, 031008 (2019).
13. Betrie, A.H., Brock, J.A., Harraz O.F., Bush, A.I., He, G.-W., Nelson, M.T., Angus, J.A., Wright, C.E., Ayton, S., Zinc drives vasorelaxation by acting in sensory nerves, endothelium and smooth muscle. *Nat. Commun.* **12**, 3296 (2021).
14. Matsumoto, T., Tsuchida, M., Sato, M., Change in intramural strain distribution in rat aorta due to smooth muscle contraction and relaxation. *Am. J. Physiol.* **271**, H1711-H1716 (1996).
15. Lacolley, P., Regnault, V., Segers, P., Laurent, S., Vascular smooth muscle cells and arterial stiffening: relevance in development, aging, and disease. *Physiol. Rev.* **97**, 1555-1617 (2017).
16. Ratz, P.H., Berg, K.M., Urban, N.H., Miner, A.S., Regulation of smooth muscle calcium sensitivity: KCl as a calcium sensitizing stimulus. *Am. J. Physiol. Cell. Physiol.* **288**, C769-C783 (2005).
17. Rachev, A., Hayashi, K., Theoretical study of the effects of vascular smooth muscle contraction on strain and stress distributions in arteries. *Ann. Biomed. Eng.* **27**, 459-468 (1999).

18. Zulliger, M.A., Rachev, A., Stergiopoulos, N., A constitutive formulation of arterial mechanics including vascular smooth muscle tone. *Am. J. Physiol. Heart Circ. Physiol.* **287**, H1335–H1343 (2004).
19. Baek, S., Gleason, R.L., Rajagopal, K.R., Humphrey, J.D., Theory of small on large: Potential utility in computations of fluid–solid interactions in arteries. *Comput. Methods Appl. Mech. Engrg.* **196**, 3070–3078 (2007).
20. Wagner, H.P., Humphrey, J.D., Differential passive and active biaxial mechanical behaviors of muscular and elastic arteries: basilar versus common carotid. *J. Biomech. Eng.* **133**, 051009 (2011).
21. Murtada, S.C., Arner, A., Holzapfel, G.A., Experiments and mechanochemical modeling of smooth muscle contraction: significance of filament overlap. *J. Theor. Biol.* **297**, 176-186 (2012).
22. Murtada, S.-I., Lewin, S., Arner, A., Humphrey, J.D., Adaptation of active tone in the mouse descending thoracic aorta under acute changes in loading. *Biomech. Model. Mechanobiol.* **15**, 579–592 (2016).
23. Haspinger, D.C., Murtada, S.-I., Niestrawska, J.A., Holzapfel, G.A., Numerical analyses of the interrelation between extracellular smooth muscle orientation and intracellular filament overlap in the human abdominal aorta. *Z. Angew. Math. Mech.* **98**, 2198–2221 (2018).
24. Gade, J.-L., Thore, C.-J., Sonesson, B., Stålhand, J., In vivo parameter identification method for arteries is extended to account for smooth muscle activity. *Biomech. Model. Mechanobiol.* in press (2021). <https://doi.org/10.1007/s10237-021-01462-4>
25. Amabili, M., *Nonlinear Mechanics of Shells and Plates in Composite, Soft and Biological Materials*. Cambridge University Press, New York (2018).
26. Breslavsky, I.D., Franchini, G., Amabili, M., Effect of fiber exclusion in uniaxial tensile tests of soft biological tissues. *J. Mech. Behav. Biomed. Mater.* **112**, 104079 (2020).
27. Amabili, M., Asgari, M., Breslavsky, I.D., Franchini, G., Giovanniello, F., Holzapfel, G.A., Microstructural and mechanical characterization of the layers of human descending thoracic aortas. *Acta Biomaterialia* in press (2021).
28. Holzapfel, G.A., Gasser, T.C., Ogden, R.W., A new constitutive framework for arterial wall mechanics and a comparative study of material models. *J. Elasticity* **61**, 1-48 (2000).
29. Amabili, M., Balasubramanian, P., Bozzo, I., Breslavsky, I.D., Ferrari, G., Layer-specific hyperelastic and viscoelastic characterization of human descending thoracic aortas. *J. Mech. Behav. Biomed. Mater.* **99**, 27-46 (2019).
30. Holzapfel, G.A., Niestrawska, J.A., Ogden, R.W., Reinisch, A.J., Schriefl, A.J., Modelling non-symmetric collagen fibre dispersion in arterial walls. *J. R. Soc. Interface* **12**, 20150188 (2015).
31. Amabili, M., Balasubramanian, P., Bozzo, I., Breslavsky, I.D., Ferrari, G., Franchini, G., Giovanniello, F., Pogue, C., Nonlinear dynamics of human aortas for material characterization. *Phys. Rev. X* **10**, 011015 (2020).

## Chapter 5

### Conclusions

Accordingly to the previously described investigations, it was possible to characterize the passive and active static and dynamic behavior of the descending thoracic human aorta. Firstly, we proceeded in a passive characterization of the individual layers and the full wall; then, we confirmed the results of the full wall by using a mock circulatory loop, which mimics the physiological conditions. Finally, it was possible to appreciate the role of the activated muscle fibers on the mechanical response of the aortic material by using vasoactive agents in a chemically controlled environment.

Results show a significant effect of the pre-stretch on the dynamic stiffness ratio, while the pre-stretch has a smaller effect on the loss factor; and largest values of the dynamic stiffness ratio were obtained for the physiological conditions (about 50 kPa of engineering stress). But more importantly, all layers contribute in a similar way to viscoelastic (passive) behavior. In active condition the results show that Vascular Smooth Muscles activation has a significant quasi-static stiffness increase of the descending thoracic aortic tissue in both the circumferential and longitudinal directions. Moreover, the viscoelastic effects increase in case of Vascular Smooth Muscles activation.

In Chapter 2, we statically characterized the material in strips taken in the two main directions, longitudinal and circumferential ones. To clarify the multilayered behavior of the material, experiments were performed by separating the samples into intima, media and adventitia. A cyclic harmonic excitation of physiological amplitude allowed to extract the dynamic parameters: dynamic stiffnesses ratio and loss factor. This dynamic study was carried out for different levels of initial aortic stretch, to investigate the different behavior of the material given the highly non-linear behavior in the quasistatic regime.

Chapter 2 paves the way to the following Chapter 3. By changing the configuration of the system, the static and dynamic behavior of an aortic segment placed into a mock circulatory loop is investigated. The aorta is now seen as a passively pulsating cylindrical structure conveying a pulsatile liquid flow; the liquid is composed of a mixture of water and glycerin to replicate the dynamic viscosity and mass density of the blood flow. The study was carried out at different pulse rates (beats per minute) in order to extract data that can be compared to those obtained by the

uniaxial tests presented in Chapter 2. Results fundamentally confirm the previously obtained dynamic stiffnesses ratio and loss factor values.

The fundamental novelty of this thesis is the full mechanical characterization of the aortic material in the "activated" state. The purpose of Chapter 4 is to analyze the influence of the activation of the vascular smooth muscles (VSM) through the use of noradrenaline and KCl. As demonstrated by the novel results, the VSM activation is in fact significant and has the function of helping in regulating the blood pressure. Since the average activation values are greater in the circumferential direction, we can assert that the VSM has a prevalent, but not exclusive, orientation in circumferential direction. Furthermore, there is an increase in the dynamic values of dynamic stiffnesses ratio and loss factor in case of activated VSM.

Chapter 2, "Viscoelastic characterization of human descending thoracic aortas under cyclic load" [ <https://doi.org/10.1016/j.actbio.2021.05.025> ], was published in *Acta Biomaterialia*, a journal with an Impact Factor of 10.633. Chapter 3, "Viscoelasticity of human descending thoracic aorta in a mock circulatory loop" [ <https://doi.org/10.1016/j.jmbbm.2022.105205> ], was published in the *Journal of the Mechanical Behavior of Biomedical Materials* with an I.F. of 3.902. Finally, Chapter 4, "Role of smooth muscle activation in the static and dynamic mechanical characterization of human aortas" [ <https://doi.org/10.1073/pnas.2117232119> ], was published in *PNAS – Proceeding of the National Academy of Sciences of the United States of America* – with an I.F. of 12.779.

Based on the results of this PhD thesis, a new model of the aortic tissue, that encompasses both active and passive behavior, was developed. This model makes possible the simulation of the behavior of the natural aorta without performing multiple additional experiments, which is invaluable in the design of grafts that can be implanted for aortic repair; for example in case of aneurysms. Cardiovascular diseases are the costliest group of diseases in Canada and aortic diseases are one of the most common vascular disorders. Our findings will help in the creation of mechanically compatible aortic grafts, that will not alter blood flow and require costly and dangerous subsequent surgeries. Thus, there is a pressing need for a new generation of aortic prostheses. Making a good prosthesis requires really good knowledge of the mechanical properties of the native aorta, and this is our motivation for studying healthy human aortas. These novel

prostheses will improve the quality of life of the patient and reduce the burden on the economy and the healthcare system.

I am looking forward to transferring the knowledge developed here at McGill University for the development of the aortic prosthesis of the future.

## Chapter 6

### Other Contributions

The PhD candidate contributed as author to the following additional papers (not discussed in this thesis) during the doctoral period:

- Microstructural and mechanical characterization of the layers of human descending thoracic aortas;  
Marco Amabili, Meisam Asgari, Ivan D Breslavsky, Giulio Franchini, Francesco Giovanniello, Gerhard A Holzapfel  
Acta Biomaterialia, vol. 134, 401-421 (2021).  
[ <https://doi.org/10.1016/j.actbio.2021.07.036> ]
- Effect of fiber exclusion in uniaxial tensile tests of soft biological tissues  
Ivan Breslavsky, Giulio Franchini, Marco Amabili;  
Journal of the Mechanical Behavior of Biomedical Materials, vol. 112, 104079 (2020).  
[ <https://doi.org/10.1016/j.jmbbm.2020.104079> ]
- Nonlinear Dynamics of Human Aortas for Viscoelastic Mechanical Characterization;  
Marco Amabili, Prabakaran Balasubramanian, Isabella Bozzo, Ivan D Breslavsky, Giovanni Ferrari, Giulio Franchini;  
ASME International Mechanical Engineering Congress and Exposition (2020)  
[ <https://doi.org/10.1115/IMECE2020-24296> ]
- Identification of viscoelastic properties of Dacron aortic grafts subjected to physiological pulsatile flow;  
Marco Amabili, Prabakaran Balasubramanian, Giovanni Ferrari, Giulio Franchini, Francesco Giovanniello, Eleonora Tubaldi  
Journal of the Mechanical Behavior of Biomedical Materials, vol. 110, 103804 (2020).  
[ <https://doi.org/10.1016/j.jmbbm.2020.103804> ]
- Nonlinear dynamics of human aortas for material characterization;  
Marco Amabili, Prabakaran Balasubramanian, Isabella Bozzo, Ivan D Breslavsky, Giovanni Ferrari, Giulio Franchini, Francesco Giovanniello, Chloé Pogue;  
Physical Review X, vol. 10, 011015 (2020).  
[ <https://doi.org/10.1103/PhysRevX.10.011015> ]

## Chapter 7

### Reference

- Agrafiotis, E., Geith, M.A., Golkani, M.A., Hergesell, V., Sommer, G., Spiliopoulos, S., Holzapfel, G.A., 2021. An active approach of pressure waveform matching for stress-based testing of arteries. *Artificial Organs* 45(12), 1562-1575.
- Amabili, M., Balasubramanian, P., Bozzo I., Breslavsky, I.D., Ferrari, G., Franchini G., Giovanniello, F., Pogue C., Nonlinear dynamics of human aortas for material characterization, *Phys. Rev. X*, 10 (2020) 011015, doi: 10.1103/PhysRevX.10.011015.
- Amabili, M., Balasubramanian, P., Breslavsky, I.D., Ferrari, G., Tubaldi, E., Viscoelastic characterization of woven Dacron for aortic grafts by using direction-dependent quasi-linear viscoelasticity, *J. Mech. Behav. Biomed. Mater.* 82 (2018) 282-290, doi:10.1016/j.jmbbm.2018.03.038.
- Amabili, M., Balasubramanian, P., Ferrari, G., Franchini, G., Giovanniello, F., Tubaldi, E., Identification of viscoelastic properties of Dacron aortic grafts subjected to physiological pulsatile flow, *J. Mech. Behav. Biomed. Mater.* 110 (2020) 103804, doi: 10.1016/j.jmbbm.2020.103804.
- Amabili, M., Balasubramanian, P., Bozzo, I., Breslavsky, I.D., Ferrari, G., Layer-specific hyperelastic and viscoelastic characterization of human descending thoracic aortas, *J. Mech. Behav. Biomed. Mater.* 99 (2019) 27-46, doi: 10.1016/j.jmbbm.2019.07.008.
- Amabili, M., Balasubramanian, P., Breslavsky, I., Anisotropic fractional viscoelastic constitutive models for human descending thoracic aortas, *J. Mech. Behav. Biomed. Mater.* 99 (2019) 186-197, doi: 10.1016/j.jmbbm.2019.07.010.
- Amabili, M., Arena, G.O., Balasubramanian, P., Breslavsky, I.D., Cartier, R., Ferrari, G., Holzapfel, G.A., Kassab, A., Mongrain, R., Biomechanical characterization of a chronic Type A dissected aorta, *J. Biomech.* 110 (2020) 109978, doi: 10.1016/j.jbiomech.2020.109978.
- Amabili, M., *Nonlinear Mechanics of Shells and Plates in Composite, Soft and Biological Materials*, Cambridge University Press, New York, 2018.
- Amabili, M., Asgari, M., Breslavsky, I.D., Franchini, G., Giovanniello, F., Holzapfel, G.A., 2021. Microstructural and mechanical characterization of the layers of human descending thoracic aortas. *Acta Biomaterialia* 134, 401-421.
- Armentano, R.L., Gabriel Barra, J., Martin Pessana, F., Craiem, D.O., Graf, S., Bia Santana, D., Sanchez, R.A., Smart smooth muscle spring-dampers, *IEEE Eng. Med. Biol. Mag.* 26 (2007) 62-70, doi: 10.1109/MEMB.2007.289123.
- Armentano, R.L., Barra, J.G., Levenson, J., Simon, A., Pichel, R.H., Arterial wall mechanics in conscious dogs. Assessment of viscous, inertial, and elastic moduli to characterize aortic wall behavior, *Circ. Res.* 76 (1995) 468-478, doi: 10.1161/01.RES.76.3.468.
- Armentano, R.L., Barra, J.G., Pessana, F.M., Craiem, D.O., Graf, S., Santana, D.B., Sanchez R.A., 2007. Smart smooth muscle spring-dampers. Smooth muscle smart filtering helps to more efficiently protect the arterial wall. *IEEE Eng. Med. Biol. Mag.* 26, 62–70.
- Attinger, F.M.L., Two-dimensional in-vitro studies of femoral arterial walls of the dog. *Circ. Res.* 22, 829-840 (1968).
- Baek, S., Gleason, R.L., Rajagopal, K.R., Humphrey, J.D., Theory of small on large: Potential utility in computations of fluid–solid interactions in arteries. *Comput. Methods Appl. Mech. Engrg.* 196, 3070–3078 (2007).

- Bank, A.J., Wang, H., Holte, J.E., Mullen, K., Shammass, R., Kubo, S.H., Contribution of collagen, elastin, and smooth muscle to in vivo human brachial artery wall stress and elastic modulus. *Circulation* 94, 3263–3270 (1996).
- Bazilevs, Y., Calo, V.M., Hughes, T.J.R., Zhang, Y., 2008. Isogeometric fluid-structure interaction: theory, algorithms, and computations. *Computational Mechanics* 43, 3–37.
- Bergel, D.H., The dynamic elastic properties of the arterial wall, *J. Physiology*, 156 (1961) 458-469, doi: 10.1113/jphysiol.1961.sp006686.
- Berjamin, H., Destrade, M., Parnell, W.J., On the thermodynamic consistency of quasi-linear viscoelastic models for soft solids, *Mech. Res. Commun.* 111 (2021) 103648, doi: 10.1016/j.mechrescom.2020.103648.
- Betrie, A.H., Brock, J.A., Harraz O.F., Bush, A.I., He, G.-W., Nelson, M.T., Angus, J.A., Wright, C.E., Ayton, S., Zinc drives vasorelaxation by acting in sensory nerves, endothelium and smooth muscle. *Nat. Commun.* 12, 3296 (2021).
- Breslavsky, I.D., Franchini, G., Amabili, M., Effect of fiber exclusion in uniaxial tensile tests of soft biological tissues, *J. Mech. Behav. Biomed. Mater.* 112 (2020) 104079, doi: 10.1016/j.jmbbm.2020.104079.
- Breslavsky, I.D., Amabili, M., Nonlinear model of human descending thoracic aortic segments with residual stresses, *Biomech. Model. Mechanobiol.* 17 (2018) 1839-1855, doi:10.1007/s10237-018-1060-5.
- Caulk, A.W., Humphrey, J.D., Murtada, S.-I., Fundamental roles of axial stretch in isometric and isobaric evaluations of vascular contractility. *J. Biomech. Eng.* 141, 031008 (2019).
- Chandra, S., Raut, S. S., Jana, A., Biederman, R. W., Doyle, M., Muluk, S. C., Finol, E. A., 2013. Fluid-structure interaction modeling of abdominal aortic aneurysms: the impact of patient-specific inflow conditions and fluid/solid coupling. *J. Biomechanical Engineering* 135, 81001.
- Courtial, E.-J., Fanton, L., Orkisz, M., Douek, P.C., Huet, L., Fulchiron, R., Hyper-viscoelastic behavior of healthy abdominal aorta, *IRBM* 37 (2016) 158-164, doi:10.1016/j.irbm.2016.03.007.
- Cox, R.H., Effects of norepinephrine on mechanics of arteries in vitro. *Am. J. Physiol.* 231, 420-425 (1976).
- Damughatla, A.R., Raterman, B., Sharkey-Toppen, T., Jin, N., Simonetti, O.P., White, R.D., Kolipaka, A., 2015. Quantification of aortic stiffness using MR Elastography and its comparison to MRI-based pulse wave velocity. *J. Magn. Reson. Imaging* 41, 44–51.
- Dhume, R.H., Barocas, V.H., Emergent structure-dependent relaxation spectra in viscoelastic fiber networks in extension, *Acta Biomater.* 87 (2019) 245-255, doi: 10.1016/j.actbio.2019.01.027.
- Di Giuseppe, M., Alotta, G., Agnese, V., Bellavia, D., Raffa, G.M., Vetri, V., Zingales, M., Pasta, S., Pilato, M., Identification of circumferential regional heterogeneity of ascending thoracic aneurysmal aorta by biaxial mechanical testing, *J. Mol. Cell. Cardiol.* 130 (2019) 205-215, doi: 10.1016/j.yjmcc.2019.04.010.
- Dobrin, P.B., Rovick, A.A., Influence of vascular smooth muscle on contractile mechanics and elasticity of arteries. *Am. J. Physiol.* 217, 1644-1651 (1969).
- Dobrin, P.B., Mechanical behavior of vascular smooth muscle in cylindrical segments of arteries in vitro. *Ann. Biomed. Eng.* 12, 497–510 (1984).
- Driska, S.P., Mechanical properties and regulation of vascular smooth muscle contraction. In *Physiology and Pathophysiology of the Heart* (2nd ed.), edited by N. Sperlakis, Kluwer, 879-898 (1989).

- Federico, S., Gasser, T.C., Nonlinear elasticity of biological tissues with statistical fibre orientation, *J. R. Soc. Interface*, 7 (2010) 955-966, doi: 10.1098/rsif.2009.0502.
- Ferrari, G., Balasubramanian, P., Tubaldi, E., Giovanniello, F., Amabili, M., Experiments on dynamic behaviour of a Dacron aortic graft in a mock circulatory loop, *J. Biomech.* 86 (2019) 132-140, doi:10.1016/j.jbiomech.2019.01.053.
- Franchini, G., Breslavsky, I.D., Holzapfel, G.A., Amabili, M., 2021. Viscoelastic characterization of human descending thoracic aortas under cyclic load. *Acta Biomaterialia* 130, 291-307.
- Franchini, G., Breslavsky, I.D., Giovanniello, F., Kassab, A., Holzapfel, G.A., Amabili, M., 2022. Role of smooth muscle activation in the static and dynamic mechanical characterization of human aortas. *PNAS* 119(3), e2117232119.
- Franchini, G., Giovanniello, F., Amabili, M., Viscoelasticity of human descending thoracic aorta in a mock circulatory loop. *Journal of the Mechanical Behavior of Biomedical Materials*. 130 105205. 2021
- Fridez, P., Makino, A., Kakoi, D., Miyazaki, H., Meister, J.J., Hayashi, K., Stergiopoulos, N., Adaptation of conduit artery vascular smooth muscle tone to induced hypertension. *Ann. Biomed. Eng.* 30, 905–916 (2002).
- Fung, Y.C., *Biomechanics: Circulation*, second ed., Springer, New York, 1997.
- Fung, Y.C., *Biomechanics: Mechanical Properties of Living Tissues*, second ed, Springer, New York, 1993.
- Gaballa, M.A., Jacob, C.T., Raya, T.E., Liu, J., Simon, B., Goldman, S., Large artery remodeling during aging: biaxial passive and active stiffness. *Hypertension* 32, 437–443 (1998).
- Gade, J.-L., Thore, C.-J., Sonesson, B., Stålhand, J., In vivo parameter identification method for arteries is extended to account for smooth muscle activity. *Biomech. Model. Mechanobiol.* in press (2021). <https://doi.org/10.1007/s10237-021-01462-4>
- Gasser, T.C., Ogden, R.W., Holzapfel, G.A., Hyperelastic modelling of arterial layers with distributed collagen fibre orientations, *J. R. Soc. Interface*, 3 (2006) 15-35, doi:10.1098/rsif.2005.0073.
- Ghigo, A.R., Wang, X.F., Armentano, R., Fullana, J.M., Legrée, P.-Y., Linear and nonlinear viscoelastic arterial wall models: applications on animals, *J. Biomech. Eng.* 139 (2017) 011003, doi: 10.1115/1.4034832.
- Haspinger, D.C., Murtada, S.-I., Niestrawska, J.A., Holzapfel, G.A., Numerical analyses of the interrelation between extracellular smooth muscle orientation and intracellular filament overlap in the human abdominal aorta. *Z. Angew. Math. Mech.* 98, 2198–2221 (2018).
- Herlihy, J.T., Murphy, R.A., Length-tension relationship of smooth muscle of the hog carotid artery. *Circ. Res.* 33, 275-283 (1973).
- Holzapfel, G.A., Gasser, T.C., Ogden, R.W., A new constitutive framework for arterial wall mechanics and a comparative study of material models, *J. Elasticity* 61 (2000) 1-48, doi:10.1023/A:1010835316564.
- Holzapfel, G.A., Determination of material models for arterial walls from uniaxial extension tests and histological structure, *J. Theor. Biol.* 238 (2006) 290-302, doi:10.1016/j.jtbi.2005.05.006.
- Holzapfel, G.A., Niestrawska, J.A., Ogden, R.W., Reinisch, A.J., Schriefl, A.J., Modelling non-symmetric collagen fibre dispersion in arterial walls, *J. R. Soc. Interface* 12 (2015) 20150188, doi:10.1098/rsif.2015.0188.
- Holzapfel, G.A., Gasser, T.C., Stadler, M., A structural model for the viscoelastic behavior of arterial walls: continuum formulation and finite element analysis, *European J. Mech. A/Solids* 21 (2002) 441-463, doi:10.1016/S0997-7538(01)01206-2.

- Holzapfel, G.A., Ogden, R.W., Sherifova, S., 2019. On fibre dispersion modelling of soft biological tissues: a review. *Proc. Royal Soc. London A* 475, 20180736.
- Horný, L., Netušil, M., Voňavková, T., 2014. Axial prestretch and circumferential distensibility in biomechanics of abdominal aorta. *Biomech. Model. Mechanobiol.* 13, 783–799.
- Humphrey, J.D., *Cardiovascular Solid Mechanics. Cells, Tissues, and Organs*, Springer-Verlag, New York, 2002.
- Imura, T., Yamamoto, K., Kanamori, K., Mikami, T., Yasuda, H., In vivo viscoelastic behavior in the human aorta, *Circ. Res.* 66 (1990) 1413-1419, doi: 10.1161/01.RES.66.5.1413.
- Imura, T., Yamamoto, K., Satoh, Kanamori, T., K., Mikami, T., Yasuda, H., Non-invasive ultrasonic measurement of the elastic properties of the human abdominal aorta, *Cardiovasc. Res.* 20 (1986) 208-214, doi: 10.1093/cvr/20.3.208.
- Jadidi, M., Habibnezhad, M., Anttila, Maleckis, E., K., Desyatova, A., MacTaggart, J., Kamenskiy, A., Mechanical and structural changes in human thoracic aortas with age, *Acta Biomat.* 103 (2020) 172-188, doi: 10.1016/j.actbio.2019.12.024.
- Jayendiran, R., Nour, B., Ruimi, A., 2018. Computational fluid–structure interaction analysis of blood flow on patient-specific reconstructed aortic anatomy and aneurysm treatment with Dacron graft. *Journal of Fluids and Structures* 81, 693-711.
- Labrosse, M.R., Gerson, E.R., Veinot, J.P., Beller, C.J., Mechanical characterization of human aortas from pressurization testing and a paradigm shift for circumferential residual stress, *J. Mech. Behav. Biomed. Mater.* 17 (2013) 44-55, doi:10.1016/j.jmbbm.2012.08.004.
- Lacolley, P., Regnault, V., Segers, P., Laurent, S., Vascular smooth muscle cells and arterial stiffening: relevance in development, aging, and disease. *Physiol. Rev.* 97, 1555–1617 (2017).
- Matsumoto, T., Tsuchida, M., Sato, M., Change in intramural strain distribution in rat aorta due to smooth muscle contraction and relaxation. *Am. J. Physiol.* 271, H1711–H1716 (1996).
- Morrison, T.M., Choi, G., Xaris, C.K., C.A. Taylor, Circumferential and longitudinal cyclic strain of the human thoracic aorta: age-related changes, *J. Vasc. Surg.* 49 (2009) 1029-1036, doi:10.1016/j.jvs.2008.11.056.
- Murtada, S.C., Arner, A., Holzapfel, G.A., Experiments and mechanochemical modeling of smooth muscle contraction: significance of filament overlap. *J. Theor. Biol.* 297, 176-186 (2012).
- Murtada, S.-I., Lewin, S., Arner, A., Humphrey, J.D., Adaptation of active tone in the mouse descending thoracic aorta under acute changes in loading. *Biomech. Model. Mechanobiol.* 15, 579–592 (2016).
- Niestrawska, J.A., Viertler, C., Regitnig, P., Cohnert, T.U., Sommer, G., Holzapfel, G.A., Microstructure and mechanics of healthy and aneurysmatic abdominal aortas: experimental analysis and modelling, *J. R. Soc. Interface*, 13 (2016) 20160620, doi: 10.1098/rsif.2016.0620.
- Ogden, R.W., Saccomandi, G., Introducing mesoscopic information into constitutive equations for arterial walls, *Biomech. Model. Mechanobiol.* 6 (2007) 333-344, doi:10.1007/s10237-006-0064-8.
- Rachev, A., Hayashi, K., Theoretical study of the effects of vascular smooth muscle contraction on strain and stress distributions in arteries. *Ann. Biomed. Eng.* 27, 459–468 (1999).
- Ratz, P.H., Berg, K.M., Urban, N.H., Miner, A.S., Regulation of smooth muscle calcium sensitivity: KCl as a calcium sensitizing stimulus. *Am. J. Physiol. Cell. Physiol.* 288, C769–C783 (2005).

- S. Pejcic, S., Najjari, M.R., Bisleri, G., Rival, D.E., 2021. Characterization of the dynamic viscoelastic response of the ascending aorta imposed via pulsatile flow. *J. Mech. Behavior Biomed. Mater.* 118, 104395.
- Safar, M.E., Arterial stiffness as a risk factor for clinical hypertension, *Nat. Rev. Cardiol.* 15 (2018) 97-105, doi: 10.1038/nrcardio.2017.155.
- Sassani, S.G., Kakisis, J., Tsangaris, S., Sokolis, D.P., Layer-dependent wall properties of abdominal aortic aneurysms: Experimental study and material characterization. *J. Mech. Behav. Biomed. Mater.* 49 (2015) 141-161, doi:10.1016/j.jmbbm.2015.04.027.
- Sassani, S.G., Tsangaris, S., Sokolis, D.P., Layer- and region-specific material characterization of ascending thoracic aortic aneurysms by microstructure-based models, *J. Biomech.* 48 (2015) 3757-3765, doi: 10.1016/j.jbiomech.2015.08.028.
- Schaafs, L.-A., Tzschätzsch, H., Reshetnik, A., van der Giet, M., Braun, J., Hamm, B., Sack, I., Elgeti, T., 2019. Ultrasound time-harmonic elastography of the aorta: effect of age and hypertension on aortic stiffness. *Invest. Radiol.* 54, 675-680.
- Southard, J.H., Belzer, F.O., The University of Wisconsin organ preservation solution: components, comparisons, and modifications, *Transplant. Rev.* 7 (1993) 176-190, doi: 10.1016/S0955-470X(05)80025-4.
- Valdez-Jasso, D., Bia, D., Zocalo, Y., Armentano, R.L., Haider, M.A., Olufsen, M.S., Linear and nonlinear viscoelastic modeling of aorta and carotid pressure–area dynamics under in vivo and ex vivo conditions, *Ann. Biomed. Eng.* 39 (2011) 1438-1456, doi:10.1007/s10439-010-0236-7.
- Valdez-Jasso, D., Haider, M.A., Banks, H.T., Bia, S.D., Zocalo, G.Y., Armentano, R.L., Olufsen, M.S., Analysis of viscoelastic wall properties in ovine arteries. *IEEE Trans. Biomed. Eng.* 56 (2009) 210-219, doi:10.1109/TBME.2008.2003093.
- Valdez-Jasso, D., Bia, D., Zócalo, Y., Armentano, R. L., Haider, M.A., Olufsen, M.S., 2011. Linear and nonlinear viscoelastic modeling of aorta and carotid pressure–area dynamics under in vivo and ex vivo conditions. *Annals Biomed. Eng.* 39, 1438–1456.
- Wagner, H.P., Humphrey, J.D., Differential passive and active biaxial mechanical behaviors of muscular and elastic arteries: basilar versus common carotid. *J. Biomech. Eng.* 133, 051009 (2011).
- Weisbecker, H., Pierce, D.M., Regitnig, P., Holzapfel, G.A., Layer-specific damage experiments and modeling of human thoracic and abdominal aortas with non-atherosclerotic intimal thickening, *J. Mech. Behav. Biomed. Mater.* 12 (2012) 93-106, doi:10.1016/j.jmbbm.2012.03.012.
- Westerhof, N., Noordergraaf, A., Arterial viscoelasticity: A generalized model, *J. Biomech.* 3 (1970) 357-379, doi: 10.1016/0021-9290(70)90036-9.
- Yang, Z., Ma, Z., Liu, S., Li, J., 2021. Tissue adhesion with tough hydrogels: Experiments and modeling. *Mechanics of Materials* 157, 103800.
- Yang, S., Wu, Q., Huang, S., Wang, Z., Qi, F., Sevoflurane and isoflurane inhibit KCl induced Class II phosphoinositide 3-kinase  $\alpha$  subunit mediated vasoconstriction in rat aorta. *BMC Anesthesiol.* 16, 63 (2016).
- Zulliger, M.A., Rachev, A., Stergiopoulos, N., A constitutive formulation of arterial mechanics including vascular smooth muscle tone. *Am. J. Physiol. Heart Circ. Physiol.* 287, H1335–H1343 (2004).